Universiteit Gent
Faculteit Ingenieurswetenschappen
Vakgroep Informatietechnologie

Silicon Photonics for Optical Fiber Communication

Siliciumgebaseerde fotonische circuits voor optische glasvezelcommunicatie

Diedrik Vermeulen

Proefschrift tot het bekomen van de graad van
Doctor in de Ingenieurswetenschappen:
Fotonica
Academiejaar 2012-2013

Promotoren:

Prof. Dr. Ir. Dries Van Thourhout
Prof. Dr. Ir. Günther Roelkens

Examencommissie:

Prof. Dr. Ir. Roel Baets	UGent, INTEC
Prof. Dr. Ir. Wim Bogaerts	UGent, INTEC

Universiteit Gent
Faculteit Ingenieurswetenschappen

Vakgroep Informatietechnologie
Sint-Pietersnieuwstraat 41, B-9000 Gent, België

Dit werk kwam tot stand in het kader van een specialisatiebeurs van het agentschap voor Innovatie door Wetenschap en Technologie.

Thank You

I have so many people to thank, it's crazy. Maybe I should just
Günther Wim Roel Dries Peter Geert
Joost Dirk Jonathan Shankar
Peter Eva Bart Karel Marie Wout

Gent, februari 2013
Diedrik Vermeulen

Table of Contents

List of Acronyms

A

AM	Amplitude Modulation

B

BPD	Balanced Photodetector
BER	Bit Error Rate
BCB	Benzocyclobutene
BPON	Broadband Passive Optical Network
BOX	Buried Oxide

C

CATV	Cable Television
CO	Central Office
CDC	Chromatic Dispersion Compensation
CMOS	Complimentary Metal-Oxide-Semiconductor
CW	Continuous Waveform
CWDM	Coarse Wavelength Demultiplexing
CMMR	Common Mode Rejection Ratio

D

DQPSK	Differential Quadrature Phase-Shift Keying
DBR	Distributed Bragg Reflector
DFB	Distributed Feedback
DWDM	Dense Wavelength Demultiplexing
DSP	Digital Signal Processing
DS	Downstream
DB	Duobinary

E

EDFA	Erbium-Doped Fiber Amplifier
EPON	Ethernet-based PON
ER	Extinction Ratio

F

FP	Fabry-Perot
FTTH	Fiber-To-The-Home
FSR	Free Spectral Range
FlexPON	Flexible Passive Optical Network

G

GPON	Gigabit PON
GSGSG	Ground Signal Ground Signal Ground

I

IMF	Index Matching Fluid
IL	Insertion Loss
IEEE	Institute of Electrical and Electronics Engineers
IPTV	Internet Protocol Television

L

LO	Local Oscillator
LN	Lithium Niobate

M

MZI	Mach-Zehnder Interferometer
MMI	Multi-Mode Interferometer

O

OLT	Optical Line Terminal
ONT	Optical Network Terminal
ODL	Optical Delay Line
OSNR	Optical Signal-To-Noise Ratio
OOK	On-Off Keying
ONU	Optical Network Unit

P

PON	Passive Optical Network
PIC	Photonic Integrated Circuit
PCG	Planar Concave Grating
PTP	Point-To-Point
PDL	Polarization Dependent Loss
PM	Polarization Multiplexing (also Pol-mux)
PCB	Printed Circuit Board
PRBS	Pseudo-Random Binary Sequence
PCE	Polarization Conversion Efficiency
PM-DQPSK	Polarization Multiplexed Differential Quadrature Phase-Shift Keying

PM-QPSK	Polarization Multiplexed Quadrature Phase-Shift Keying

Q

QPSK	Quadrature Phase-Shift Keying

R

ROADM	Reconfigurable Optical Add-Drop Multiplexer
RSOA	Reflective Semiconductor Optical Amplifier
RN	Remote Node

S

SEM	Scanning Electron Microscope
SOI	Silicon-on-Insulator
SMF	Single-Mode Fiber
SFP	Small-Form-Factor-Pluggable
SLED	Super-Luminescent Emitting Diode
Si	Silicon
SIO2	Silicon Dioxide
SOI	Silicon-on-Insulator

T

TE	Transverse Electric
TIR	Total Internal Reflection
TM	Transverse Magnetic
TIA	Transimpedance Amplifier
TO	Transverse Optical
TDM	Time Division Multiplexing

U

UV	Ultraviolet

W

WDM	Wavelength Division Multiplexing
WWW	World Wide Web
WG	Waveguide
WR	Wavelength Router

Nederlandse samenvatting –Summary in Dutch–

Optische glasvezelcommunicatienetwerken vereisen zenders en ontvangers (transceivers) aan elke zijde van de glasvezel. Deze converteren de optische signalen naar elektrische signalen en vice versa. Transceiver optiek volgt nu hetzelfde pad als elektronica in de 20^{e} eeuw. Fotonische componenten kunnen worden gemonteerd op een optisch platform (equivalent met een Printed Circuit Board (PCB)) of geïntegreerd in een fotonische chip (Photonic Integrated Circuit (PIC)). Deze trend is een van de belangrijkste drijfveren voor de vooruitgang in transceivertechnologie. Fotonische integratie, in de zin dat het licht volledig gecontroleerd wordt door middel van golfgeleiders op de chip, heeft een heel nieuwe dimensie van fotonische componenten geopend en het vermogen om complexe circuits op een enkele chip te integreren. In dit werk zal ik de haalbaarheid van siliciumgebaseerde fotonische chips als integratie platform voor optische communicatietoepassingen evalueren en dit door middel van drie integratie voorbeelden.

1 Fiber-To-The-Home (FTTH) point-to-point (PTP) central office (CO) meerkanaals zendontvanger

Voor de datacom en access markt heb ik een Fiber-To-The-Home (FTTH) point-to-point (PTP) central office (CO) transceiver array ontwikkeld. Grote economische besparingen kunnen worden bereikt door het verminderen van de CO ruimte. Ik heb hierbij gebruik gemaakt van de schaalbaarheid die fotonische integratie biedt zodat men moeiteloos meerdere transceivers kan dupliceren op een enkele chip. Normaal gezien bevat een Small-Form-Factor-Pluggable (SFP) behuizing exact één optische transceiver. Door middel van optische integratie kunnen we nu 4 tot 24 FTTH transceivers integreren in dezelfde SFP behuizing (zie Fig. 1).
De uiteindelijke multi-transceiver chip moet voldoen aan de FTTH transceiver specificaties, gebaseerd op de IEEE 802.3ah 1000Base-BX10 standaard. Daaren-

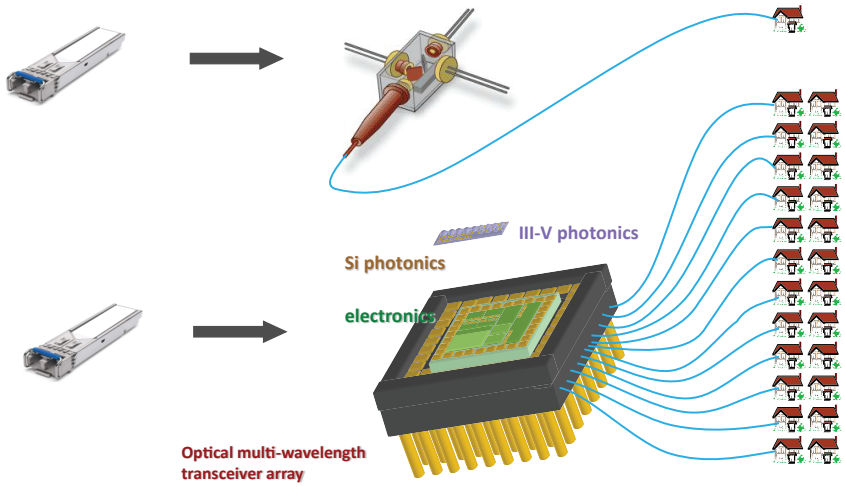

Figuur 1: SFP behuizing die een enkele FTTH transceiver bevat en gebaseerd is op discrete optica (bovenaan) en een SFP behuizing die 24 transceivers bevat door middel van geïntegreerde optica op een silicium chip (onderaan).

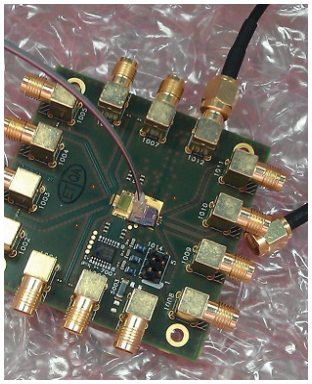

Figuur 2: 4-kanaals FTTH transceiver demonstrator, gerealizeerd in samenwerking met Genexis, Caliopa en de Technische Universiteit van Eindhoven in het kader van het Nederlands Smartmix-Memphis project.

boven heb ik de chip ontworpen zodat het gebruik van technologie overgenomen van de CMOS industrie wordt gemaximaliseerd. Hiertoe heb ik glasvezelkoppelingstechnieken die het licht uit het vlak van de chip koppelen, geoptimaliseerd en gebruikt voor elektrooptische testen op waferschaal. Dit reduceert de verpakkingskosten aanzienlijk en is daardoor essentieel in de korte afstand transceivermarkt die heel prijsgevoelig is. Naast het oplossen van het glasvezelchip koppelingsprobleem moest ik ook andere componenten optimaliseren of uitvinden om aan de IEEE specificaties te kunnen voldoen. Enkele voorbeelden hiervan zijn een Planar Concave Grating (PCG) demultiplexer die de upstream golflengtes splitst en een III/V transparante fotodetector die de downstreamgolflengtes detecteert en tegelijkertijd transparant is voor de upstream golflengtes. Al deze ontwikkelde componenten heb ik uiteindelijk gebruikt in een 4-kanaal demonstrator. De demonstrator is te zien in Fig. 2 en is gerealizeerd in samenwerking met Genexis, Caliopa en de Technische Universiteit van Eindhoven in het kader van het Nederlands Smartmix-Memphis project. Met uitzondering van de modulator drivers, waren alle elementen aanwezig in de demonstrator. Deze zijn de op silicium gebaseerde fotonische chip, de III/V transparante fotodetector array, de Transimpedance Amplifier (TIA) array en een optische glasvezel array. Ik concludeer dat het mogelijk is om aan de FTTH specificaties te voldoen voor deze 4-kanaals transceiver. Het integreren van meer dan 4 kanalen is beperkt door het optisch vermogen budget. Hiervoor zou men een verbetering in modulatorverlies of een geïntegreerde optische versterker of meer dan één laser nodig hebben.

2 Polarizatie-multiplex (PM) differentiële quadrature fase shift keying (DQPSK) ontvanger

Voor de lange-afstand en mogelijks korte-afstand markt hebben we een ontvanger onderzocht die een complex modulatieformaat demoduleert. Dit modulatieformaat is Differential Quadrature Phase-Shift Keying (DQPSK) die de spectrale efficiëntie verhoogt. Daarnaast kunnen we ook beide orthogonale polarisaties gebruiken om de bitrate te verdubbelen. Dit noemen we Polarization Multiplexing (PM or Pol-mux). Een microscoopfoto van de DQPSK ontvanger is te zien in Fig. 3, gerealizeerd in samenwerking met DAS photonics, Universidad Politecnica de Valencia, CEA Leti en het Institut d'Electronique Fondamentale (IEF) in het kader van het Europees Helios project. We hebben DUV lithografie en Ge fotodetector integratie gebruikt voor het maken van deze DPQSK ontvanger. Dit circuit heeft een 90° hybrid en gebalanceerde fotodetectoren nodig. Succesvolle werking aan 10 Gb/s en 20 Gb/s is aangetoond. Als laatste voorbeeld hebben we een PM-DQPSK ontvanger onderzocht en ontworpen gebruik makend van een

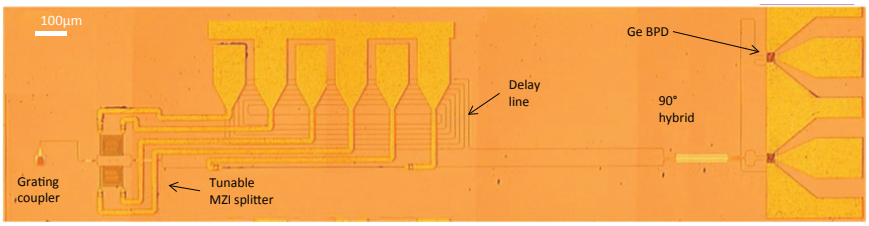

Figuur 3: DQPSK ontvanger demonstrator met gebalanceerd Ge fotodetectoren, gerealizeerd in samenwerking met DAS photonics, Universidad Politecnica de Valencia, CEA Leti en het Institut d' Electronique Fondamentale (IEF) in het kader van het Europees Helios project.

2D polarisatie splittende roosterkoppelaar om beide polarisaties in te koppelen, te splitsen en te roteren. Als alternatief voor deze 2D roosterkoppelaar hebben we horizontale koppeling onderzocht door middel van een geïnverteerde taper. Hiertoe hebben we een polarisatie splitter en polarisatie rotator ontwikkeld.

3 FlexPON golflengte router

Een laatste voorbeeld is een Reconfigurable Optical Add-Drop Multiplexer (ROADM) voor een Passief Optisch Netwerk (PON). Deze architectuur, genaamd FlexPON, is ontwikkeld door Genexis en de Technische Universiteit van Eindhoven. Ringresonatoren worden gebruikt om gebruikerspecifieke golflengtes af te leiden of bij te voegen op een dynamische en flexibele manier. Deze architectuur is mogelijk dankzij siliciumgebaseerde geïntegreerde fotonica. Een microscoop afbeelding van de gefabriceerde FlexPON golflengterouter is te zien in Fig. 4. We hebben de nodige subcomponenten onderzocht en geoptimaliseerd zodat de golflengterouterspecificaties kunnen vervuld worden. Een polarisatieafhankelijk verlies (PDL) compensatie methode voor het gebruik van 2D roosterkoppelaars als koppelingselementen is aangetoond, waarbij een PDL van slechts 0.15 dB is bereikt. Ringresonatoren zijn de hoofdcomponenten voor golflengteschakelaars. We hebben deze verbeterd en hebben een ultrahoge kwaliteitsfactor van 1 miljoen bereikt. We hebben ook de reflectie van roosterkoppelaars geminimaliseerd tot −45 dB.

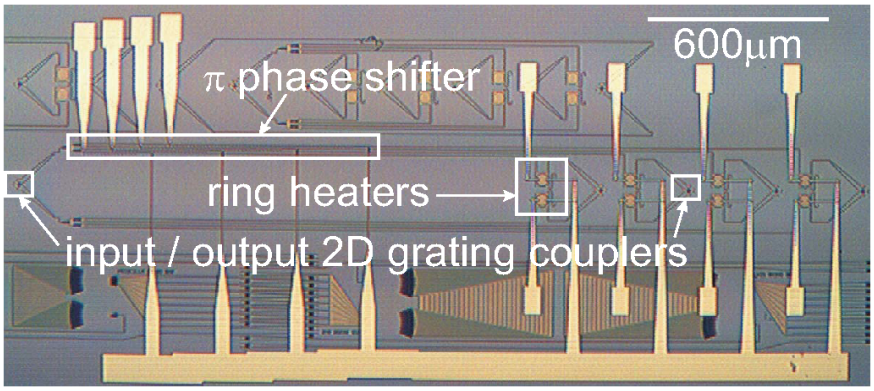

Figuur 4: Microscoopfoto van een gefabriceerde silicium chip met FlexPON golflengterouter.

English summary

Optical fiber communication networks require transceivers on each side of the fiber. These convert the optical signals to electrical signals and vice versa. Transceiver optics is now following the same path as electronics in the 20th century. Photonic components can be assembled on an optical board (equivalent to a Printed Circuit Board (PCB)) or integrated on a Photonic Integrated Circuit (PIC). This trend is a main enabler in transceiver advancements. Photonic integration, in the sense that the light is fully controlled using on-chip waveguides, has opened up a whole new dimension of photonic components and the ability to squeeze complex circuits onto a single chip. In this work I evaluate the feasibility of Silicon Photonics technology as integration platform for optical communication applications by means of three integration examples.

4 Fiber-To-The-Home (FTTH) point-to-point (PTP) central office (CO) transceiver array

For the access and short-reach market I have developed a Fiber-To-The-Home (FTTH) point-to-point (PTP) central office (CO) transceiver array. Large economic savings can be accomplished by reducing the CO space. I exploited the scalability of photonic integration to duplicate effortless multiple transceivers on a single chip. Normally a single Small-Form-Factor-Pluggable (SFP) package contains exactly one optical transceiver. Optical integration enables integrating 4 to 24 FTTH transceivers in a single SFP package (see Fig. 5).
The eventual transceiver array has to fulfill the FTTH transceiver specifications based on the IEEE 802.3ah 1000Base-BX10 standard. Moreover, I designed the circuit such that the use of technology leveraged from the CMOS industry is maximized. Out-of-plane fiber-to-chip coupling techniques were optimized and used to enable electro-optical wafer-scale testing. This reduces the packaging cost substantially and is therefore thus essential in the cost sensitive access transceiver market. Besides solving the fiber-to-chip problem, other components had to be optimized or invented to be able to reach the IEEE specifications. A Planar Concave Grating (PCG) demultiplexer splitting the upstream wavelengths

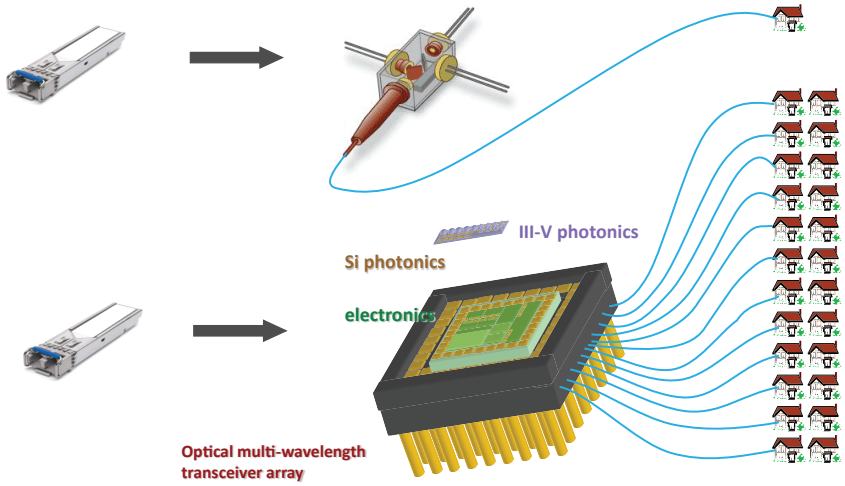

Figure 5: SFP package containing one FTTH transceiver using discrete optics (top) and 24 FTTH transceivers (bottom) using Silicon Photonics technology.

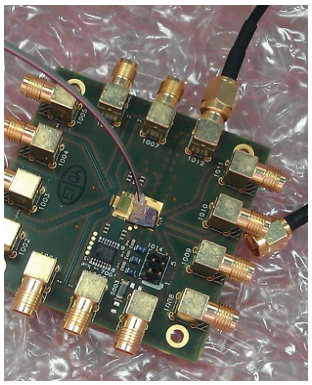

Figure 6: 4-channel FTTH transceiver demonstrator, developed in cooperation with Genexis, Caliopa and the Technical university of Eindhoven in the framework of the Dutch Smartmix-Memphis project.

and a III/V transparent photodetector which is transparent for the upstream wavelengths and detects the downstream wavelengths were demonstrated.
All the developed components were eventually used in a 4-channel demonstrator. The demonstrator can be seen in Fig. 6 and is realized in cooperation with Genexis, Caliopa and the Technical university of Eindhoven in the framework of the Dutch Smartmix-Memphis project. Except for the modulator drivers, all components including the Silicon Photonics chip, the III/V transparent photodetector array, the Transimpedance Amplifier (TIA) array and optical fiber array were present. I concluded that for this 4-channel transceiver array it is possible to reach the FTTH specifications. Going to a higher number of channels is restricted by the power budget. This would require an improvement in modulator loss or the use of inegrated optical amplifiers or more than one laser.

5 Polarization-multiplexed (PM) differential quadrature phase shift keying (DQPSK) receiver

For the long-reach and potentially access market I have investigated a receiver which demodulates a complex modulation format, named Differential Quadrature Phase-Shift Keying (DQPSK), thereby increasing the spectral efficiency. Furthermore, by using both orthogonal polarizations, the bitrate can be doubled. This is called Polarization Multiplexing (PM or Pol-mux). A microscope picture of the DQPSK receiver demonstrator is shown in Fig. 7. This demonstrator was realized in cooperation with DAS photonics, Universidad Politecnica de Valencia, CEA Leti, the Institut d'Electronique Fondamentale (IEF) and the Technical university of Eindhoven in the framework of the European Helios project. I employed DUV lithography including Ge photodetector integration to make the DPQSK receiver. This circuit requires a 90° hybrid and balanced photodetectors. Successful operation at 10 Gb/s and 20 Gb/s was achieved. Finally I investigated and designed a PM-DQPSK receiver using a 2D polarization splitting grating coupler to couple, split and rotate the polarizations. As an alternative, horizontal coupling by means of an inverted taper was considered. For this I developed a polarization splitter and polarization rotator.

6 FlexPON wavelength router

A last example is a Reconfigurable Optical Add-Drop Multiplexer (ROADM) for a Passive Optical Network (PON). The particular architecture is quite unique and is called FlexPON. It is invented by Genexis and the Technical university of Eindhoven. Ring resonators are used to add and drop user specific wavelengths in

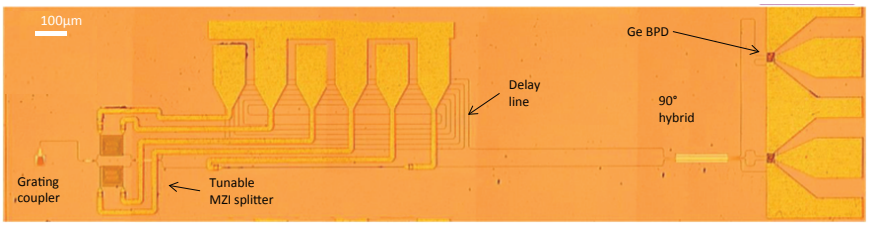

Figure 7: DQPSK receiver demonstrator with balanced Ge photodetectors, realized in cooperation with DAS photonics, Universidad Politecnica de Valencia, CEA Leti, the Institut d'Electronique Fondamentale (IEF) and the Technical university of Eindhoven in the framework of the European Helios project.

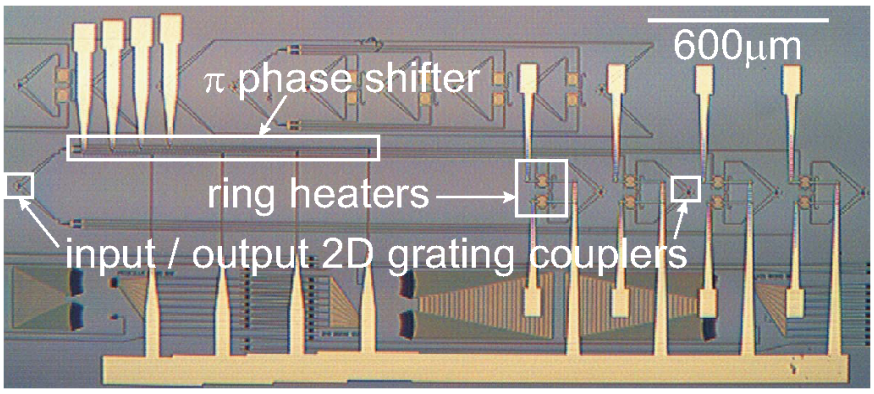

Figure 8: Microscope picture of a fabricated FlexPON wavelength router SOI chip.

a dynamic and flexible way. This architecture is enabled by integrated photonics. A microscope picture of the fabricated FlexPON wavelength router chip is shown in Fig. 8. I investigated the necessary subcomponents and optimized them such that the wavelength router specs can be reached. A PDL compensation method in the case of fiber-to-chip coupling by means of 2D grating couplers has been demonstrated achieving a PDL as low as 0.15 dB. Ring resonators, serving as the main component for wavelength switching, have been improved to achieve ultra-high Q's of one million. Furthermore, the return loss of grating couplers have been improved up to 45 dB.

1 Introduction

1.1 Optical fiber communication

Humankind's crazy progress started with the early usage of primitive tools in order to shape the world to his needs. Now, as we are on the brink of conquering our solar system, creating artificial life and revealing the most fundamental theory of the universal laws. None of which would have been possible without the following three basic properties: a big tight and flexible interconnected brain that enables self-awareness and the ability to learn complicated sequences of movements or thoughts. Manipulators (hands, legs) to physically interact with our surroundings and manipulate objects. Receivers (senses) and transmitters (speech, touch) to extract/inject information from and into our surroundings. Early human communication happened by means of sounds and together with the human brain as powerful signal processor, complex languages were created such that the information density of the sounds increased. Information was spread from generation to generation by oral communication, thereby keeping the obtained information, knowledge and technology and steadily creating new insights. In order to spread information over greater distances and over greater time periods, in order to enhance the information density, people invented alternative communication methods such as painting, writing, audio/video recording,... Inventions such as the printing press, telegraph and laser are at the basis of communication advancements. The tendancy toward increased information

density, increased information reach and increased information speed has been a constant through human history. It is the enabler of fast technological progress and world peace.
In modern society we digitalize information and communicate by manipulating particles/waves.[1] Physically speaking the most suitable carrier would be a neutrino as it only interacts by the weak interaction. For example, we could transmit signals through the earth core since the chance that neutrino's interact with matter is extremely small. However, this makes these particles also difficult to manipulate [2]. Another example of a good particle candidate is the photon. Since it is massless and mainly interacts by the electromagnetic force, it can be used to communicate over very long distances using optically transparent media. A photon can be guided by forming a waveguide using optical materials with different refractive indices and by the principle of total internal reflection. The lowest cost photon waveguide is an optical fiber [3]. The most common Single-Mode Fiber (SMF) is Corning SMF-28e and its current price is about $ 0.2 per meter. In Fig. 1.1, the intercontinental fiber connections are shown. It are these transmission networks that are at the core of today's communication infrastructure and enable the worldwide internet.
Transceivers are the components at the end of a fiber network that convert electrical to optical signals and vice versa [4]. The main components of a transceiver are lasers (light source), modulators (light manipulators) and photodetectors (light sensors). Besides the optical fiber itself and the deployment costs, a big cost of a transmission network are the optical transceivers. Optical communication advancements typically coincide with transceiver advancements. A straightforward advancement is reducing the inherent cost of the transceiver. The operating cost can be decreased by reducing the power consumption, reducing the footprint of the transceiver or increasing tunability/flexibility. The performance can be improved, as well as the reliability and self-testing capabilities can be included. All these transceiver advancements will eventually decrease the cost per bit of a transmission network.

1.2 Distance weighted transceiver cost reduction

The cost of a transmission network is determined by the optical link cost, i.e. the fiber, amplifier and deployment costs. In submarine (~ 3000 km), long-haul ($80-3000$ km) and metro ($20-80$ km) networks, the optical link cost is much higher than the cost of the transceivers. The main transceiver advancements for these long-reach networks are thus related to increased performance and in a lesser manner to reduced operating cost. High spectral efficiency (bit/s/Hz)

[1] Recently, a particle free communication method using quantum mechanical superposition principles has been demonstrated [1].

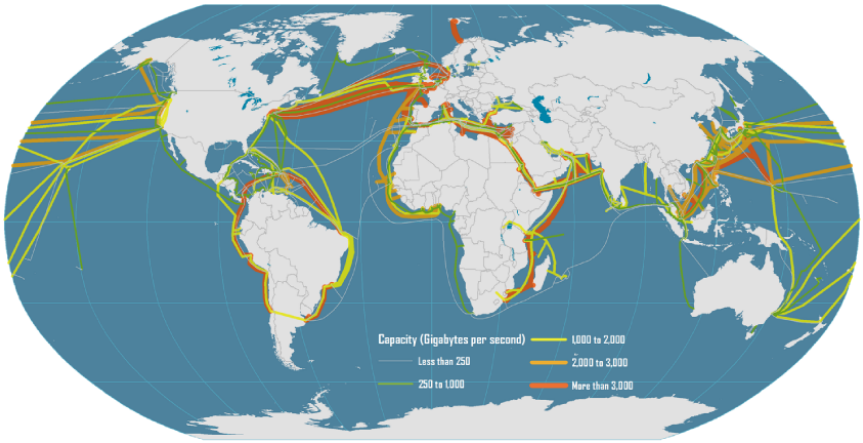

Figure 1.1: Submarine optical fiber networks on earth.

is of utter importance. Techniques which enhance the optical reach such as Chromatic Dispersion Compensation (CDC), high Optical Signal to Noise Ratio (OSNR) and high launch power/sensitivity are necessary and reduce the number of amplifiers and/or exclude regeneration [5]. These transceivers need to operate over several decades and need to be very reliable [6]. For the mid-range and access transmission networks transceiver power consumption and footprint also play a major role in decreasing the network cost. For the ultra-short-reach (such as active optical cables in data centers) the optical link becomes very inexpensive and thus the optical transceiver value is mainly determined by its fabrication cost, compactness, power consumption and short-term reliability [7].

1.3 Optical integration value proposition

Transceiver optics is now following the same path as electronics in the 20th century. Photonic components can be assembled on an optical board (equivalent to a Printed Circuit Board (PCB) board) [8] or integrated on a Photonic Integrated Circuit (PIC) [9]. This trend is a main enabler in transceiver advancements. Photonic integration, in the sense that the light is fully controlled using on-chip waveguides, has opened up a whole new dimension of photonic components and the ability to squeeze complex circuits onto a single chip. However, the early cases of photonic integration (in the broad context of photonics on a chip) were single photonic components such as photodetectors, modulators [10] and wavelength demultiplexers having a superior performance over their discrete counterparts. This increased performance is mainly achieved by tuning the integration platform accordingly to the specific component needs. A couple of

examples are the III-V materials for lasers and photodetectors, silica glass for passive optical filters [11] and Lithium Niobate for modulators [12]. Photonic systems quickly became an assembly of fiber based components and single integrated components, merging the best of all worlds. But, as research and technology in integrated photonics advances, the chance that these multi-systems dominate the photonics landscape is decreasing dramatically. Factors such as size, cost and power consumption are becoming more important every day and are the main driving force behind the search for the holy grail of complete photonic integration.
The applications of integrated photonic circuits are numerous and range from active cables [13, 14] to sensing [15] and free space applications [16]. However, although integrated photonics technology has the potential to become a major player in all these fields, for future telecom applications it is the only possible solution due to the inexistence of any alternative to meet future size and complexity requirements. The main challenge in all of this is to develop a complete photonic integration platform that has the potential to meet the required specifications.

1.4 Photonic integration platform choice

There are several approaches for complete photonic integration. Historically, the most successful is using InP or in general Group III/V materials as platform for integration [17]. The main reason for the success can be contributed to the direct bandgap, enabling straightforward integration of active optical components using a gain section. Also the fact that the bandgap can be engineered contributed to the success of the III/V platform. At the end of the 20^{th} century people started looking seriously into silicon or more generally Group IV materials as integration platform candidate for telecom applications. This platform is what one calls Silicon Photonics [18]. Research was driven by the fact that Silicon Photonics could leverage on all the existing tools and progress made in the silicon industry for micro-electronics [19]. Silicon technology has been massively optimized during several decades now and forms a perfect platform for integrated photonics with a potentially ultra-low cost-yield ratio. Combining germanium with Silicon has been proven to be quite straightforward and paved the way for high quality photodetectors [20]. Furthermore, using doped waveguides high-speed modulation can be achieved [21]. However, one major problem is the integration of light sources due to the indirect bandgap of Silicon. Several solutions are developed based on the integration of III-V material on the Silicon platform by means of hybrid or heterogeneous integration ([22], [23]). None of them could be called elegant but until the germanium laser, which has recently shown to be very promising [24] , or other truly compatible Complimentary Metal-Oxide-Semiconductor (CMOS)-compatible laser deliver,

these solutions are second to none. Another alternative approach could be to completely separate the lasers and the rest of the circuit using a co-packaged III-V laser and Silicon Photonics chip but at the cost of increased packaging costs.

Putting the laser issue aside as this is at the moment a very application dependent problem and solutions come in many flavors, one big general problem that Silicon Photonics is fighting with are the total circuit losses and specifically the fiber-to-chip coupling losses [25]. Furthermore, due to the high birefringence of the silicon waveguides, both orthogonal polarizations are treated preferably independently using a polarization diversity circuit [26]. In order to have full benefit from the cost-yield ratio of the Silicon Photonics platform, low-cost chip testing is a must and this can only be provided if surface couplers such as grating couplers are used [27, 28], thereby enabling wafer-scale testing and thus pre-packaging die selection. I will take the coupling problem as a starting point for discussing silicon photonic integration for applications such as Fiber-To-The-Home (FTTH) Point-To-Point (PTP) [29] and coherent optical transceivers [30].

1.5 Trends for integrated photonics

The quest for the ultimate complete integrated photonics platform is pursued on different levels. First of all the III/V community is trying to mature the InP platform [31, 32]. Although very good progress has been made, the InP platform is in terms of reliability and killer defects, about 20 years behind the CMOS industry. Silicon Photonics on the other hand, instead of trying to catch up with the CMOS industry, makes direct use of the materials, CMOS processes, tools and infrastructure. In this sense Silicon Photonics is surfing the CMOS wave.
The main problem of the group IV platform is the absence of lasers or amplifiers. One way forward is to make Silicon Photonics complete by achieving gain in silicon or germanium. Very interesting work can be found in [33] where successful lasing has been demonstrated. Still there are some fundamental difficulties to be addressed.
An integration strategy which combines the best of both worlds is integrating III-I/V materials onto a Silicon Photonics platform. Although this is the least elegant method, it is a strategy with the least uncertainty and risk. Hybrid integration can take many forms. Prefabricated devices can be hybridly combined with a silicon PIC by means of butt or out-of-plane coupling. A more intimate marriage is to bond III/V dies on the silicon PIC whereafter the III/V is processed, achieving lithographic alignment between the silicon and III/V devices [34].

1.6 Structure of this PhD thesis

In this work I will focus on the use of PICs for transceiver-like applications. Especially telecom applications are addressed but a lot of the developed designs can be used for other applications such as on-chip interconnects or bio sensing. The telecom transceiver market is separated according to the optical link distances. For access and short-reach market I have developed a Fiber-To-The-Home (FTTH) point-to-point (PTP) central office (CO) transceiver array (see Chapter 2). For this case the scalability of photonic integration is exploited to duplicate effortless multiple transceivers on a single chip and achieve a central office space reduction. I was the main coordinator in this work and part of all stages in the development process. This work was realized in cooperation with *imec* (fabrication), Genexis (design and characterization) and the Technical university of Eindhoven (characterization) in the framework of the Dutch Smartmix-Memphis project. Due to the achieved technical success and big market potential of the developed technology, an independent startup, Caliopa, was created to commercialize the technology pioneered in this work.
For the long-reach and potentially access market I have investigated a receiver which uses a complex modulation format, named Differential Quadrature Phase-Shift Keying (DQPSK), thereby increasing the spectral efficiency (see Chapter 3). Moreover, both orthogonal polarizations are used to double the bitrate. This is called Polarization Multiplexing (PM or Pol-mux). This work was realized in cooperation with DAS photonics (main coordinator), Universidad Politecnica de Valencia (fabrication), CEA Leti (fabrication), the Institut d'Electronique Fondamentale (IEF) (design) and the Technical university of Eindhoven (characterization) in the framework of the European Helios project. My contribution was mainly focused on design and layout.
A last example is a Reconfigurable Optical Add-Drop Multiplexer (ROADM) for a Passive Optical Network (PON) (see Chapter 4). The particular architecture is quite unique and is called FlexPON. Ring resonators are used to add and drop user specific wavelengths in a dynamic and flexible way. This architecture is enabled by integrated photonics. This work was realized in cooperation with Genexis and the Technical university of Eindhoven in the framework of the Dutch Smartmix-Memphis project. My work in this project was mainly focused on design and layout.

References

[1] Hatim Salih, Zheng-Hong Li, M. Al-Amri, and M. Suhail Zubairy. *Protocol for Direct Counterfactual Quantum Communication.* Physical Review Letters, 110(17):170502, 2013.

[2] D. D. STANCIL, P. ADAMSON, M. ALANIA, L. ALIAGA, ..., G. ZAVALA, D. ZHANG, L. Y. ZHU, and B. P. ZIEMER. *DEMONSTRATION OF COMMUNICATION USING NEUTRINOS.* Modern Physics Letters A, 27(12):1250077, 2012.

[3] R. Ramaswami. *Optical fiber communication: from transmission to networking.* IEEE Communications Magazine, 40(5):138–147, 2002.

[4] Avigdor Brillant. *Digital and Analog Fiber Optic Communications for CATV and FTTx Applications.* 2008.

[5] Peter J. Winzer and Greg Raybon. *100G Ethernet A Review of Serial Transport Options.* In 2007 Digest of the IEEE/LEOS Summer Topical Meetings, pages 7–8, 2007.

[6] R. Dinu, a. Barklund, E. Miller, C. Wei, and J. Vemagiri. *Environmental Stress Testing of ElectroâĂŞOptic Polymer Modulators.* Journal of Lightwave Technology, 27(11):1527–1532, 2009.

[7] a. F. Benner, M. Ignatowski, J. a. Kash, D. M. Kuchta, and M. B. Ritter. *Exploitation of optical interconnects in future server architectures.* IBM Journal of Research and Development, 49(4.5):755–775, 2005.

[8] R. T. Chen, H. Lu, D. Robinson, Z. Sun, T. Jannson, D. V. Plant, and H. R. Fetterman. *60 GHz board-to-board optical interconnection using polymer optical buses in conjunction with microprism couplers.* Applied Physics Letters, 60(5):536, 1992.

[9] Radhakrishnan Nagarajan, Damien Lambert, Masaki Kato, Vikrant Lal, Gilad Goldfarb, Jeff Rahn, Matthias Kuntz, Jacco Pleumeekers, Andrew Dentai, Huan-Shang Tsai, Roman Malendevich, Mark Missey, Kuang-Tsan Wu, Han Sun, John McNicol, Jie Tang, Jiaming Zhang, Tim Butrie, Alan Nilsson, Mike Reffle, Fred Kish, and Dave Welch. *10 Channel, 100Gbit/s per Channel, Dual Polarization, Coherent QPSK, Monolithic InP Receiver Photonic Integrated Circuit.* Optical Fiber Communication Conference/National Fiber Optic Engineers Conference 2011, page OML7, 2011.

[10] G. T. Reed, G. Mashanovich, F. Y. Gardes, and D. J. Thomson. *Silicon optical modulators.* Nature Photonics, 4(8):518–526, 2010.

[11] Y. Hibino. *Recent advances in high-density and large-scale AWG multi/demultiplexers with higher index-contrast silica-based PLCs.* IEEE Journal of Selected Topics in Quantum Electronics, 8(6):1090–1101, 2002.

[12] E.L. Wooten, K.M. Kissa, A. Yi-Yan, E.J. Murphy, D.A. Lafaw, P.F. Hallemeier, D. Maack, D.V. Attanasio, D.J. Fritz, G.J. McBrien, and D.E. Bossi. *A review of lithium niobate modulators for fiber-optic communications systems.* IEEE Journal of Selected Topics in Quantum Electronics, 6(1):69–82, 2000.

[13] Jurgen Michel, J. F. Liu, D. H. Ahn, D. Sparacin, R. Sun, C. Y. Hong, W. P. Giziewicz, M. Beals, L. C. Kimerling, A. Kopa, A. B. Apsel, M. S. Rasras, D. M. Gill, S. S. Patel, K. Y. Tu, Y. K. Chen, A. E. White, A. Pomerene, D. Carothers, and M. J. Grove. *No Title.* pages 64770P–64770P–11, 2007.

[14] N. Adithyaram, S. Abdalla, C. Bradbury, A. Clark, J. Clymore, J. Coyne, A. Dahl, S. Gloeckner, A. Gruenberg, D. Guckenberger, S. Gutierrez, M. Harrison, D. Kucharski, K. Leap, R. LeBlanc, Y. Liang, M. Mack, D. Martinez, G. Masini, A. Mekis, R. Menigoz, C. Ogden, M. Peterson, T. Pinguet, J. Redman, J. Rodriguez, S. Sahni, M. Sharp, T. J. Sleboda, D. Song, Y. Wang, B. Welch, J. Witzens, W. Xu, K. Yokoyama, and P. De Dobbelaere. *An ultra low power CMOS photonics technology platform for H/S optoelectronic transceivers at less than $1 per Gbps.* In Optical Fiber Communication Conference (OFC), 2010.

[15] C. Monat, P. Domachuk, and B. J. Eggleton. *Integrated optofluidics: A new river of light.* Nature Photonics, 1(2):106–114, 2007.

[16] Tiehui Su, Ryan P Scott, Stevan S Djordjevic, Nicolas K Fontaine, David J Geisler, Xinran Cai, and S J B Yoo. *Demonstration of free space coherent optical communication using integrated silicon photonic orbital angular momentum devices.* Optics express, 20(9):9396–402, 2012.

[17] D.F. Welch, F.A. Kish, S. Melle, R. Nagarajan, M. Kato, C.H. Joyner, J.L. Pleumeekers, R.P. Schneider, J. Back, A.G. Dentai, V.G. Dominic, P.W. Evans, M. Kauffman, D.J.H. Lambert, S.K. Hurtt, A. Mathur, M.L. Mitchell, M. Missey, S. Murthy, A.C. Nilsson, R.A. Salvatore, M.F. Van Leeuwen, J. Webjorn, M. Ziari, S.G. Grubb, D. Perkins, M. Reffle, and D.G. Mehuys. *Large-Scale InP Photonic Integrated Circuits: Enabling Efficient Scaling of Optical Transport Networks.* IEEE Journal of Selected Topics in Quantum Electronics, 13(1):22–31, 2007.

[18] R.A. Soref. *Silicon-based optoelectronics.* Proceedings of the IEEE, 81(12):1687–1706, 1993.

[19] W. Bogaerts, R. Baets, P. Dumon, V. Wiaux, S. Beckx, D. Taillaert, B. Luyssaert, J. Van Campenhout, P. Bienstman, and D. Van Thourhout. *Nanophotonic waveguides in silicon-on-insulator fabricated with CMOS technology.* Journal of Lightwave Technology, 23(1):401–412, 2005.

[20] L. Vivien, J. Osmond, J.-M. Fédéli, D. Marris-Morini, P. Crozat, J.-F. Damlencourt, E. Cassan, Y Lecunff, and S. Laval. *42 GHz p.i.n Germanium photodetector integrated in a silicon-on-insulator waveguide.* Optics express, 17(8):6252–7, 2009.

[21] F. Y. Gardes, G. T. Reed, a. P. Knights, and G. Mashanovich. *Evolution of optical modulation using majority carrier plasma dispersion effect in SOI.* Proceedings of SPIE, 6898:68980C–68980C–10, 2008.

[22] G. Roelkens, J Van Campenhout, J. Brouckaert, D Van Thourhout, R. Baets, P Rojo Romeo, P Regreny, A Kazmierczak, C Seassal, X Letartre, G Hollinger, J. M. Fedeli, and L Di Cioccio. *III-V/Si photonics by die-to-wafer bonding.* Materials Today, 10(7):36–43, 2007.

[23] A.W. Fang, B.R. Koch, R. Jones, Erica Lively, and J.E. Bowers. *A Distributed Bragg Reflector Silicon Evanescent Laser.* IEEE Photonics Technology Letters, 20(20):1667–1669, 2008.

[24] R. E. Camacho-Aguilera, Y. Cai, N. Patel, Jonathan T. Bessette, M. Romagnoli, Lionel C. Kimerling, and J. Michel. *An electrically pumped germanium laser.* Optics express, 20(10):11316–20, 2012.

[25] L Zimmermann, T Tekin, H Schroeder, P. Dumon, and W. Bogaerts. *How to bring nanophotonics to application-silicon photonics packaging*, 2008.

[26] Hiroshi Fukuda, Koji Yamada, Tai Tsuchizawa, Toshifumi Watanabe, Hiroyuki Shinojima, and Sei-ichi Itabashi. *Silicon photonic circuit with polarization diversity.* Quantum Electron, 16(7):4872–4880, 2008.

[27] D. Taillaert, P. Bienstman, and R. Baets. *Compact efficient broadband grating coupler for silicon-on-insulator waveguides.* Optics letters, 29(23):2749–51, 2004.

[28] A. Mekis, S. Gloeckner, G. Masini, A. Narasimha, T. Pinguet, S. Sahni, and P. Dobbelaere. *A Grating-Coupler-Enabled CMOS Photonics Platform.* Selected Topics in Quantum Electronics, IEEE Journal of, (99):1–12, 2010.

[29] D. Vermeulen, G. Roelkens, J. Brouckaert, D. Van Thourhout, R. Baets, R. Duijn, E. Pluk, and G. Van den Hoven. *Silicon-on-insulator nanophotonic waveguide circuit for fiber-to-the-home transceivers.* In 2008 34th European Conference on Optical Communication (ECOC), volume 2, pages 1–2, 2008.

[30] C. R. Doerr, L. Buhl, Y. Baeyens, R. Aroca, S. Chandrasekhar, X. Liu, L. Chen, and Y. K. Chen. *Packaged monolithic silicon 112-Gb/s coherent receiver*. Photonics Technology Letters, IEEE, 23(99):1–1, 2011.

[31] R. Nagarajan, M. Kato, J. Pleumeekers, D. Lambert, V. Lal, A. Dentai, M. Kuntz, J. Rahn, H.-S. Tsai, R. Malendevich, G. Goldfarb, J. Tang, J. Zhang, T. Butrie, M. Raburn, B.E. Little, A. Nilsson, M. Reffle, F. Kish, and D. Welch. *10 Channel, 45.6 Gb/s per Channel, Polarization-Multiplexed DQPSK, InP Receiver Photonic Integrated Circuit*. Lightwave Technology, Journal of, 29(4):386–395, 2010.

[32] M. Smit, J. van der Tol, and M. Hill. *Moore's law in photonics*. Laser & Photonics Reviews, 6(1):1–13, 2012.

[33] J. Michel, R. E. Camacho-aguilera, Y. Cai, N. Patel, J. T. Bessette, B. R. Dutt, and L. C. Kimerling. *An Electrically Pumped Ge-on-Si Laser*. In OFC, pages 5–7, 2012.

[34] G. Roelkens, J. Brouckaert, D. Taillaert, P. Dumon, W. Bogaerts, D. Van Thourhout, R. Baets, Richard Nötzel, and Meint Smit. *Integration of InP/InGaAsP photodetectors onto silicon-on-insulator waveguide circuits*. Optics express, 13(25):10102–8, 2005.

2

Fiber-To-The-Home (FTTH) point-to-point (PTP) central office (CO) transceiver array

In this chapter I will analyze the feasibility of realizing a transceiver array for the Central Office (CO) for a Fiber-To-The-Home (FTTH) network in the case of a Point-To-Point (PTP) topology [1, 2]. The PTP topology has the drawback of requiring a huge amount of optical transceivers in the CO. By integrating the optical transceiver functionalities on a chip, multiple transceivers can be squeezed into the same Small-Form-Factor-Pluggable (SFP) package which traditionally contains just one single transceiver.[1] Such transceiver arrays would reduce the required CO space considerably and thus decrease the total cost of a FTTH network [3]. I will evaluate Silicon Photonics candidature as integration platform. The eventual transceiver array has to fulfill the FTTH transceiver specifications based on the IEEE 802.3ah 1000Base-BX10 standard. Moreover, I will design the circuit such that the use of technology leveraged from the CMOS industry is maximized. Out-of-plane fiber-to-chip coupling techniques for example enable electro-optical wafer-scale testing reducing the packaging cost substantially which is very important in the cost sensitive access transceiver

[1] We compare a single and multi-channel transceiver using an SFP package but this package is not appropriate for a multi-channel device.

market. First I will try to solve the vertical coupling problem using special grating couplers. However, as these grating couplers are inherently not very broadband, I will conclude that it is impossible to use grating couplers as a viable coupling technique to conform the FTTH transceiver specifications. To solve the problem I will introduce a new kind of photodetector which is transparent for the upstream wavelengths (1490nm and 1550nm) and has a high responsivity for the 1310nm wavelength band. This transparent photodetector simplifies the coupling problem and makes it possible to use grating couplers while fulfilling all IEEE specifications. Finally I will demonstrate a packaged 4-channel FTTH transceiver array. This demonstrator was realized in cooperation with Genexis, Caliopa and the Technical university of Eindhoven in the framework of the Dutch Smartmix-Memphis project.

2.1 Introduction to Fiber-To-The-Home

Fiber-To-The-Home, abbreviated FTTH, is a service that provides narrowband/broadband services over an optical fiber to the residential customer. It replaces the traditional copper wiring. The residential broadband service is mainly spurred by the exponential growth of the commercial internet and the World Wide Web (WWW). In order to meet these broadband needs, existing copper or more hybrid fiber-copper networks have been pushed to the limit using DSL (Digital Subscriber Line) technology such as VDSL (Very High Bit Rate DSL). Speeds on the order of 50 Mbps can be delivered to the customer using this technology. However, this kind of speeds are only possible over distances up to 300 m. Cable modem services have similar performance. FTTH service is by far superior to these traditional technologies. Instead of copper twistes pairs or coax cable, the last mile to the home is an optical fiber. Back in the mid- to late 1980s, when telephone and broadcast video services were largely provided to residential customers, the exponential increase in bandwidth demand was not predicted and copper or cable instead of optical fiber was deployed. Consequently, huge infrastructural investments have to be made in order to provide existing residential houses with a direct optical fiber connection. This is probably the biggest hurdle for FTTH to replace existing broadband services. However, the large demand for bandwidth and the fact that new residential districts are automatically equipped with optical fiber connections, will largely spur the acceleration of FTTH adoption.
The bandwidth provided by an optical fiber is huge. Typical record bitrates using the C and L band are in the order of Tb/s over thousands of kilometer. However, these kind of bitrates require very high cost optical transceivers and are only utilized in submarine or long-haul networks. For an access network such as a FTTH network, the cost of the optical transceivers is key and a suitable architec-

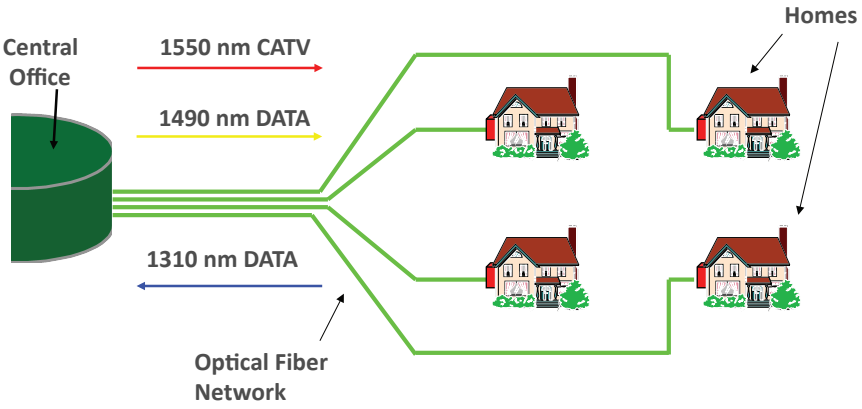

Figure 2.1: Optical wavelengths used in a Fiber-To-The-Home PTP triple-play network.

ture has to be chosen in order to meet this requirement. Long-haul networks operate in the C and L band for which the fiber optic loss is minimal. Access network operation wavelengths are more determined by the laser and transceiver cost. The most common FTTH system is a "triple play" system offering voice (telephone), video (TV) and data (internet access). This is shown in Fig. 2.1. To provide all three services over one fiber, signals are sent bidirectionally over a single fiber using two or three separate wavelengths of light. Three different protocols are in use today. Broadband PON (BPON), uses a third wavelength for Amplitude Modulation (AM) video, while Ethernet-based PON (EPON) and Gigabit PON (GPON) use digital Internet Protocol Television (IPTV) transmission. Digital signals from the CO to the home are sent at 1490 nm and 1550 nm. The 1490 nm signal carries both voice and data to the home. On BPON systems the video transmission signal uses the same technology as Cable Television (CATV), an analog modulated signal which is broadcasted separately at the 1550 nm wavelength. This signal is typically generated using a single laser and modulator for multiple customers. At the home an inexpensive 1310 nm laser (Fabry-Perot laser) is used to send upstream digital signals for voice and data back to the CO.

When deploying a FTTH network, the service provider will have to choose between two kind of network topologies, i.e. a passive optical network (PON) or point-to-point (PTP) network as shown in Fig. 2.2(a) and Fig. 2.2(b) respectively. I will focus on these two topologies, but note that variations on these network topologies exist. A PON network will passively split an optical fiber link among different users, typically 16 to 32. This has some clear advantages. First of all it needs less optical fiber being deployed between the CO and passive splitter. Furthermore, at the CO just one transceiver is needed for multiple users. However, the PON network has some key drawbacks with respect to a PTP network

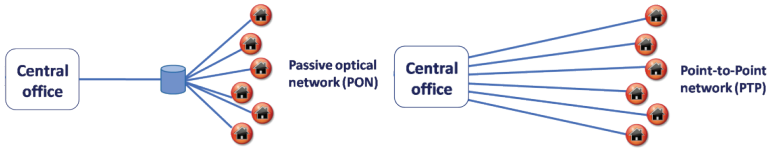

(a) PON (b) PTP

Figure 2.2: FTTH network topologies

where every customer has his dedicated fiber link to the CO. In a PON network the bandwidth is shared and for privacy concerns, the data is strongly encrypted which increases the complexity of the network. Furthermore, in practice, the number of customers which subscribe to a FTTH service is rarely reached.[2] This reduces the effective cost reduction a PON network theoretically offers. A PTP network on the other hand is a simple concept and uses the Ethernet standard. It is easy to upgrade and future proof. Every customer has a dedicated optical fiber to the CO and thus dedicated bandwidth. At the same time it is very secure [3].

2.2 Central office (CO) problem

For a PTP topology more fibers need to be deployed such that it is less backwards compatible with existing technologies such as copper cable. However, the inherent fiber cost is much lower than the deployment cost itself. This makes deploying a PTP network in a newly built residential area not significantly more expensive than deploying a PON network. The biggest cost difference between a PTP and PON network are the number of optical transceivers needed in the CO. For a PON network only one transceiver is needed for 2, 4, 8 and even 16 to 32 customers. For a PTP network every customer needs a dedicated transceiver. The problem in the CO that accompanies a PTP network is schematically illustrated in Fig. 2.3.

A conventional FTTH transceiver is typically packaged in an SFP, having dimensions of 5 cm × 1.5 cm × 1 cm (see Fig. 2.5). Taking the example of a CO providing PTP broadband service to 40000 homes, 40 19 inch racks are needed in the CO. This is really a huge amount of racks and comes with a high cost. Fig. 2.4 is an example of a 19 inch rack in a CO. CO space is typically very expensive and CO space and power reduction are key cost differentiators. This cost reduction is envisioned by packaging an array of 12 to 24 FTTH transceivers in a single SFP, thereby reducing the CO space, CO maintenance cost and CO power consumption. To accomplish this kind of footprint reduction, the traditional discrete

[2] In some parts of China a customer is obliged to subscribe to FTTH if it is available.

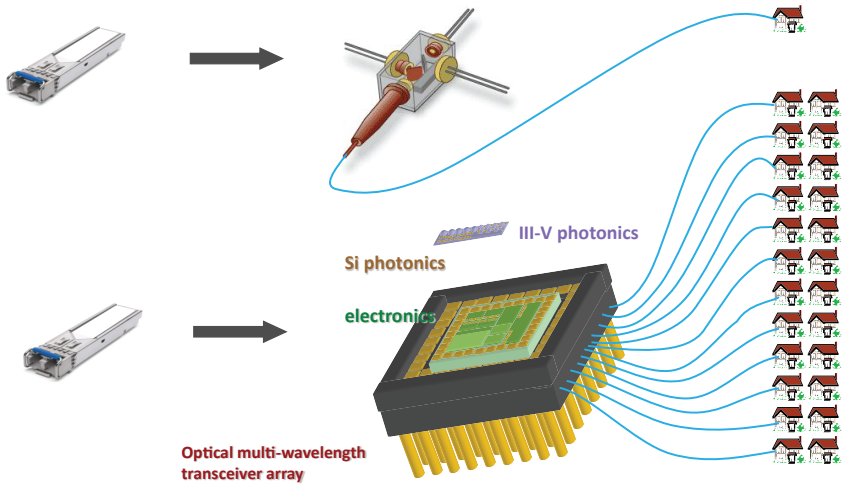

Figure 2.3: Optical integration enables multiple transceivers (12/24) in an SFP package.

optics used for 'triple play' transceivers are insufficient. The only viable solution is to integrate the optical components on board or chip level. This optical integration is the enabling and future proof technology for FTTH transceiver arrays.

2.3 Transceiver specifications

The transceiver specifications for this work were formulated in cooperation with Genexis, a trendsetting European company focused on the development, manufacturing and marketing of active equipment dedicated to FTTH networks [4]. The FTTH transceiver specifications are based on the IEEE 802.3ah 1000Base-BX10 standard. In Fig. 2.6 the optical transmitter and optical receiver specifications are listed. In Fig. 2.7 the mechanical and electrical specifications. 12 to 24 transceivers are the preferred number of transceivers to be integrated. The power consumption per transceiver channel should be less than 250 mW. Operating range is 0 °C to 70 °C at minimum and preferably −40 °C to 85 °C. The upstream wavelengths (from the CO point of view) are 1490 nm and 1550 nm and are treated equally. 1550 nm for CATV is not always used but should be multiplexed if needed with a flat top bandwidth of ±10 nm. 1490 nm on-off keying signals with a minimum extinction ratio (ER) of 6 dB should be transmitted with an average launch power of −9 dBm to −3 dBm. The required data rate for this first wave of FTTH PTP services is 1.25 Gb/s. Further specifications are made about the return losses and transmitter laser performance. The downstream wavelength is 1310 nm and

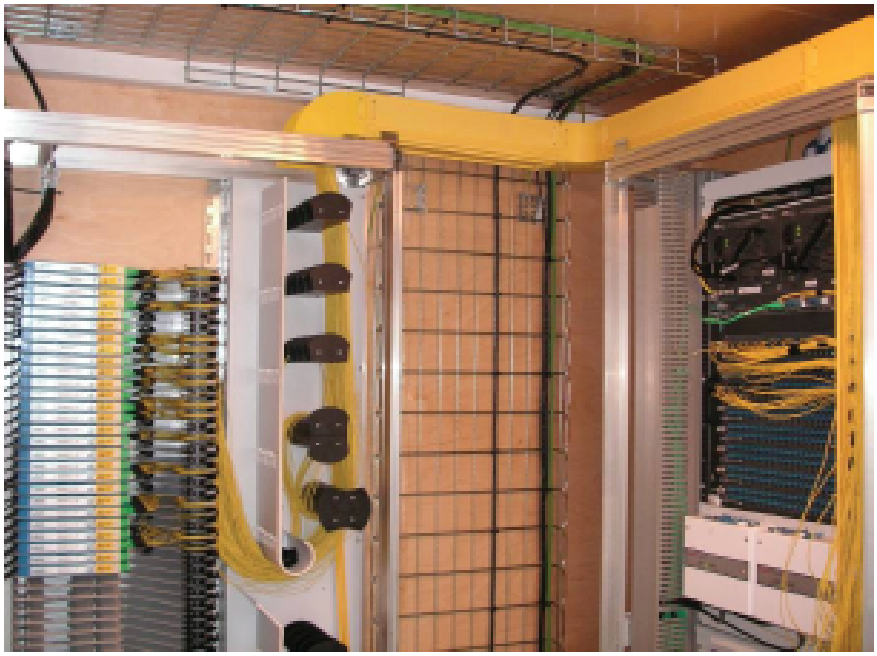

Figure 2.4: 19 inch *racks in a central office (CO).*

Figure 2.5: Picture of a Small-Form-Factor-Pluggable (SFP) transceiver. The dimensions are 5 cm × 1.5 cm × 1 cm

needs to be demultiplexed with a bandwidth of 100 nm to accommodate the wavelength shift of the uncooled FP laser from the customers transceiver. The sensitivity of the receiver needs to be better than −19.5 dBm and the 3 dB cutoff frequency 1.5 GHz. Further specifications are made about the jitter and return losses.
If we would measure the optical spectrum in the optical fiber at the CO it would look like the one in Fig. 2.8. For the downstream part there is a low power 1310 nm modulated signal with unknown polarization and having a wavelength which can range from 1260 nm till 1360 nm. The upstream band exists out of high power signals at 1490 nm and/or 1550 nm ranging from 1480 nm to 1500 nm and 1540 nm to 1560 nm respectively. The crosstalk specification between 1310 nm and 1490 nm for the receiver can be estimated by using the performance criterion for digital receivers, i.e. the bit-error rate (BER). If we see the crosstalk as an intensity fluctuation then the power penalty is $\delta = -10\log(1 - r^2 Q)$ with Q = 6 for a BER of 10^{-9} and r the ratio of the crosstalk and the receiver sensitivity which is −19.5 dBm. For a δ = 0.02 dB power penalty we need an r = 1% ratio, translating in a 33.5 dB crosstalk specification for our transceiver.

2.4 General FTTH transceiver array layout for Silicon Photonics

Nowadays discrete optical components are used such as thin film filters and discrete photodetectors and lasers in Transverse Optical (TO) packages. As an example we will have a closer look at the optical equipment needed for two customers. The schematic layout is shown in Fig. 2.9. Since discrete components are quite big, one SFP package can only contain a single transceiver. This means that going from one to two customers is accompanied by doubling the optical equipment, doubling the central office space and cost.
When we consider integrating the optical functionalities on a chip, we have the ability to increase the number of transceivers in a single SFP package. Rather than doubling the optical components in the package, certain components can be shared and will further decrease the cost. The schematic layout of an integrated 2-channel FTTH transceiver array is shown in Fig. 2.10. As explained in Chapter 1 we have chosen Silicon Photonics as integration platform. The layout which is specifically targeted for Silicon Photonics integration is shown in Fig. 2.11. The chip contains power splitters and modulators such that only one laser is needed per upstream wavelength. These power splitters and modulators are well-known and are off-the-shelf components. Also, Ge photodetectors can be integrated and detect 1310nm signals [5, 6]. Silicon does not have direct gain because of the indirect bandgap and hybrid integration of III/V lasers or gain

DESCRIPTION	VALUE
Optical Transmitter Specifications	
Average minimum launch power	-9 dBm
Average maximum launch power	-3 dBm
Average launch power of OFF transmitter	< -45 dBm
Extinction ratio	> 6 dB
Wavelength	1490 nm ± 20 nm
Spectrum width (RMS)	< 0.88 nm
Relative intensity noise (RIN)	< -113 dB / Hz
Data rate	1.25 Gbps
Optical return loss tolerance	< 12 dB
Transmitter reflectance	< -10 dB
Transmitter and dispersion penalty (TDP)	< 3.3 dB
Optical Receiver Specifications	
Average minimum receive power (Sensitivity)	-19.5 dBm
Average maximum receive power	-3 dBm
Wavelength	1310 ± 50 nm
Receiver reflectance	< -12 dB
Receive electrical 3dB upper cutoff frequency	< 1500 MHz
Signal detect threshold	> -45 dBm
Stressed eye jitter	> 0.3 UI pk-pk
Jitter corner frequency	637 kHz

Figure 2.6: FTTH optical transmitter and optical receiver specifications based on the IEEE 802.3ah 1000Base-BX10 standard.

DESCRIPTION	VALUE
Mechanical specifications	
Operating temperature (min.)	0 °C
Operating temperature (max.)	70 °C
Alternative temperature range	-40 to +85 °C
Optical connections	Preferable array connectors (e.g. MPO 12)
Array size	12, 24
Electrical specifications	
Power consumption (per transceiver path)	< 250 mW

Figure 2.7: Mechanical and electrical specifications for a FTTH transceiver array based on the IEEE 802.3ah 1000Base-BX10 standard.

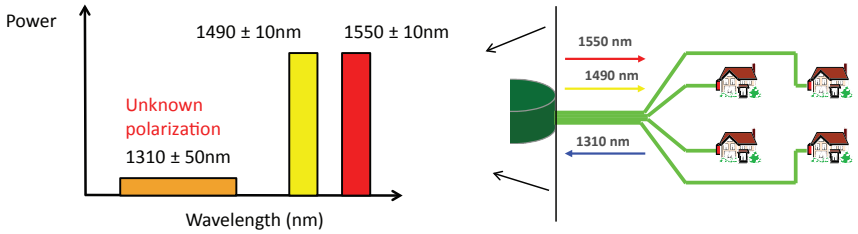

Figure 2.8: Optical spectrum for the optical fiber at the central office.

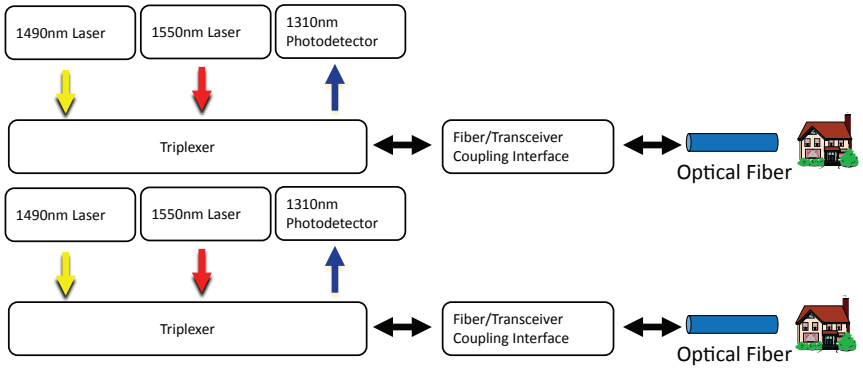

Figure 2.9: Optical equipment needed for two customers using discrete components and packaged in two separate SFP packages.

mediums is still in development [7–9]. Co-packaging, either by butt-coupling or vertical coupling, has proven to be a good solution in the short-term [10, 11] and is definitely a compact option for our application. The most straightforward solution is to use pig-tailed lasers. A fiber array is used to align multiple fibers at once with the coupling interfaces of the chip. A missing building block in our layout is the fiber-to-chip coupling interface. This interface needs to be low-loss for both wavelength bands around 1310 nm and 1520 nm in order to meet the FTTH transceiver specifications. Furthermore, it needs to be polarization independent for 1310 nm. Another building block challenge is the wavelength demultiplexer (triplexer) which has to split the 1310 nm, 1490 nm and 1550 nm signals with their respective wavelength bands and polarization independent for 1310 nm.

2.5 Grating couplers as fiber-to-chip interface for FTTH transceivers

2.5.1 Horizontal versus vertical coupling

The coupling interface is regarded as the most challenging problem for this application and will be addressed in much detail in the rest of this chapter. This interface needs to convert the large mode-size of the fiber ($\sim 100\,\mu m^2$) to the mode-size of the submicrometer silicon wire. There are two general strategies to make a mode-size convertor, i.e. horizontal or vertical coupling. Both methods can be implemented with different components. Besides fulfilling the required specifications, the full story of fiber-to-chip coupling also includes more practical considerations such as packaging and alignment convenience, yield and pre-

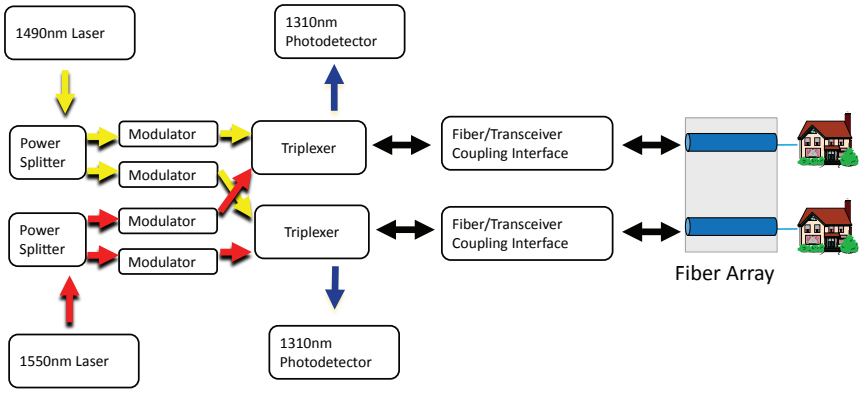

Figure 2.10: Integration scheme for 2-channel FTTH transceiver array using on-chip lasers, modulators and photodetectors.

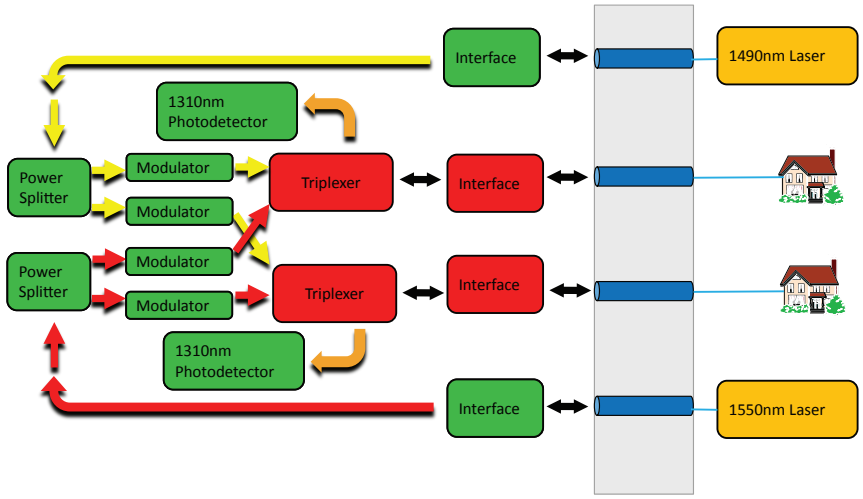

Figure 2.11: Integration scheme for 2-channel FTTH transceiver array using on-chip modulators and photodetectors. The lasers are external pigtailed lasers.

packaging testing possibilities. Horizontal coupling is the most commonly used method in optics. The benefit is that it is very straightforward to butt-couple a waveguide to a fiber and it is very broadband and efficient for both orthogonal polarizations. Inverted tapers [12–14] can easily convert the waveguide mode to a $3\,\mu m \times 3\,\mu m$ mode in silica such that coupling to lensed/tapered fibers can be very efficient. However, these custom fibers are more expensive and have small alignment tolerances. Moreover, the wafer has to be diced and semi-packaged before a chip can be tested.
Vertical spot-size conversion can be achieved by means of grating couplers [15, 16]. Although these devices are inherently wavelength and polarization dependent, they have the big advantage of being vertical optical ports such that wafer-scale testing is possible. This is the reason why test structures are typically measured using grating couplers. They can couple to regular optical fibers with a large $10\,\mu m$ core and thus have large alignment tolerances. Grating couplers are also planar structures and thus highly compatible with the planar CMOS process flow. Today grating coupler based fiber-to-chip coupling techniques are the most popular in the Silicon Photonics datacom market [17], despite their wavelength and polarization dependency. I will investigate if grating couplers can be used for our FTTH transceiver chip.

2.5.2 High-efficiency grating couplers

The first issue that needs to be addressed is the coupling efficiency. In order to meet the required power budget, the grating coupler efficiency needs to be increased considerably. *Imec*' standard passive platform (see Fig. 2.12) is a Silicon-on-Insulator (SOI) wafer with $2\,\mu m$ Buried Oxide (BOX) layer and 220 nm silicon waveguide core with a 220 nm deep etch and 70 nm shallow etch. The grating couplers which can be fabricated in this platform have a coupling efficiency of around −5 dB [16] and are perfect for research purposes or applications that can tolerate high coupling losses. For a FTTH transceiver this kind of coupling efficiency is not sufficient. A back-of-the-envelope calculation, assuming a laser power of 13 dBm and modulator loss of 6 dB, learns us that we need 2 dB coupling loss to target a −6 dBm output power for an 8-channel transceiver array. According to the same power budget calculation a 5 dB coupling loss would only allow a 2-channel transceiver array. The number of transceiver channels can be scaled to 16 or 32 by increasing the number of lasers or by implementing an amplifier. However, this will be difficult to fit in a single SFP package and will also increase the power consumption. Note that the coupling loss is experienced twice, once for the external laser input and once for the optical output. Decreasing the overall losses and especially coupling losses is key to increase the number of transceiver channels while maintaining the same package and low

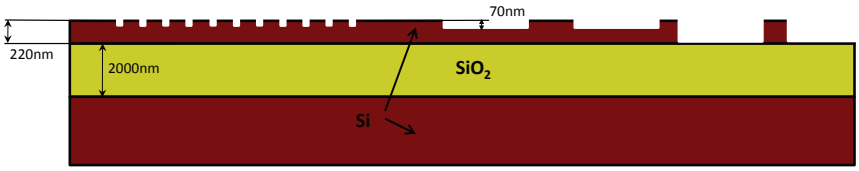

Figure 2.12: Imec' passive platform. A Silicon-on-Insulator (SOI) wafer with 2 µm *Buried Oxide (BOX) layer and* 220 nm *silicon waveguide core with a* 220 nm *deep etch and* 70 nm *shallow etch.*

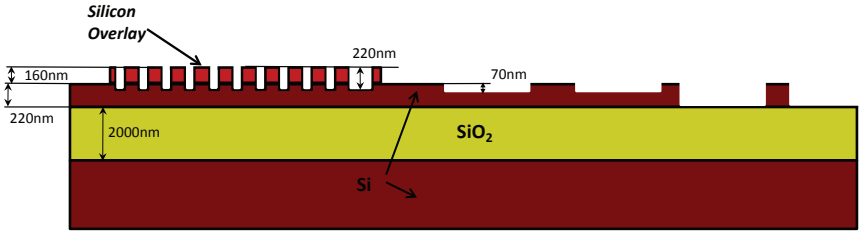

Figure 2.13: Imec's advanced passive platform. A Silicon-on-Insulator (SOI) wafer with 2 µm *BOX layer and* 220 nm *silicon waveguide core and* 160 nm *amorphous/poly-Si overlay layer. Different etch depths of* 230 nm, 70 nm *and* 220 nm *can be used.*

power consumption. Furthermore, the more relaxed the optical power budget is, the more low-cost components or low-cost packaging techniques can be used, thereby decreasing the overall transceiver cost. Such components/techniques could be: a higher optical loss MPO connector, a fiber array with a less accurate fiber pitch, passive alignment of the fiber array or optical fibers, tighter bending of the fibers, ...

In order to increase the grating coupler efficiency, we have developed a more advanced passives platform (see Fig. 2.13) together with *imec* which incorporates the integration of high efficiency grating couplers. A state-of-the art overview, grating coupler principle, fabrication details and characterization can be found in [18]. This paper has also been attached at the end of this chapter (see page 2-41). It is one of the key publications in this thesis. I have shown experimentally a coupling efficiency of −1.6 dB which is among the highest reported fiber coupling efficiency for grating couplers fabricated in a CMOS pilot line. An example spectrum of a grating coupler is shown in Fig. 2.14(a). The grating coupler uses an amorphous silicon overlay in the advanced *imec* passives platform to increase the directionality of grating to 90%. The optimal duty cycle of the grating is found to be 35% (see Fig. 2.14(b)).

A low directionality, i.e. the fraction of the light that is diffracted upwards, of

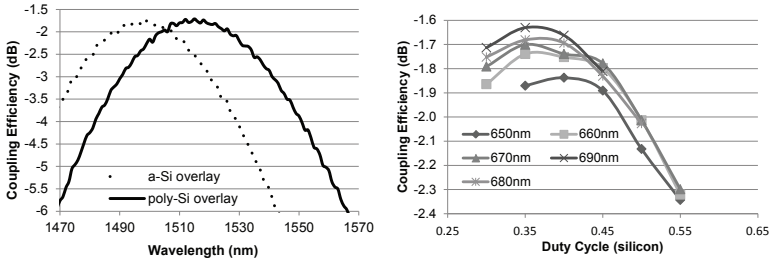

(a) (b)

Figure 2.14: The spectrum (a) of grating couplers using a Silicon overlay spectrum. The top efficiency as a function of the duty cycle for different grating periods (b).

around 50% is the biggest contributor to the high loss of regular grating couplers in the standard passives platform. Theoretically one could achieve a coupling efficiency of 80% for a uniform grating coupler if the directionality is increased to 100%. In Fig. 2.15 an overview is given for the different methods to increase the directionality of a grating coupler. The grating coupler using a silicon overlay is shown in Fig. 2.15(b). Other techniques such as using a gold bottom mirror [19] or bottom Distributed Bragg Reflector (DBR) [16, 20] have also been demonstrated. However, in order to achieve a gold bottom mirror the process flow needs be adjusted very drastically. For a DBR bottom mirror special wafers by means of molecular bonding have to be used or fabricated by a Si/SiO_2 layer stack deposition in combination with an a-Si (amorphous Silicon) waveguide layer.

In context of this work, an a-Si DBR bottom has been explored. The fabrication and measurement results can be found in [21]. I optimized the coupling structure using a rigorous 2D eigenmode solver in combination with a particle swarm optimization algorithm for a silicon waveguide core thickness of 220 nm. The field profile of the optimal design simulated with a 2D FDTD solver is shown in Fig. 2.16. The period of the grating is 630 nm with a duty cycle of 50% and the etch depth is 70 nm. The number of grating periods is 25. If the thickness of the SiO_2 buffer layer is 1.44 μm, the Bragg mirror will reflect the light constructively. The fiber is tilted under an angle of 10° to avoid a large second order reflection. For this angle the optimal waveguide width of the grating is 15 μm. The refractive index of the surrounding medium is 1.45, which corresponds to SiO_2 or Index Matching Fluid (IMF). Theoretically the coupling efficiency is 82% for TE polarized light at 1550 nm.

The grating fiber couplers with bottom mirrors were fabricated on a 200 mm Si wafer. First a 1 μm SiO_2 isolation layer is deposited on a bare Si wafer. Then the Bragg mirror, consisting of two 112 nm layers of a-Si and a 267 nm layer of SiO_2

are deposited. On top of the Bragg mirror a 1.48 μm of buffer SiO_2 and a silicon layer of 205 nm, were deposited. A Scanning Electron Microscope (SEM) picture is shown in Fig. 2.17. The grating couplers and waveguides were fabricated using 193 nm optical lithography and dry etching. The coupling efficiency is characterized with a fiber-to-fiber measurement. The test structures consist of identical input and output grating couplers connected by a waveguide. Fiber-to-fiber transmission is measured by launching light into the input coupler from a SMF connected to a Super-Luminescent Emitting Diode (SLED) and the light from the output coupler is captured by another SMF connected to a spectrum analyzer. Both fibers were positioned at an angle of 10° to the sample normal and IMF was applied between the optical fiber facet and the fiber coupler to avoid reflections at the fiber facets. The measured coupling efficiency is 69.5% for a single grating coupler with a 1 dB-bandwidth of 36 nm and a 3 dB-bandwidth of 63 nm. The simulated efficiency for the fabricated device is 76%. The non-optimal waveguide width of 10 μm explains 5% difference in coupling efficiency between measurement and simulation.

2.5.3 1310nm/1550nm grating duplexer

A 1-dimensional grating coupler is typically optimized to couple one wavelength band into a broad waveguide. To avoid second order reflection, the fiber is tilted under an angle with respect to the surface normal. For our FTTH application, we need to couple in two wavelength bands with central wavelengths at 1310 nm and 1520 nm (center of 1490 nm and 1550 nm). To this purpose we have developed a new kind of 1-dimensional grating coupler which couples a first wavelength band around 1310 nm forwards, and a second wavelength band around 1520 nm backwards. This is what we call a grating duplexer because it inherently couples and splits two wavelength bands. The principle is shown in Fig. 2.18 and the results are presented in [24] which can be found at the end of this chapter (see page 2-47). The measured coupling efficiencies of the central wavelengths are −6 dB for 1300 nm and −4 dB for 1520 nm. At the communication wavelengths 1310 nm, 1490 nm and 1550 nm the coupling efficiencies are respectively −7 dB, −6 dB and −8 dB. Further simulations show that the coupling efficiencies of the central wavelengths can be increased to −2 dB by increasing the grating directionality with a silicon overlay or bottom mirror.

2.5.4 Two-dimensional polarization splitting grating duplexer

The grating duplexer addresses the problem of coupling in two wavelength bands at the same time. However, this coupling is polarization dependent due to the birefringence of the high index contrast silicon/oxide waveguides. Coupling in both orthogonal polarizations can be done with 2-dimensional grating couplers

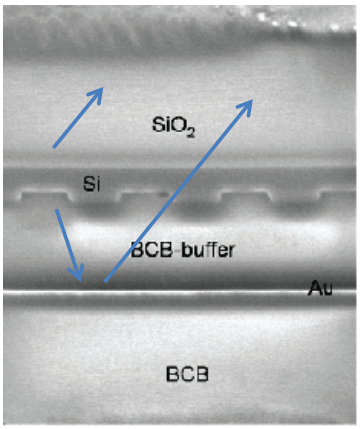

(a) gold bottom mirror [22]

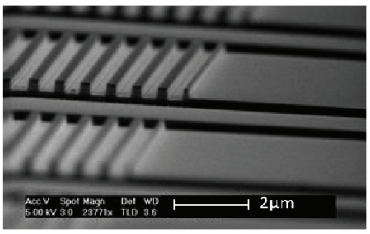

(b) silicon overlay [23]

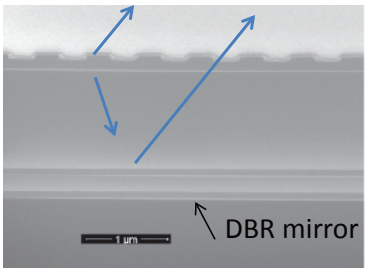

(c) DBR bottom mirror [21]

Figure 2.15: SEM images of highly directional grating couplers

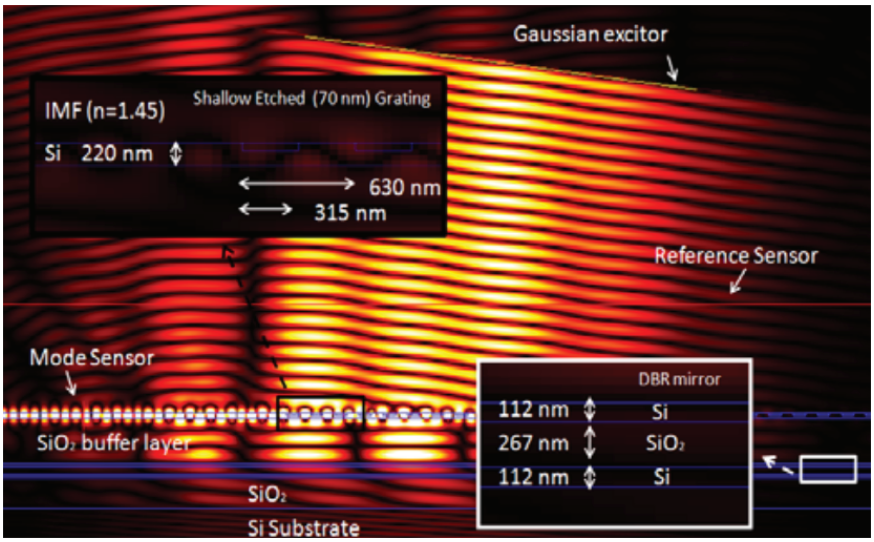

Figure 2.16: Simulated field profile of grating coupler with Bragg bottom mirror.

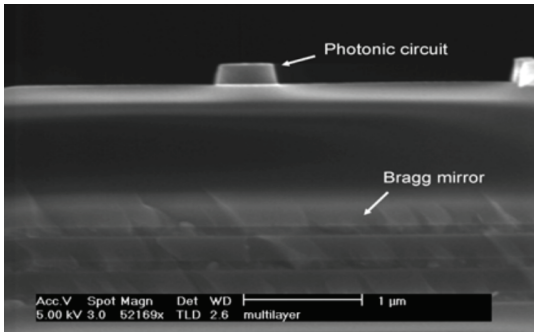

Figure 2.17: Cross-section SEM image of the fabricated grating coupler with DBR bottom mirror.

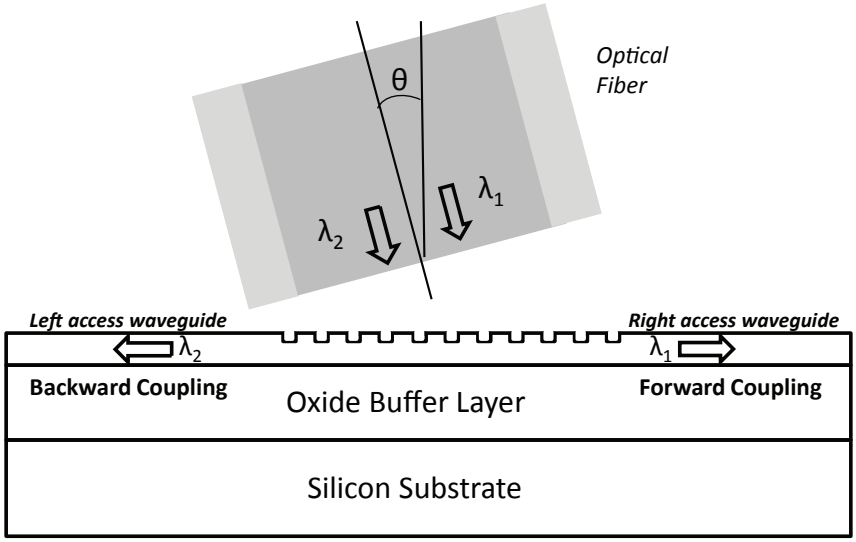

Figure 2.18: Working principle of grating duplexer.

[25, 26]. Similarly I investigated a 2-dimensional grating duplexer, as shown in Fig. 1(a) of [27] (attached at the end of this chapter on page 2-49). However, the coupling efficiency of these grating couplers was quite low (around −7 dB at the central wavelengths). Furthermore, the Polarization Dependent Loss (PDL) was very high since the fiber needs to be tilted under an angle of about 15°. But the biggest problem with these 2D grating couplers is the low 1 dB/3 dB-bandwidth of 25 nm/50 nm. This bandwidth is insufficient to couple in the 1310 nm FTTH wavelength band. An in-depth investigation of the bandwidth can be found in [28]. It is proven that the bandwidth of a grating coupler is inverseley proportional to the effective refractive index of the grating. Increasing the bandwidth of a grating coupler can thus be done by using a lower index grating material such as SiN.

2.5.5 TM tapers

A 2-dimensional grating coupler will couple in both orthogonal polarizations in near-perpendicular waveguides. In both waveguides the fundamental TE mode is excited. Due to the birefringence of the waveguide (n_{eff}(TE) ≠ n_{eff}(TM)), the TM mode is not excited. We also designed a grating coupler for coupling to the TM mode. In theory and according to the Bragg condition, this is perfectly possible. However, in some cases the TM grating coupler didn't seem to work. We solved this problem and the physical interpretation is explained in [29], attached

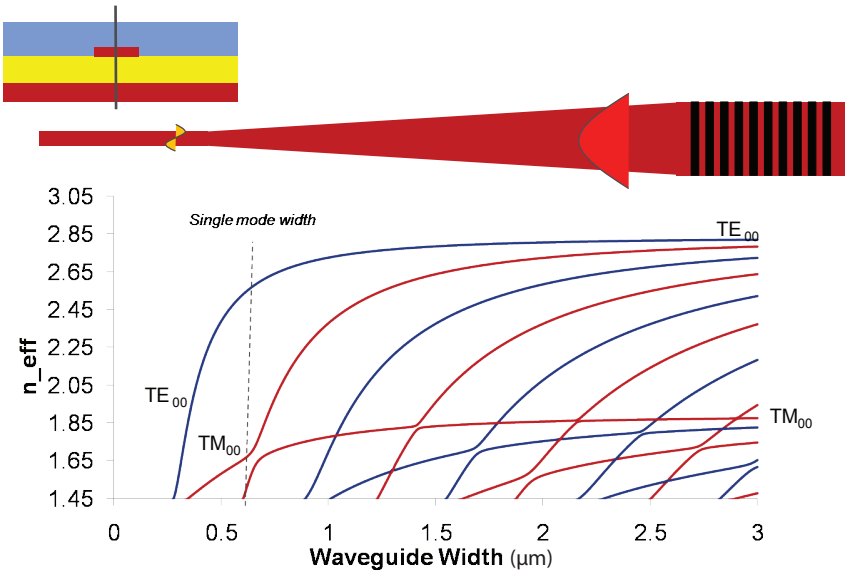

Figure 2.19: Effective refractive index of the waveguide modes as a function of the waveguide width. The fundamental TM mode couples to higher order TE modes when the waveguide width is decreased. (blue lines = even modes, red lines = odd modes)

at the end of this chapter page 2-59. It was found that the taper from a broad multi-mode waveguide to a single-mode waveguide was to blame. Depending on the cladding symmetry of the taper, the fundamental TM mode will be coupled to itself (symmetric cladding) or to higher order TE modes (asymmetric cladding). This mode coupling in the asymmetric case can be derived from Fig. 2.19 where the effective refractive index of the modes is plotted as a function of the waveguide width. Using a curved grating coupler which focuses the light instead of tapering it, a 13% fiber-to-chip coupling efficiency could be achieved for the TM polarization and for an asymmetric cladding.

2.5.6 Polarization splitting 1-dimensional grating coupler/duplexer

I explored the possibility to use a single 1D grating coupler to couple in both orthogonal polarizations. This led to a grating coupler which couples in the TE polarization in the forward direction and the TM polarization in the backward direction, exciting their corresponding waveguide mode. This approach was unique and we have patented this grating coupler which couples in both TE and TM polarization simultaneously [30]. I envision this to be an important coupling structure in future integrated transceivers. In [27] I presented the

experimental data of a first generation of these grating couplers. A detailed analysis can be found in an unpublished paper at the end of this chapter on page 2-49. The presented grating coupler is a combination of a 1D polarization splitting grating coupler and grating duplexer, thus coupling in both polarizations in opposite directions at 1300 nm while at the same time coupling in 1520 nm TE polarized light in the backward direction. We reported an insertion loss of −6 dB for 1300 nm and −6 dB for 1520 nm. The measured fiber-to-fiber PDL ranges between 0.4 dB and 1.8 dB within a bandwidth of 100 nm around 1300 nm. These efficiencies can be increased by increasing the directionality using for example a silicon overlay as discussed earlier. However, the FTTH specifications are very strict and the 100 nm bandwidth around 1310 nm is not fulfilled. I conclude that it is almost surely impossible to couple in all three FTTH wavelength bands using grating couplers while fulfilling all IEEE FTTH specifications.

2.6 Silicon photonics FTTH transceiver using a transparent photodetector

As discussed in the previous section, in order to design a transceiver which couples to a fiber vertically or near-vertically, we have to come up with a new concept to tackle the coupling problem. In this section I investigate the possibility to use a III/V transparent photodetector which has a high responsivity for the 1310 nm band and which is transparent for 1490 nm and 1550 nm.

2.6.1 Transparent photodetector

The first step to design a transparent photodetector is to choose an appropriate absorption layer. This layer needs to detect the 1310 nm band, i.e. 1260 nm till 1360 nm, but needs to be optically transparent for 1480 nm and higher wavelengths. Furthermore, the responsivity at these higher wavelengths needs to be sufficiently small such that the responsivity difference (which I will refer to as crosstalk) is better than 42 dB as was calculated from the transceiver specifications in Section 2.3. In order to get a low crosstalk we need a material with a well-defined bandgap. In Fig. 2.20 the absorption spectra of some candidate materials are plotted. The quaternary material InGaAsP seems to be the perfect as the absorption spectrum rolls of very quickly and the bandgap can be chosen to be 1370 nm.

In Fig. 2.21 the cross section of the transparent photodetector is schematically shown. The photodetector is a pin photodetector with top and bottom layers p and n doped InP respectively and with a Q1.37 InGaAsP layer in the middle. Each individual layer is transparent for wavelengths higher than 1370 nm,

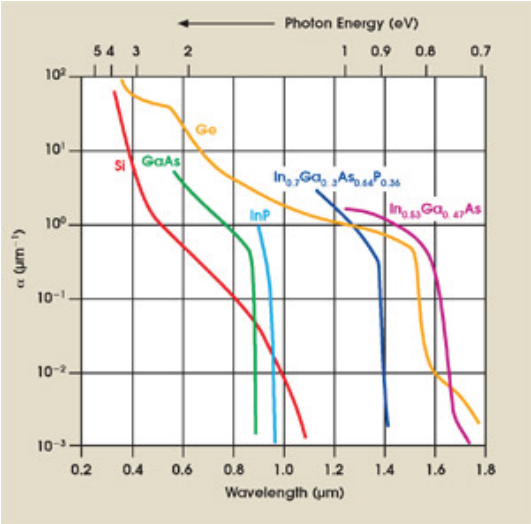

Figure 2.20: Absorption spectra of different materials.

but in order to make the whole photodetector transparent, the layer thicknesses have to be optimized to minimize losses due to reflection. The cross section of a possible circuit using a transparent photodetector is shown in Fig. 2.22. A transparent photodetector is heterogeneously integrated on a Silicon Photonics circuit which uses grating couplers for fiber-to-chip coupling. The photodetector is positioned on top of the grating coupler and under the optical fiber such that 1310 nm light from the fiber gets detected in the photodetector and 1490 nm and 1550 nm light can be coupled out of the chip using the grating coupler and into fiber while passing the transparent photodetector. In the attached paper [31] (see page 2-61) the fabrication details and measurement results of such a circuit are described. The transparent photodetector is integrated 1 μm above a grating coupler using heterogeneous III/V integration by means of Benzocyclobutene (BCB) bonding. The bonding thickness is not crucial and can be in the order of microns. This makes the heterogeneous BCB bonding, which is one of the most crucial process steps, potentially very high yield. I was able to demonstrate the basic properties of this transparent photodetector proof-of-principle. The absorption region thickness determines the trade-off between 1310 nm responsivity and 1490 nm/1550 nm crosstalk. The measured responsivity was 0.4 A/W and the crosstalk 32 dB and 42 dB for 1490 nm and 1550 nm respectively. The PDL was smaller than 0.5 dB over the whole 1310 nm bandwidth. A penalty of around 1 dB was observed for the grating coupling with transparent photodetector on top. These results show the feasibility of the transparent photodetector concept and are an important result of this work.

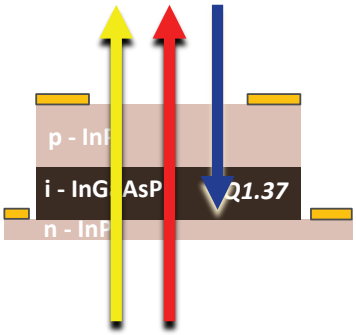

Figure 2.21: Cross section of the transparent photodetector. The InP layers and quaternary layer thicknesses are optimized for transparency of the upstream wavelengths 1490 nm *and* 1550 nm.

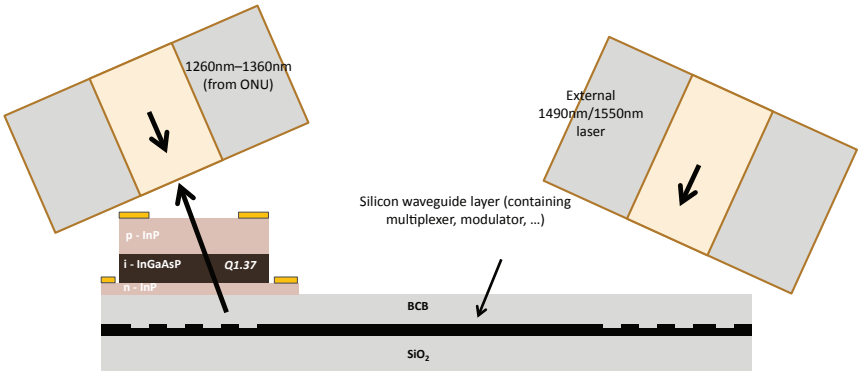

Figure 2.22: Silicon photonics circuit with integrated transparent photodector on a grating coupler.

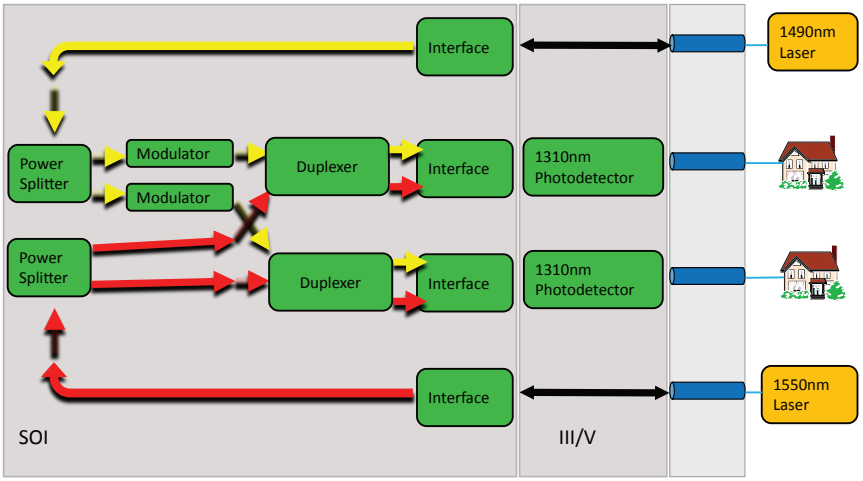

Figure 2.23: 2-channel FTTH transceiver layout using transparent photodetectors to detect the 1310 nm *downstream band.*

2.6.2 Transceiver array layout

The transparent photodetector solves our coupling problem to the chip. Instead of coupling in all three FTTH wavelengths into waveguides and detecting the 1310 nm band using waveguide Ge photodetectors, we can now use these vertical incident III/V transparent photodetectors to detect the 1310 nm band prior to coupling in to the chip. This simplifies our coupling section to the chip dramatically as only one wavelength band around 1520 nm (1480 nm to 1560 nm) needs to be coupled in and out.[3] Furthermore, the coupling can be polarization dependent. 1-dimensional high-efficiency grating couplers described earlier in Section 2.5.2 are perfect candidates for such a coupling section. The wavelength dependence of these grating couplers acts a filter for 1310 nm light that is not absorbed in the transparent photodetector. The triplexers in our previous layout in Fig. 2.11 can now be replaced with diplexers to multiplex the upstream wavelengths 1490 nm and 1550 nm.

2.6.3 1490nm/1550nm Planar Concave Grating (PCG) (de)multiplexer

The multiplexing of 1490 nm and 1550 nm can be easily performed using a planar concave grating (PCG) demultiplexer [32–34]. This multiplexer is based on an on-chip reflector grating in a slab region. It is very similar to free space grating demultiplexers with the main difference that it uses a birefringent planar slab

[3] In future transceivers only the DATA upstream wavelength 1490 nm is necessary.

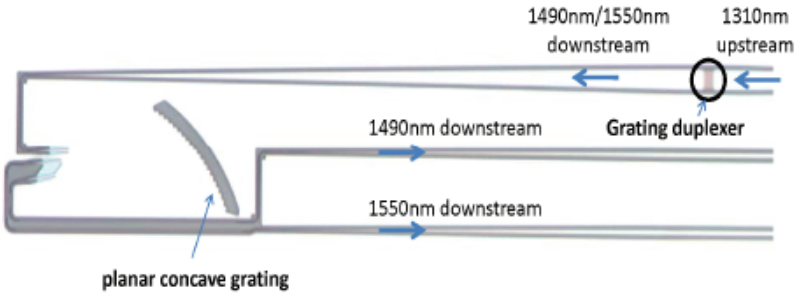

Figure 2.24: Microscope image of a grating duplexer in combination with a Planar Concave Grating (PCG) demultiplexer splitting 1490 nm *and* 1550 nm.

region instead of a free space region. The demultiplexer is thus polarization dependent and sensitive to slab height variations. Luckily, for our purposes the PCG multiplexer can be made very compact due the large required Free Spectral Range (FSR) of 60 nm. A 1490 nm/1550 nm PCG demultiplexer has been published in [24] (see Fig. 2.24 and page 2-47), achieving −5.4 dB insertion loss (IL) for 1485 nm and −7.6 dB for 1542 nm. This IL was limited by the Fresnel reflection at the Silicon/Air interface of the PCG. The crosstalk at these maxima was very high and about 30 dB and 40 dB respectively.
The PCG demultiplexer was improved by including small DBR reflectors at the facets of the PCG [33]. This boosts the facet reflectivity from 30% to 90% (see Fig. 2.25). The measured channel spectra are shown in Fig. 2.26. The IL was −0.97 dB for 1490 nm and −1.81 dB for 1550 nm. The difference in IL is mainly attributed to the higher reflectivity of the DBR's at lower wavelengths. The large FSR of this PCG demultiplexer makes it very compact and less dependent on process variations such as height variations of the Si core slab. The measured crosstalk was better than 30 dB which is close to the desired crosstalk levels.

2.6.4 4-channel FTTH CO transceiver array demonstrator

A proof-of-principle 4-channel transceiver array was developed in cooperation with Genexis, Caliopa and the Technical university of Eindhoven in the framework of the Dutch Smartmix-Memphis project. The general layout of the silicon chip is shown in Fig. 2.27 [31] (see page 2-61). An 8-channel fiber array is used to align 8 fibers to the chip simultaneously. The fiber array is actively aligned using an alignment loop between the two outer fibers. The remaining 6 fibers comprise the 4 channels and two inputs for 1490 nm Continuous Wave (CW) and 1550 nm which can be CW or amplitude modulated for CATV. These wavelengths

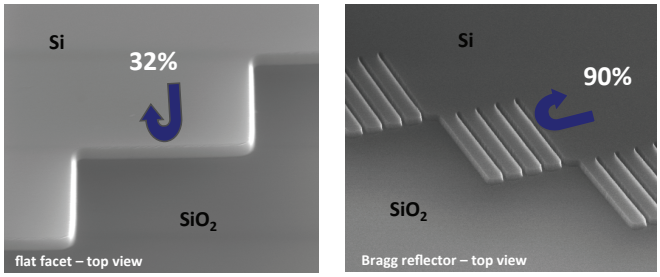

Figure 2.25: Planar concave grating reflectors with flat facet (left) and DBR facets (right). (Courtasy of Joost Brouckaert [33])

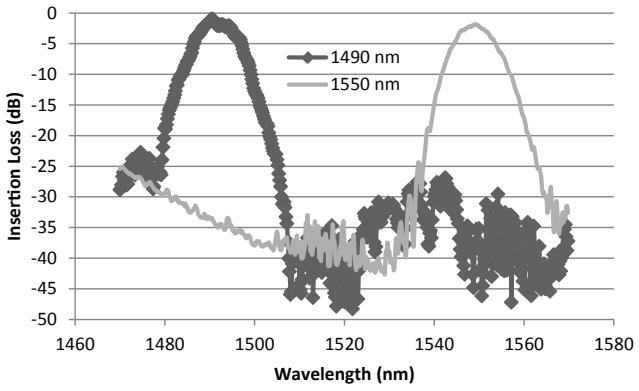

Figure 2.26: 2-channel PCG demultiplexer insertion loss spectra.

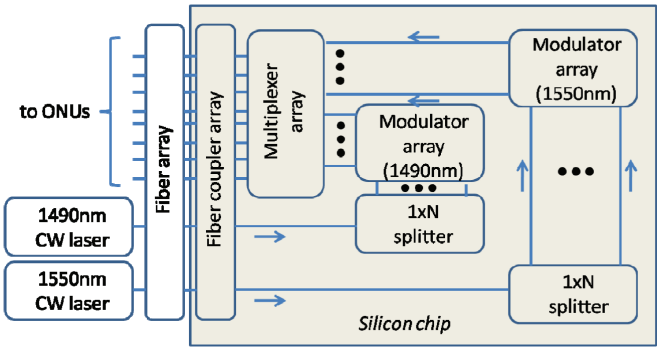

Figure 2.27: Silicon chip configuration for the integrated transceiver arrays for FTTH CO equipment.

are then divided among the 4 channels using a tree of 1x2 and 2x2 on-chip MMI power splitters [34]. This 1x4 splitting tree uses a 2x2 MMI as a first component such that two inputs can be chosen. The alternative input was connected to a 1D grating coupler, designed such that a near-vertical emitting 1490 nm Distributed Feedback (DFB) laser can be actively aligned and co-packaged with the Silicon Photonics chip (see Fig. 2.28). After the splitting tree, the 1490 nm light is amplitude modulated using Mach-Zehnder Interferometers (MZI's) in combination with single-ended lateral pn junction carrier depletion phase modulators [35–37]. Silicon phase modulation is based on the plasma dispersion effect. By modulating the free carrier density either by depleting or injecting carriers, the optical refractive index of silicon is changed. In our demonstrator two out of four channels used 3 mm long carrier depletion phase modulators in an unbalanced MZI configuration. The remaining channels used 5 mm long carrier depletion phase modulators in a balanced MZI configuration. The 1550 nm light is split in two using a 1x2 MMI and multiplexed with the 1490 nm light of 2 channels by means of the PCG duplexer with grating DBR's as discussed in section 2.6.3. The modulator contact pads and photodetector contact pads to connect to the Transimpedance Amplifiers (TIA) chip were placed on opposite sides of the chip to allow for easy wirebonding. The inter-modulator electrical crosstalk was neglected as the spacing was determined by the available mask space, limiting it to 80 μm which should be sufficient for 1.25 Gb/s applications. In order to minimize optical crosstalk and optical loss the layout of the chip was optimized such that a amount of crossings necessary was reduced to two. The details of the crossing design can be found in [38] and is based on a double patterned waveguide crossing exhibiting a crossing loss less than 0.5 dB and a -40 dB crosstalk. All routings were performed with single-mode waveguides (typical 2 dB/cm loss) and 5 μm waveguide bends. Typical routing length is about 1 cm translating in a 2 dB routing loss penalty. This loss can be decreased to 0.5 dB by using low-loss multimode waveguides or low-loss rib waveguides [39].

A colour picture of the fabricated Silicon Photonics chip is shown in Fig. 2.29. The grating coupler array to couple to the 8-channel fiber array is clearly visible and numbered. The chip is illuminated under angle and visible wavelengths are diffracted at the gratings into the camera. The colour is dependent on the pitch of the gratings. The two outer red grating couplers and grating coupler number 3 are optimized for 1550 nm coupling. Grating coupler number 2 in green is optimized for the coupling of 1490 nm light. Grating couplers number 4 till 7 are optimized for 1520 nm coupling, exactly in between 1490 nm and 1550 nm.

The demonstrator is designed for transparent photodetector integration as explained in section 2.6.1 by means of III/V heterogeneous integration. Furthermore, the Al contact pads were arranged such that the demonstrator is also suited for flip chipping of pre-processed III/V transparent photodetectors. I pursued

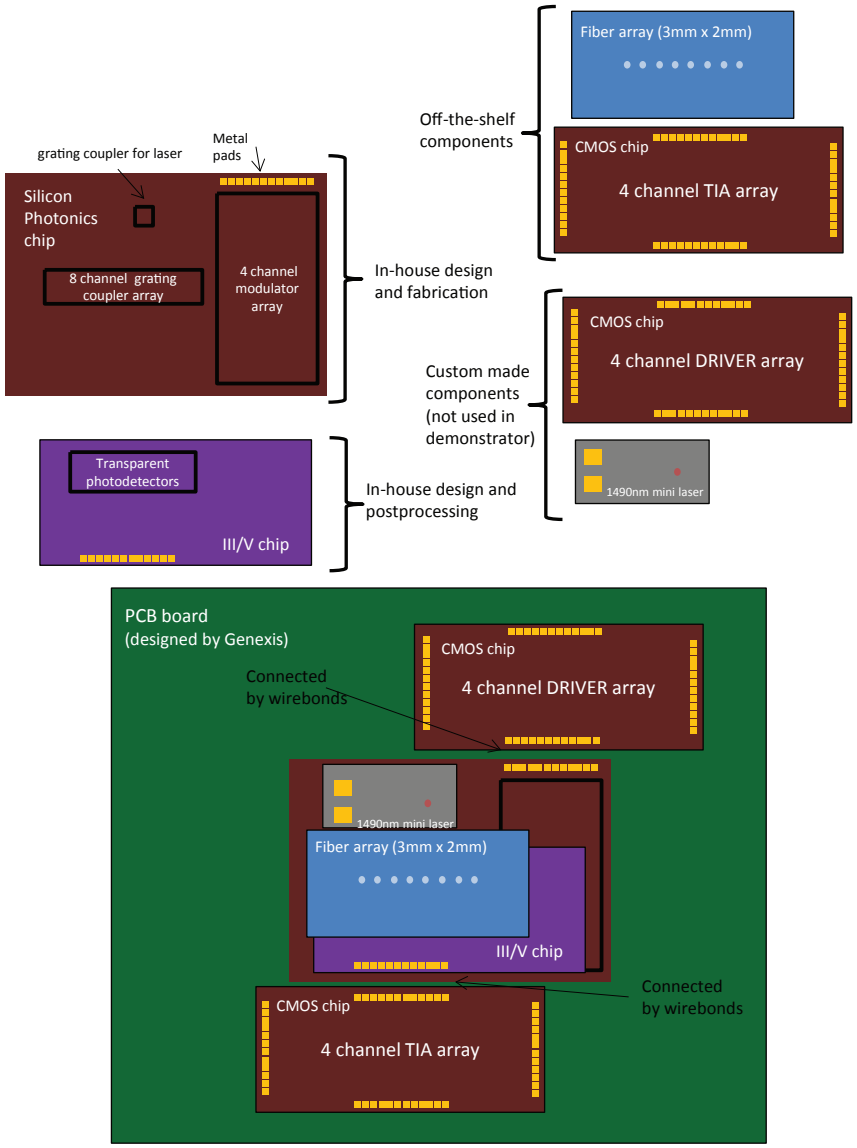

Figure 2.28: General layout of the 4-channel FTTH transceiver array demonstrator. A III/V chip and mini laser are attached to the Silicon Photonics chip using an epoxy. This chip is mounted on a pcb board wirebonded to a driver and TIA chip. An 8-channel fiber array is actively aligned and attached to the chip.

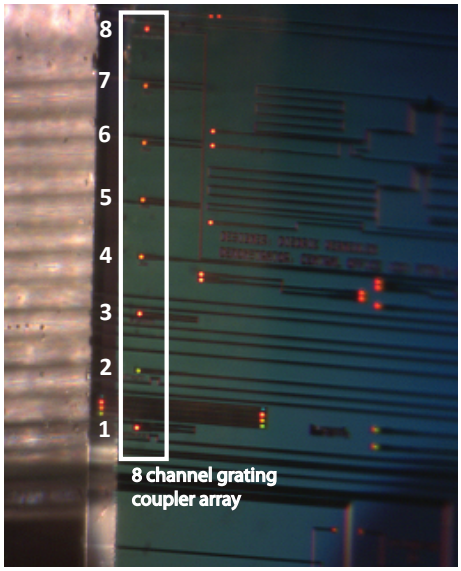

Figure 2.29: Picture of the Silicon Photonics chip for the 4-channel FTTH transceiver array demonstrator. The chip was illuminated under an angle.

both integration schemes. Using pre-processed III/V photodetectors has the advantage of using a commercially proven technology and thus being able to obtain high yield. However, in order to minimize the coupling loss of 1490 nm and 1550 nm due to diffraction between the fiber and the grating coupler, the thickness of the pre-processed photodetector has to be kept to a minimum. These discrete transparent photodetectors were developed by a third party in accordance with [31] (see page 2-61). The detectors were thinned down to 80 μm which corresponds to a 1 dB penalty in coupling efficiency for the upstream wavelengths due to diffraction in the photodetector.
The fabricated silicon photonics wafers with Al metallization for flip-chip integration showed extremely high waveguide loss of 30 dB/cm. Consequently, the flip-chip integration was ruled out. The wafer without Al pads, but with Cu pads and SiC flash passivation showed better performance. Especially at the edge of the wafer some relatively low loss dies were found by means of wafer-scale automated testing, see Fig. 2.30. Around 10 dies with a workable waveguide loss of 6 – 8 dB/cm were extracted from the quarter wafer. This waveguide loss is still too high for a product but enough for a proof-of-principle demonstrator.

In order to integrate the discrete transparent photodetector array without the need of flipchipping, I developed a rapid prototyping integration method by means of SU8 chip-to-chip local attachment. Before integration, the III/V dies with transparent photodetectors are post-processed. I processed metal tracks

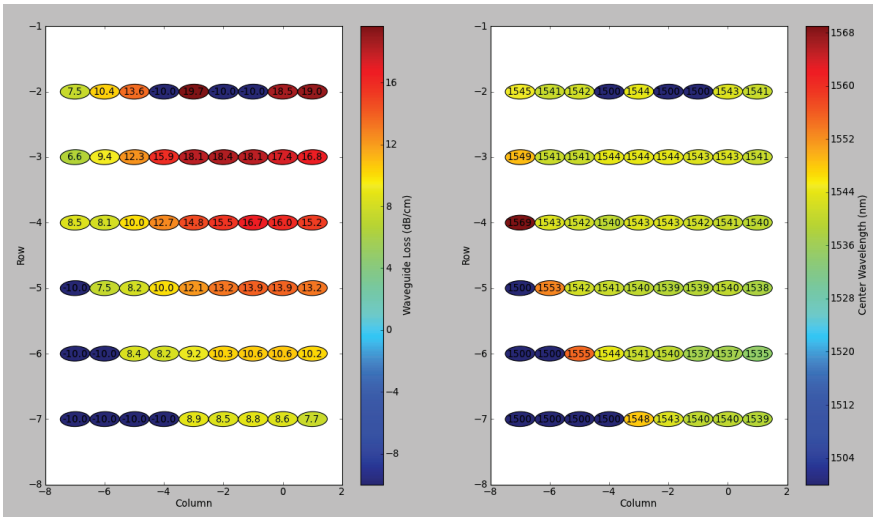

Figure 2.30: Wafer-scale automated testing of quarter wafer. The waveguide loss of a single-mode waveguide and central wavelength of standard test grating couplers are plotted as a function of the row and column number.

using an insulating layer of BCB and Au to route the signals from under the fiber array which will be attached in the final stage of the demonstrator assembly. The photodetector array with metal tracks is shown in Fig. 2.31. After dicing the III/V chips, they are attached with SU8-2 epoxy to the silicon chip using a Finetech flipchip machine with micron alignment accuracy. This is shown in Fig. 2.32. Care was taken such that the SU8 was only applied locally and that the contact pads of the modulators were not covered which would prevent wirebonding.

A couple of demonstrators were placed on a PCB board as can be seen in Fig. 2.33(a). The photodetectors were wirebonded to a 4-channel TIA array supporting speeds up to 3 Gb/s. The TIA's are then routed differentially to SMA connectors at the end of the PCB board. In Fig. 2.33(b) the wirebonds from the photodetector array to the TIA array are shown. The modulator drivers were not integrated in order to have large flexibility for characterization. They were connected to microstrip lines ending in SMA connectors.

A standard low-cost 8-channel fiber array polished under an angle of 8° was attached to the chip using UV-curable epoxy. This is shown in Fig. 2.34. The demonstrator was then packaged in a 3D printed package which allowed for easy characterization and transportation (see Fig. 2.35(a)). The demonstrator was characterized at TUe in cooperation with Genexis. The eye diagrams of the modulator at 1.25 Gb/s and 2.5 Gb/s are shown in Fig. 2.36(a) and 2.36(b) for a Pseudo-Random Binary Sequence (PRBS) of $2^{31} - 1$ and at 1510 nm optical

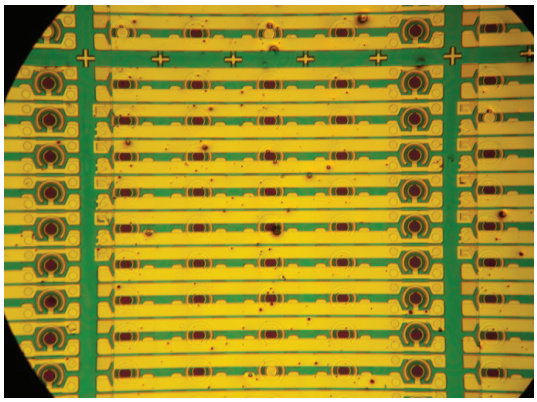

Figure 2.31: III/V transparent photodetector array with metal track routings.

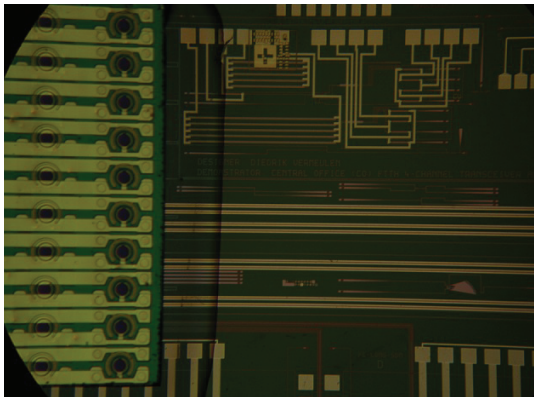

Figure 2.32: Picture of silicon chip demonstrator with SU8 epoxy attached III/V transparent photodetector array.

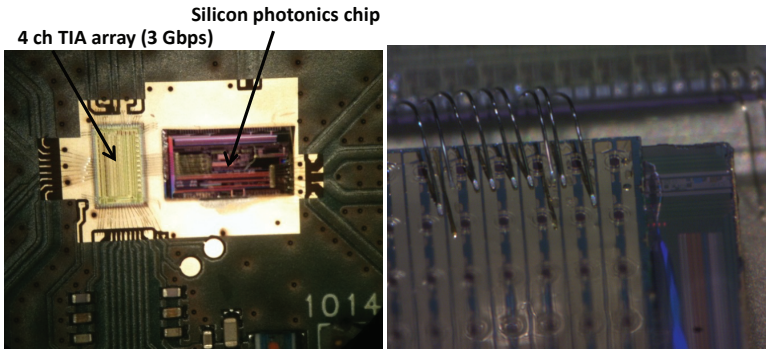

(a) SOI chip wirebonded to a PCB board and a 4-channel 3 Gb/s TIA array.

(b) Zoom-in picture of wirebonds from the metal tracks of the III/V photodetectors integrated on the SOI chip to the contact pads on a TIA array.

Figure 2.33: 4*-channel FTTH transceiver array demonstrator with PCB board.*

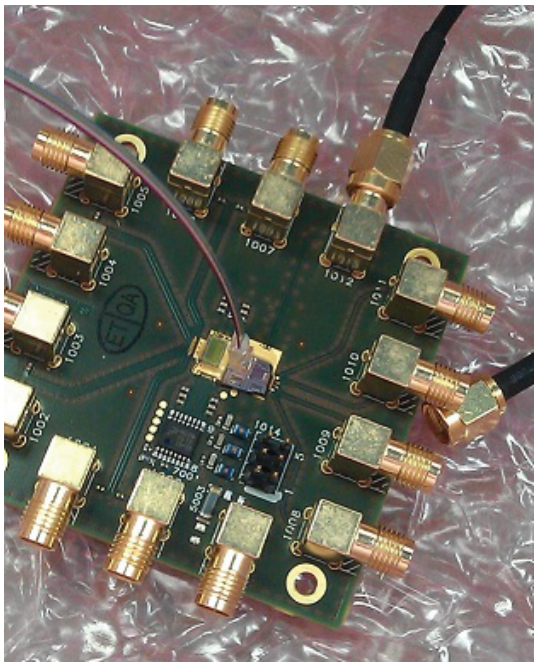

Figure 2.34: 8*-channel fiber array attachement with UV-curable epoxy.*

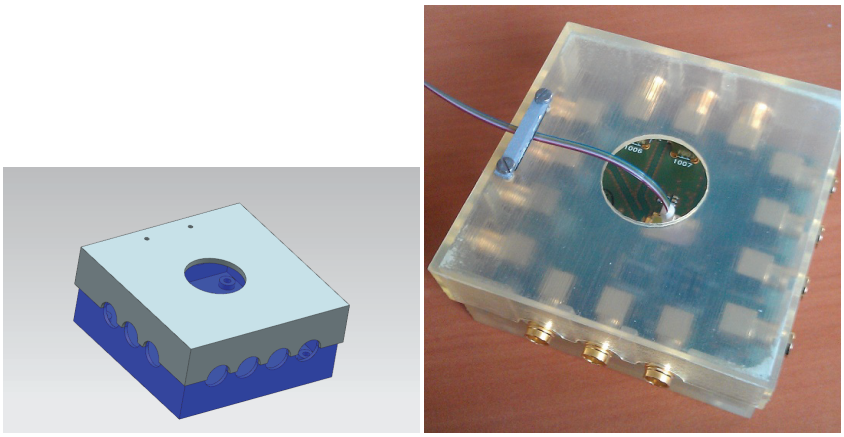

(a) 3D package CAD drawing (b) Packaged demonstrator

Figure 2.35: Packaged 4-channel FTTH transceiver array demonstrator using a 3D printed package.

wavelength. The optical loss of the modulators is about 6dB. The measured Extinction Ratio (ER) was 17 dB for a 5 mm long balanced modulator with a 1.5 V bias and 2 V peak-to-peak voltage. Error-free measurement was achieved. The eye diagram of a transparent photodetector is shown in Fig. 2.37. It was measured at 1.25 Gb/s with a PRBS of 2^7-1 and for 1310 nm. The discrete transparent photodetectors only worked at high-speed if the fiber was positioned closely to the contact metals. This was due to the absence of a p++ InGaAs top layer in the 80 μm diameter transparent region of the photodetector. Consequently, sufficient coupling efficiency for the upstream wavelengths was not possible while achieving high-speed operation for the transparent photodetectors, prohibiting bi-directional experiments.

2.7 Conclusion

I have investigated Silicon Photonics as integration platform for increasing the number of transceivers per package. An interesting example where this kind of scaling would introduce huge economic benefits are Fiber-To-The-Home (FTTH) Point-to-Point (PTP) networks. This network type requires a dedicated transceiver per user, which means that thousands of transceivers are necessary at the Central Office (CO). By integrating the optical components on a chip we can form an array of transceivers with a minimal increase in footprint and cost. A Passive Optical Network (PON) on the other hand shares a single transceiver at

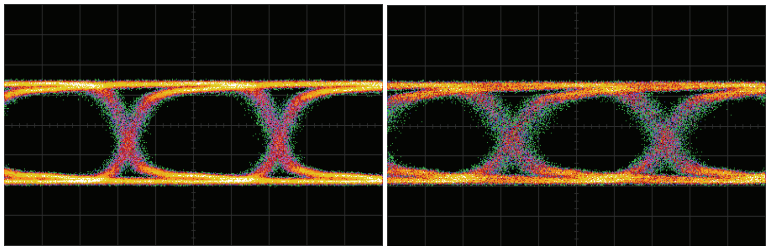

(a) 1.25 Gb/s (b) 2.5 Gb/s

Figure 2.36: Measured modulator eye diagrams at 1510 nm *and for a PRBS of* $2^{31}-1$ *achieving an ER of* 17 dB.

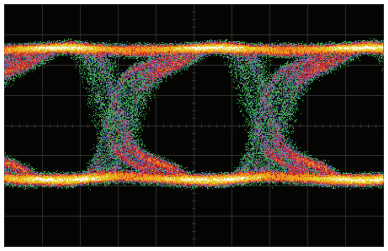

Figure 2.37: Channel 3 1310 nm *transparent photodetector eye diagram at* 1.25 Gb/s *and PRBS of* 2^7-1.

the CO with multiple users and thus benefits less from this transceiver scaling. Furthermore, the transceiver requirements in a PON network are much more stringent than those for a PTP network, making the PTP FTTH transceiver market an ideal candidate for integrated photonics such as Silicon Photonics.
I investigated how the transceiver array specifications could be met in the Silicon Photonics platform and identified the shortcomings. A major hurdle was meeting the power budget. To this extent I developed a new type of highly-efficient grating coupler for the fiber-to-chip interface, decreasing the coupling loss with more than 3 dB and achieving a typical coupling efficiency for a single polarization and wavelength of −2 dB. A big effort was made to design a grating coupler which can couple in all FTTH wavelengths, i.e. 1310 nm (both polarizations) and 1490 nm/1550 nm, at the same time while maintaining the high coupling efficiency of $-2dB$. In the process I demonstrated a grating duplexer which couples in two wavelength bands such as 1310 nm and 1490 nm/1550 nm in opposite directions. Another design was a polarization splitting 1D grating coupler, coupling in both orthogonal polarizations while splitting them. Efforts to improve 2D polarization splitting grating couplers and to combine above functionalities were made. However, a grating coupler which is compatible with all FTTH specs was not found.
To solve the coupling problem I changed gear and invented a heterogeneous integrated III/V transparent photodetector. This photodetector detects 1310 nm polarization independently. It is transparent for 1490 nm/1550 nm and sits on top of a high-efficiency 1D grating coupler, which provides the fiber-to-chip coupling interface for these upstream wavelengths. A proof-of-principle of this transparent photodetector showed promising performance with a crosstalk of 32 dB and 42 dB at 1490 nm and 1550 nm respectively with a responsivity of 0.4 A/W. The measured penalty for the upstream wavelength coupling was about 1 dB.
The developed building blocks enabled us to design a FTTH PTP 4-channel transceiver array, which can fulfill all the IEEE FTTH specifications. This demonstrator includes a full process flow of active and passive components. The light modulation (OOK) is performed with carrier depletion Mach-Zehnder modulators. The 1490 nm and 1550 nm light is splitted with a PCG demultiplexer using DBR back mirrors to achieve an IL of 1 dB. Low-loss MMI splitters and crossings were employed. The III/V transparent photodetectors were integrated with a SU8 flipchip method. The chip was mounted on a PCB board and connected to the board and a TIA array by means of wirebonding. An 8-channel SMF fiber array was attached to the demonstrator and it was packaged in a 3D printed package. The required 1.25 Gbps operation for the transmitter and receiver was demonstrated.
In the future an 8-channel and even 16 or 32-channel transceiver array should be

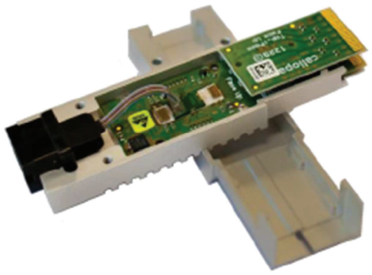

Figure 2.38: 12-channel commercial FTTH transceiver product from Caliopa (imec/UGent Silicon Photonics startup) using similar transparant photodetector technology pioneered in this work.

possible. The biggest challenge is meeting the optical power budget. The biggest improvement would be to optimize the modulator for this specific application, reducing the 6 dB IL with a couple of dB. Together with fully optimized waveguide components, optimized fiber-to-chip coupling interfaces and by going to a laser with more than 13 dBm output power or integrating an amplifier, a 32-channel device is achievable with Silicon Photonics.
Fig. 2.38 is a commercial 12-channel FTTH transceiver from Caliopa, an *imec*/UGent Silicon Photonics startup. This product includes an array of transparent photodetectors based on the technology pioneered in this work.

References

[1] P.E. Green. *Fiber to the home: the next big broadband thing.* IEEE Communications Magazine, 42(9):100–106, 2004.

[2] K Kim. *On the evolution of PON-based FTTH solutions.* Information Sciences, 149(1-3):21–30, 2003.

[3] Wei-ping Huang, Xun Li, Chang-qing Xu, Xiaobin Hong, Chenglin Xu, and Wanguo Liang. *Optical Transceivers for Fiber-to-the-Premises Applications: System Requirements and Enabling Technologies.* Journal of Lightwave Technology, 25(1):11–27, 2007.

[4] R. Duijn, E. Pluk, and G. Van den Hoven. *Genexis, a trendsetting European company focused on the development, manufacturing and marketing of active equipment dedicated to fiber-to-the-home (FTTH) networks.*

[5] P. Verheyen, Guy Lepage, J. Van Campenhout, Marianna Pantouvaki, P. Absil, P. De Heyn, W. Bogaerts, P. Dumon, and S.K. Selvaraja. *Co-integration of Ge detectors and Si modulators in an advanced Si photonics platform.* pages 843114–843114–8, 2012.

[6] L. Vivien, A. Polzer, D. Marris-Morini, J. Osmond, J. M. Hartmann, P. Crozat, E. Cassan, C. Kopp, H. Zimmermann, and J.-M. Fédéli. *Zero-bias 40Gbit/s germanium waveguide photodetector on silicon.* Optics express, 20(2):1096–101, 2012.

[7] A.W. Fang, B.R. Koch, R. Jones, Erica Lively, and J.E. Bowers. *A Distributed Bragg Reflector Silicon Evanescent Laser.* IEEE Photonics Technology Letters, 20(20):1667–1669, 2008.

[8] M. N. Sysak, H. Park, A. W. Fang, O. Raday, J. E. Bowers, and R. Jones. *Reduction of hybrid silicon laser thermal impedance using Poly Si thermal shunts.* In Optical Fiber Communication Conference and Exposition (OFC/NFOEC), 2011.

[9] S. Stankovic, R. Jones, Matthew N Sysak, John M Heck, G. Roelkens, and D. Van Thourhout. *Hybrid IIIâĂŞV/Si Distributed-Feedback Laser Based on Adhesive Bonding.* IEEE Photonics Technology Letters, 24(23):2155–2158, 2012.

[10] N. Adithyaram, S. Abdalla, C. Bradbury, A. Clark, J. Clymore, J. Coyne, A. Dahl, S. Gloeckner, A. Gruenberg, D. Guckenberger, S. Gutierrez, M. Harrison, D. Kucharski, K. Leap, R. LeBlanc, Y. Liang, M. Mack, D. Martinez,

G. Masini, A. Mekis, R. Menigoz, C. Ogden, M. Peterson, T. Pinguet, J. Redman, J. Rodriguez, S. Sahni, M. Sharp, T. J. Sleboda, D. Song, Y. Wang, B. Welch, J. Witzens, W. Xu, K. Yokoyama, and P. De Dobbelaere. *An ultra low power CMOS photonics technology platform for H/S optoelectronic transceivers at less than $1 per Gbps.* In Optical Fiber Communication Conference (OFC), 2010.

[11] A. J. Zilkie, P. Seddighian, B. J. Bijlani, W. Qian, D. C. Lee, S. Fathololoumi, J. Fong, R. Shafiiha, D. Feng, B. J. Luff, X. Zheng, J. E. Cunningham, a. V. Krishnamoorthy, and M. Asghari. *Power-efficient III-V/Silicon external cavity DBR lasers.* Optics Express, 20(21):23456, 2012.

[12] T. Shoji, T. Tsuchizawa, T. Watanabe, K. Yamada, and H. Morita. *Low loss mode size converter from 0.3μm square Si waveguides to singlemode fibres.* Electronics Letters, 38(25):1669, 2002.

[13] S. McNab, N. Moll, and Y. Vlasov. *Ultra-low loss photonic integrated circuit with membrane-type photonic crystal waveguides.* Optics express, 11(22):2927–39, 2003.

[14] G. Roelkens, P. Dumon, W. Bogaerts, D. Van Thourhout, and R. Baets. *Efficient silicon-on-insulator fiber coupler fabricated using 248-nm-deep UV lithography.* IEEE Photonics Technology Letters, 17(12):2613–2615, 2005.

[15] T.W. Ang, G.T. Reed, A. Vonsovici, A.G.R. Evans, P.R. Routley, and M.R. Josey. *Effects of grating heights on highly efficient unibond SOI waveguide grating couplers.* IEEE Photonics Technology Letters, 12(1):59–61, 2000.

[16] D. Taillaert, W. Bogaerts, P. Bienstman, T.F. Krauss, P. Van Daele, I. Moerman, S. Verstuyft, K. De Mesel, and R. Baets. *An out-of-plane grating coupler for efficient butt-coupling between compact planar waveguides and single-mode fibers.* IEEE Journal of Quantum Electronics, 38(7):949–955, 2002.

[17] A. Mekis, S. Gloeckner, G. Masini, A. Narasimha, T. Pinguet, S. Sahni, and P. Dobbelaere. *A Grating-Coupler-Enabled CMOS Photonics Platform.* Selected Topics in Quantum Electronics, IEEE Journal of, (99):1–12, 2010.

[18] D. Vermeulen, S.K. Selvaraja, P. Verheyen, G. Lepage, W. Bogaerts, P. Absil, D. Van Thourhout, and G. Roelkens. *High-efficiency fiber-to-chip grating couplers realized using an advanced CMOS-compatible silicon-on-insulator platform.* Optics express, 18(17):18278–83, 2010.

[19] F. Van Laere, W. Bogaerts, P. Dumon, G. Roelkens, D. Van Thourhout, and R. Baets. *Focusing polarization diversity gratings for Silicon-on-Insulator integrated circuits.* In Group IV Photonics, 2008 5th IEEE International Conference on, volume 1, pages 203–205, 2008.

[20] D. Taillaert, W. Bogaerts, P. Bienstman, T.F. Krauss, I. Moerman, P. Van Daele, and R. Baets. *A high-efficiency out-of-plane fibre coupler for coupling to high index contrast waveguides.* Proceedings 27th European Conference on Optical Communication (Cat. No.01TH8551), 6(l):30–31.

[21] S.K. Selvaraja, D. Vermeulen, Marc Schaekers, Erik Sleeckx, W. Bogaerts, G. Roelkens, P. Dumon, D. Van Thourhout, and R. Baets. *Highly efficient grating coupler between optical fiber and silicon photonic circuit.* In Lasers and Electro-Optics, 2009 and 2009 Conference on Quantum electronics and Laser Science Conference. CLEO/QELS 2009. Conference on, volume 1, pages 1–2, 2009.

[22] F. Van Laere, G. Roelkens, M. Ayre, J. Schrauwen, D. Taillaert, D. Van Thourhout, Thomas F. Krauss, and R. Baets. *Compact and Highly Efficient Grating Couplers Between Optical Fiber and Nanophotonic Waveguides.* Journal of Lightwave Technology, 25(1):151–156, 2007.

[23] D. Vermeulen, S.K. Selvaraja, P. Verheyen, G Lepage, W. Bogaerts, and G. Roelkens. *High-efficiency silicon-on-insulator fiber-to-chip grating couplers using a silicon overlay.* In Group IV Photonics, pages post–deadline, San Francisco, United States, 2009.

[24] D. Vermeulen, G. Roelkens, J. Brouckaert, D. Van Thourhout, R. Baets, R. Duijn, E. Pluk, and G. Van den Hoven. *Silicon-on-insulator nanophotonic waveguide circuit for fiber-to-the-home transceivers.* In 2008 34th European Conference on Optical Communication (ECOC), volume 2, pages 1–2, 2008.

[25] D. Taillaert, P.I. Borel, L.H. Frandsen, R.M. De La Rue, and R. Baets. *A compact two-dimensional grating coupler used as a polarization splitter.* IEEE Photonics Technology Letters, 15(9):1249–1251, 2003.

[26] W. Bogaerts, D. Taillaert, P. Dumon, D. Van Thourhout, R. Baets, and E. Pluk. *A polarization-diversity wavelength duplexer circuit in silicon-on-insulator photonic wires.* Optics express, 15(4):1567–78, 2007.

[27] D. Vermeulen, G. Roelkens, D. Van Thourhout, and R. Baets. *SOI 1D and 2D photonic crystal structures for polarization independent fiber-to-chip coupling and duplexing operation.* In 8th International Photonic and Electromagnetic Crystal Structures Meeting (PECS-VIII), volume 45, Sydney, Australia, 2009.

[28] C. R. Doerr, L. Chen, Y.K. Chen, and L.L. Buhl. *Wide bandwidth silicon nitride grating coupler.* Photonics Technology Letters, IEEE, 22(19):1461–1463, 2010.

[29] D. Vermeulen, K. Van Acoleyen, S. Ghosh, S. K. Selvaraja, W. A. D. De Cort, N. A. Yebo, E. Hallynck, K. De Vos, P. P. P. Debackere, P. Dumon, W. Bogaerts, G. Roelkens, D. Van Thourhout, and R. Baets. *Efficient Tapering to the Fundamental Quasi-TM Mode in Asymmetrical Waveguides.* In European Conference on Integrated Optics, 2010.

[30] D. Vermeulen, G. Roelkens, and D. Van Thourhout. *GRATING STRUCTURES FOR SIMULTANEOUS COUPLING TO TE AND TM WAVEGUIDE MODES (US 20100322555 A1)*, 2010.

[31] D. Vermeulen, T. Spuesens, P. De Heyn, P. Mechet, R. Notzel, S. Verstuyft, D. Van Thourhout, and G. Roelkens. *III-V/silicon-on-insulator photonic integrated circuit for fiber-to-the-home central office transceivers in a point-to-point network configuration.* In ECOC, page Tu.5.C.2, Torino, Italy, 2010.

[32] J. Brouckaert, W. Bogaerts, P. Dumon, D. Van Thourhout, and R. Baets. *Planar Concave Grating Demultiplexer Fabricated on a Nanophotonic Silicon-on-Insulator Platform.* Journal of Lightwave Technology, 25(5):1269–1275, 2007.

[33] J. Brouckaert, W. Bogaerts, S.K. Selvaraja, P. Dumon, R. Baets, and D. Van Thourhout. *Planar Concave Grating Demultiplexer With High Reflective Bragg Reflector Facets.* IEEE Photonics Technology Letters, 20(4):309–311, 2008.

[34] W. Bogaerts, S.K. Selvaraja, P. Dumon, J. Brouckaert, K. De Vos, D. Van Thourhout, and R. Baets. *Silicon-on-Insulator Spectral Filters Fabricated With CMOS Technology.* IEEE Journal of Selected Topics in Quantum Electronics, 16(1):33–44, 2010.

[35] H. Yu, W. Bogaerts, and A. De Keersgieter. *Optimization of Ion Implantation Condition for Depletion-Type Silicon Optical Modulators.* IEEE Journal of Quantum Electronics, 46(12):1763–1768, 2010.

[36] A. Liu, L. Liao, D. Rubin, and H. Nguyen. *High-speed optical modulation based on carrier depletion in a silicon waveguide.* Optics Express, 15(2):660–8, 2007.

[37] L. Chen, C. R. Doerr, P. Dong, and Y.-K. Chen. *Monolithic Silicon Chip with 10 Modulator Channels at 25 Gbps and 100-GHz Spacing.* In 37th European Conference and Exposition on Optical Communications, page Th.13.A.1, 2011.

[38] W. Bogaerts, P. Dumon, D. Van Thourhout, and R. Baets. *Low-loss, low-cross-talk crossings for silicon-on-insulator nanophotonic waveguides.* Optics letters, 32(19):2801–3, 2007.

[39] SK Selvaraja, Wim Bogaerts, and Philippe Absil. *Record Low-Loss Hybrid Rib / Wire Waveguides for Silicon Photonic Circuits.* IV Photonics, 2010.

High-Efficiency Fiber-to-Chip Grating Couplers realized using An Advanced CMOS-Compatible Silicon-On-Insulator Platform

D. Vermeulen [1], S. Selvaraja [1], P. Verheyen [2], G. Lepage [2]
W. Bogaerts [1], P. Absil [2] , D. Van Thourhout [1] and G. Roelkens [1]

[1] *Photonics Research Group, Department of Information Technology, Ghent University - imec, B-9000 Ghent, Belgium*

[2] *imec, Kapeldreef 75, B-3001 Leuven, Belgium*
Diedrik.Vermeulen@intec.ugent.be

Abstract: A new generation of Silicon-on-Insulator fiber-to-chip grating couplers which use a silicon overlay to enhance the directionality and thereby the coupling efficiency is presented. Devices are realized on a 200 mm wafer in a CMOS pilot line. The fabricated fiber couplers show a coupling efficiency of −1.6 dB and a 3 dB bandwidth of 80 nm.

OCIS codes: (000.0000) General.

References and links

1. D. Taillaert, W. Bogaerts, P. Bienstman, T.F. Krauss, P. Van Dale, I. Moerman, S. Verstuyft, K. De Mesel, and R. Baets, "An out-of-plane grating coupler for efficient butt-coupling between compact planar waveguides and single-mode fibers," IEEE J. Quantum Electron. **14,** 949–955 (2002).
2. D. Taillaert, P. Bienstman, and R. Baets, "Compact efficient broadband grating coupler for silicon-on-insulator waveguides," Opt. Lett. **29,** 2749–2751 (2004).
3. G. Roelkens, D. Van Thourhout, and R. Baets, "High Efficiency grating coupler between silicon-on-insulator waveguides and perfectly vertical optical fibers," Opt. Lett. **32,** 1495–1497 (2007).
4. X. Chen, C. Li, and H. K. Tsang, "Fabrication-tolerant waveguide chirped grating coupler for coupling to a perfectly vertical optical fiber," IEEE Photon. Technol. Lett. **20,** 1914-1916 (2008).
5. L. Vivien, D. Pascal, S. Lardenois, D. Marris-Morini, E. Cassan, F. Grillot, S. Laval, J.M. Fédéli, and L. El Melhaoui, "Light injection in SOI microwaveguides using high-efficiency grating couplers," J. Lightwave Technol. **24,** 3810–3815 (2006).
6. S. K. Selvaraja, D. Vermeulen, M. Schaekers, E. Sleeckx, W. Bogaerts, G. Roelkens, P. Dumon, D. Van Thourhout, and R. Baets, "Highly efficient grating coupler between optical fiber and silicon photonic circuit," in *Lasers and Electro-Optics/International Quantum Electronics Conference,* (2009).
7. F. Van Laere, G. Roelkens, M. Ayre, J. Schrauwen, D. Taillaert, D. Van Thourhout, T. F. Krauss, and R. Baets, "Compact and highly efficient grating couplers between optical fiber and nanophotonic waveguides," J. Lightwave Technol. **25,** 151–156 (2007).
8. J. Schrauwen, F. Van Laere, D. Van Thourhout, and R. Baets, "Focused-ion-beam fabrication of slanted grating couplers in silicon-on-insulator waveguides," IEEE Photon. Technol. Lett. **19,** 816–818 (2007).
9. G. Roelkens, D. Van Thourhout, and R. Baets, "High efficiency silicon-on-insulator grating coupler based on a poly-silicon overlay," Opt. Express **14,** 11622–11630 (2006).
10. G. Roelkens, D. Vermeulen, D. Van Thourhout, R. Baets, S. Brision, P. Lyan, P. Gautier, and J. M. Fédéli, "High efficiency diffractive grating couplers for interfacing a single mode optical fiber with a nanophotonic silicon-on-insulator waveguide circuit," Appl. Phys. Lett. **92,** 131101 (2008).
11. X. Chen, C. Li, S. M. G. Lo, K. Fung, and H. K. Tsang, "Silicon Waveguide Grating Couplers with Engineered Coupling Strength for Optimized Coupling," in *European Conference on Integrated Optics,* (2010).

12. T.K. Saha, and W. Zhou, "High efficiency diffractive grating coupler based on transferred silicon nanomembrane overlay on photonic waveguide," J. Phys. D: Appl. Phys. **42,** 085115 (2009).
13. F. Van Laere, T. Claes, J. Schrauwen, S. Scheerlinck, W. Bogaerts, D. Taillaert, L. O'Faolain, D. Van Thourhout, and R. Baets, "Compact focusing grating couplers for silicon-on-insulator integrated circuits," IEEE Photon. Technol. Lett. **27,** 612–618 (2009).
14. C. R. Doerr, L. Chen, M. Rasras, Y.K. Chen, J. Weiner, and M. Earnshaw, "Diplexer With Integrated Filters and Photodetector in Ge/Si Using $\Gamma - X$ and $\Gamma - M$ Directions in a Grating Coupler," Photon. Technol. Lett. **21,** 1698–1700 (2009).

1. Introduction

In the last decade much research has focused on silicon photonic integrated circuits, due to the scaling in size that can be accomplished because of the high refractive index contrast available on the SOI material platform. However, the scaling of the device cross-section complicates the interfacing with a single mode optical fiber. Several schemes have been proposed to tackle this problem. We focused particularly on fiber-to-chip coupling by means of subwavelength structured surfaces such as line gratings or photonic crystals. With these grating couplers one can couple out-of-plane and thus test photonic circuits on a wafer-scale without the need of any post-processing or cleaving. Furthermore because of a relaxed 1dB alignment sensitivity of $2\,\mu$m, it is even possible to align several optical fibers at the same time by using fiber arrays for wafer-scale testing or packaging. Despite the fact that these grating couplers are a very good candidate for fiber interfacing for the low cost and high volume oriented silicon photonics framework, they suffer from relatively high coupling loss, making them only useful for research purposes or specific applications with a relaxed power budget.
In 2002 we reported an SOI grating coupler with a fiber coupling efficiency of -7 dB [1]. Since then, a lot of attempts were made to improve the coupling efficiency significantly. In general there are three factors that contribute to the poor coupling efficiency of standard grating couplers. Most of the light $35\,\% - 45\,\%$ is lost because of diffraction towards the substrate and around $20\,\%$ is lost because of poor mode-matching to the Gaussian shaped mode of the fiber. For perfectly vertical coupling another $30\,\%$ is reflected back into the waveguide due to second order Bragg diffraction. This last issue can be easily solved by coupling under a small angle which breaks the symmetry and eliminates the reflection [2]. An alternative method is to etch a deep slit in front of the grating which acts together with the grating as a Fabry-Perot cavity [3]. By chirping the grating, back reflections [4] and losses due to mode-mismatch [2] can be minimized. Most attempts to increase the directionality of the grating all involve substrate engineering [5]. Other approaches are either based on amorphous silicon, which limits the thermal budget [6], or require a lot of post-processing [7]. Alternatively, one can use exotic gratings with for example slanted facets, in analogy to a blazed grating, to enhance the coupling to the first diffraction order in the superstrate [8]. In 2006 however, we proposed a rather simple and elegant way to adapt the grating and increase the coupling efficiency drastically, i.e. by defining a silicon overlay prior to etching the grating [9]. Early attempts which involved epitaxial silicon growth were promising and showed efficiencies up to -2.6 dB [10]. In this paper we demonstrate high efficiency grating couplers, fabricated in a CMOS pilot line, with -1.6 dB coupling efficiency, approaching the coupling efficiencies required in practical applications.

2. Fiber Coupler Grating Design

For designing a fiber-to-chip grating coupler, which is inherently highly efficient, several design issues have to be taken into account. These are summarized in Figure 1. The first order diffraction of a grating is described by the Bragg condition $\beta - K = k_z$ where the propagation constant of the guided mode $\beta = \frac{2\pi}{\lambda} n_{eff}$, $K = \frac{2\pi}{\Lambda}$ and the projected wave vector of the incident mode $k_z = \frac{2\pi}{\lambda} \sin\theta$ with λ the wavelength of the light, Λ the period of the grating and θ the

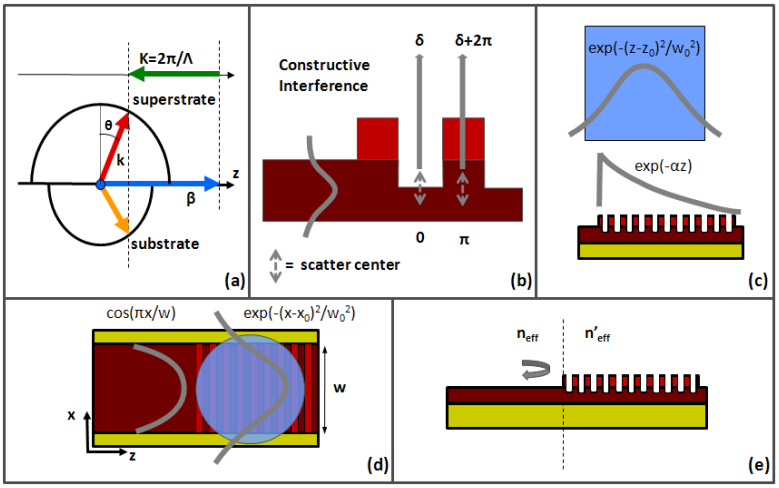

Fig. 1. Schematic illustrations of fiber-to-chip high index contrast grating coupler optimization factors: the Bragg condition (a), upwards directionality (b), 2D fiber mode-matching in z- and x-direction (c,d) and mode-matching between the waveguide and Bloch mode of the grating (e).

angle of the fiber with respect to the surface normal of the grating. In order to avoid a high second order reflection, it is convenient to couple in under a positive fiber angle as shown in Figure 1(a). In general the effective refractive index n_{eff} of the grating is a function of the grating parameters shown in Figure 2(a). However, since for a given grating period and given fiber angle it is almost always possible to find a wavelength at which the Bragg condition is fulfilled, this dependency will have a minor influence on the maximal coupling efficiency of the grating coupler but rather on the central wavelength of the coupling spectrum. In the rest of the analysis we will assume that the Bragg condition is satisfied and that the fiber coupling angle θ is close to zero.

The physical principle behind a highly directional grating as shown in Figure 1(b) can be understood as follows. Considering the diffracted field pattern as the superposition of the fields emitted by an array of scattering centers (which have a π phase shift with respect to each other for a perfect vertically coupling grating), constructive interference towards the superstrate (and hence the optical fiber) can be achieved by realizing an additional π phase shift during the propagation towards the superstrate, since light is propagating either in air (in the etched slit) or in silicon (in the grating tooth). This directionality is thus a function of the waveguide thickness h, the etch depth e in the waveguide and the silicon overlay thickness o (see Figure 2). Furthermore, in order to reach high fiber coupling efficiency, a highly directional grating is required while at the same time the grating strength needs to be optimized for maximal overlap with the Gaussian fiber mode, shown in Figure 1(c). This mode-matching requirement is a function of the same three parameters h, e and o as the high directionality condition. For high index contrast gratings, the strength of the alternating scattering centers is in general not equal, resulting in an imbalanced interference to the superstrate. The duty cycle of the grating can be used as a tuning parameter to compensate and maximize the grating directionality. Three different classes of grating cases shown in Figure 2 can be considered which can be favorable, depending on the considered photonics platform, robustness and cost considerations.

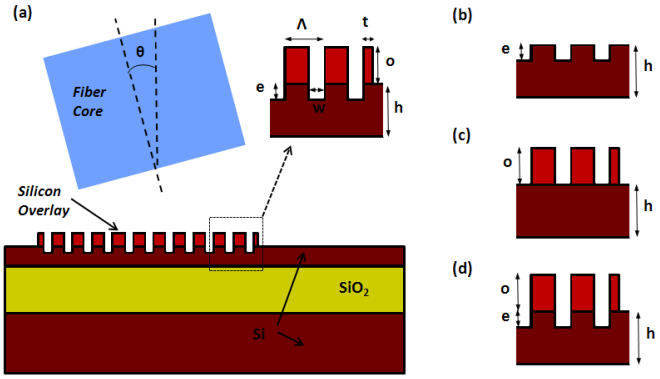

Fig. 2. Parameterized highly directional grating couplers: the general case (a), without silicon overlay (b), with silicon overlay but no waveguide etch (c) and both silicon overlay and waveguide etch (d).

The first case 2(b) is a grating without silicon overlay where high directionality and an optimal grating strength are only achieved for a certain waveguide thickness h and etch depth e. In [11] this grating type is optimized and a coupling efficiency of $-1.2\,\mathrm{dB}$ is achieved for a waveguide thickness h of 340 nm and a deep waveguide etch depth e of 200 nm. Important drawbacks are the fixed waveguide thickness which is multimode and the deep waveguide etch depth which introduces a large mode mismatch between the waveguide mode and the Bloch mode of the grating resulting in high back reflections (see Figure 1(e)). The last issue is improved by apodizing the grating, leading to reduced reflections and a better mode matching with the Gaussian fiber mode. However, an apodized grating requires feature sizes which are beyond the limit of current 193 nm DUV lithography.

For case 2(c), no waveguide etch e is required. This kind of grating coupler has been theoretically reported in [12], where a transferred silicon nanomenbrane is proposed in order to fabricate the grating. For a waveguide thickness h of 220 nm and a silicon overlay thickness o of 240 nm the simulated efficiency was 64%. We optimized this grating type and simulated for a uniform grating with $h = 150\,\mathrm{nm}$ and $o = 220\,\mathrm{nm}$ around 80% coupling efficiency, which is the theoretical upper limit because of the mode mismatch between the exponential shaped electrical field profile of the uniform grating and the Gaussian shaped mode of the optical fiber. Unfortunately, a waveguide thickness of $h = 150\,\mathrm{nm}$ leads to a lower confinement of the TE optical mode, and does not support any TM polarized waveguide modes. We also like to point out that the coupling strength of a grating with no waveguide etch is solely dependent on the silicon overlay and thus on the evanescent field of the waveguide mode. Because this evanescent field is different for orthogonal polarized waveguide modes, it is unlikely that there exists a grating which is highly efficient for both polarizations. Despite these drawbacks, this grating coupler type could be an ideal candidate for using in a single-polarization low-cost photonics platform.

The most general fiber coupler grating using a silicon overlay is case 2(d) where both a silicon overlay o and waveguide etch e is used to define the grating. This gives us the freedom to choose an appropriate waveguide thickness h of for example 220 nm. This high efficiency grating coupler type is theoretically described in [9] and shows around 80% of coupling efficiency according to simulations. Although it requires more process steps than the previous cases, it

is compatible with any high index contrast photonic platform. Moreover, the introduced additional thickness levels could be used to optimize other integrated photonic devices.
An optimization issue that is unrelated to the previous discussion is the mode-matching between the Gaussian fiber mode and the waveguide mode in the x-direction as is shown in Figure 1(d). For a 220 nm thick waveguide, the optimal waveguide width w is 15 μm. Since the taper length scales quadratic with the waveguide width, a long taper section ($\approx 500\,\mu$m) would be needed to adiabatically transform the broad waveguide of the grating into a single-mode optical waveguide. This can be easily solved by curving the grating as is demonstrated in [13], without decreasing the grating coupling efficiency.

3. Fabrication

We developed an advanced Silicon-on-Insulator process flow which is capable of realizing the most general case in Figure 2(d) of the high efficiency grating couplers. The complete fabrication process is done in the 200 mm *imec* CMOS pilot line with 193 nm DUV lithography. We start from a 200 mm SOI wafer with a buried oxide layer thickness of 2 μm and a crystalline silicon layer thickness of 220 nm. Simulations show that the thickness of the buried oxide layer is of minimal importance for the coupling efficiency, since the grating intrinsically is very directional such that only a small fraction of the light is reflected at the interface of the buried oxide and silicon substrate [9]. In a second step an amorphous silicon layer of 160 nm is deposited over the whole wafer and a deep etch is performed through the amorphous silicon reaching 70 nm into the crystalline silicon layer. This is used to define the slits of the high efficiency grating couplers. Next, the amorphous silicon is removed where necessary by dry etching using a combination of a chlorine/fluorine-based and bromine-based chemistry. The width of the first tooth will not affect the grating coupling efficiency if it is narrower than the subsequent teeth [9]. By contrast, larger first tooth widths introduce a rapid decrease of the coupling efficiency. The consequences of possible mask misalignment between the silicon overlay and the grating coupler are anticipated by designing the first tooth of the grating narrower. This can be clearly seen in Figure 3 where a bird's eye view image of the fabricated silicon overlay grating is shown. In the final step the strip waveguides are defined in the crystalline silicon layer. The measured propagation loss for a straight single-mode strip waveguide with a height of 220 nm and a width of 450 nm was 1.8 dB/cm, demonstrating the high process quality of this advanced SOI fabrication process.

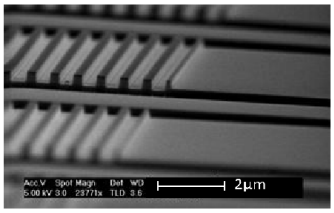

Fig. 3. Bird's eye view of a silicon overlay grating fiber coupler.

4. Experimental Results

The measurement results are shown in Figure 4. All measurements were performed with a single-mode fiber tilted under an angle of 13 degrees relative to the surface normal of the grating. Index matching fluid was applied between the grating and fiber facet to reduce Fresnel

reflections. TE polarized light is used in all experiments, because the gratings are polarization dependent. The coupling efficiency was determined by measuring the fiber-to-fiber insertion loss of two grating couplers connected with a 300 μm long and 15 μm broad waveguide. Figure 4(a) shows the central wavelength of the fiber coupling spectrum as a function of the grating period and this for several duty cycles. The central wavelength scales almost linearly with the grating period because the effective refractive index of the grating is only weakly dependent upon the wavelength. In Figure 4(b), the coupling efficiency for different grating periods is plotted versus the duty cycle. It seems that a duty cycle of 35 % (refers to the unetched silicon part) is optimal and we measured a maximum efficiency of -1.6 dB with a 1 dB and 3 dB bandwidth of respectively 44 nm and 80 nm for a grating period of 690 nm and central wavelength of 1530 nm. This is the highest fiber coupling efficiency reported to date for CMOS-compatible fiber-to-chip grating couplers.

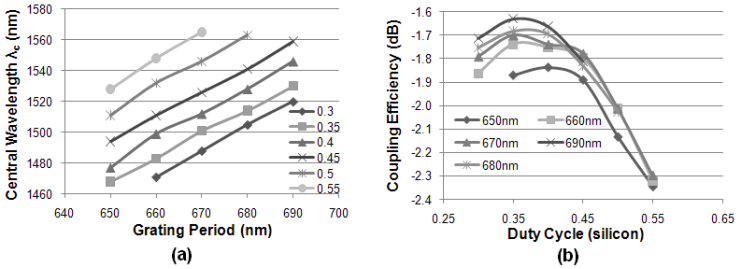

Fig. 4. Measurement results of a sweep of 1D fiber couplers (a-Si overlay) for different duty cycles (a) and different grating periods (b).

5. Conclusion

Different types of high efficiency grating couplers which are inherently highly directional are discussed. The most general case of a grating coupler with silicon overlay and etch into the optical waveguide is fabricated using 193 nm DUV lithography. We have shown experimentally a coupling efficiency of -1.6 dB which is the highest fiber coupling efficiency for grating couplers fabricated in a CMOS pilot line. The optimal duty cycle of the grating is found to be 35 %. The amorphous silicon is stable up to a temperature of 500 °C. As an alternative a polysilicon overlay could be used which is stable up to a temperature of 1000 °C. A silicon overlay could also be beneficial for more advanced grating couplers which incorporate polarization diversity and wavelength demultiplexing [14]. Besides the grating couplers, the silicon overlay can be used in other components on the SOI chip as an extra degree of design freedom.

6. Acknowledgements

Diedrik Vermeulen thanks the Institute for the Promotion of Innovation by Science and Technology in Flanders (IWT) for a grant. W. Bogaerts and G. Roelkens acknowledge the Fund for Scientific Research Vlaanderen (FWO) for a postdoctoral grant. The research leading to these results has received funding from the European Community's Seventh Framework Programme (FP7/2007-2013) under grant agreement n° 224312 HELIOS and from Ghent University through the IOF STARCHIP grant.

Silicon-on-Insulator Nanophotonic Waveguide Circuit for Fiber-to-the-Home Transceivers

D. Vermeulen(1), G. Roelkens(1), J. Brouckaert(1), D. Van Thourhout(1), R. Baets(1)
R. Duijn(2), E. Pluk(2), G. Van den Hoven(2)
1: Photonics Research Group, Ghent University-IMEC, Sint-Pietersnieuwstraat 41, B-9000 Ghent – Belgium
e-mail: Diedrik.Vermeulen@Ugent.be
2: GENEXIS B.V., Lodewijkstraat 1a, 5652 AC Eindhoven, The Netherlands
e-mail: r.duijn@genexis.nl

Abstract

We present a SOI nanophotonic waveguide circuit for FTTH transceivers. A grating duplexer and planar concave grating are combined to couple and demultiplex the 1310, 1490 and 1550nm communication channels.

Introduction

Silicon-on-insulator technology has many advantages for the realization of photonic integrated circuits. First of all the platform is CMOS-compatible and due to the high refractive index contrast, the designs are very compact. Furthermore, out-of-plane coupling can be realized by the use of a diffractive grating [1]. This makes wafer scale testing feasible. By unifying these advantages it is possible to fabricate nanophotonic integrated circuits in large volumes at a low cost.

Point-to-point Fiber-to-the-Home optical access networks require large volume and low-cost optical transceivers, both at the subscriber and the central office side. From the perspective of the transceiver at the subscriber side, 1310nm is the upstream channel and 1490nm and 1550nm are the downstream channels for data and CATV. The passive optical part of a fiber-to-the-home transceiver has to couple and demultiplex these three communication channels.

In this paper, we report on the design and fabrication of a nanophotonic waveguide circuit realizing this optical coupling and demultiplexing. With a grating duplexer [2] the light is coupled into the chip and the 1310nm upstream channel is spatially separated from the downstream channels.

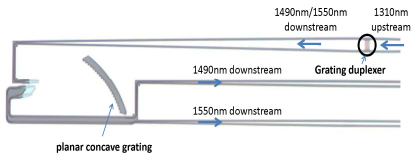

Figure 1: Microscope image of a grating duplexer in combination with a Planar Concave Grating (PCG) demultiplexer for FTTH applications

With a planar concave grating demultiplexer [3], the downstream channels 1490nm and 1550nm are splitted and the 1310nm wavelength channel is filtered to reduce the crosstalk levels. A microscope image of the fabricated structure is shown in Figure 1.

This circuit is fabricated using standard CMOS technology, on a silicon wafer with a 220 nm thick silicon waveguide core and a 2µm thick buried oxide layer.

Grating Duplexer

In order to couple and at the same time split the upstream and downstream wavelength bands, we use a 1-dimensional grating duplexer. The working principle is shown in Figure 2. Under a certain angle of the optical fiber, the Bragg condition is fulfilled for both wavelengths λ_1 and λ_2 and the 2 wavelength bands will couple in opposite directions. The grating period, duty cycle and number of periods have been optimized using a particle swarm optimization algorithm, in order to achieve maximum coupling efficiency for both the upstream and downstream wavelength bands.

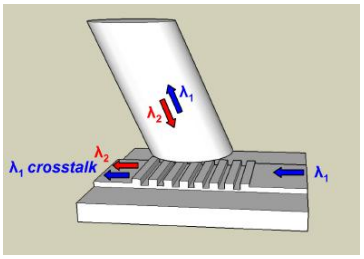

Figure 2: Operation principle of a grating duplexer. λ_1 represents the upstream wavelength band, λ_2 represents the downstream wavelength band.

The duplexer has been designed in a way that the upstream band around 1310 nm is coupled in the forward direction and the downstream band around 1520 nm is coupled backwards. The measurement results of the grating duplexer are plotted in Figure 3. The period of the grating is 520 nm and the grating duty cycle is 40%. The etch depth is 70nm. The number of grating periods is 20. Index matching fluid was applied between the optical fiber facet and the

grating duplexer to avoid reflections at the fiber facets and the fiber was tilted under an angle of 10 degrees. Standard single mode fiber was used for the experiments. The experiments were performed using TE polarized light. Making the grating duplexer polarisation independent can be done by using a two dimensional grating structure [2].

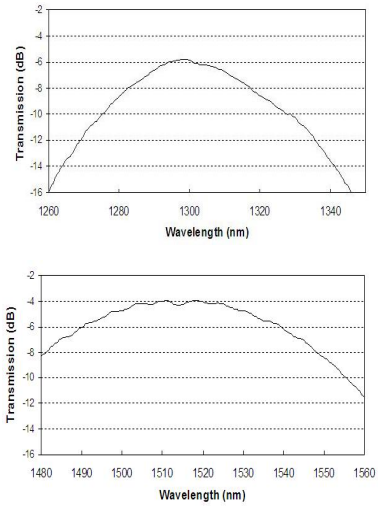

Figure 3: Transmission spectrum of the grating duplexer for the upstream band (upper graph) and the downstream band (lower graph)

The coupling efficiencies of the central wavelengths are -6 dB for 1300 nm and -4 dB for 1520 nm. At the communication wavelengths 1310, 1490 and 1550 nm the coupling efficiencies are respectively -7 dB, -6 dB and -8 dB. Decreasing these losses can be done by first depositing an extra silicon layer prior to defining the grating [4]. Simulations show that efficiencies of -1.9 dB are possible for both central wavelengths.

Planar Concave Grating Demultiplexer

Demultiplexing the downstream band is accomplished by using a planar concave grating demultiplexer (PCG) [3]. In order to avoid possible crosstalk from the grating duplexer as shown in figure 2, we also have to filter the 1310 nm wavelength in both downstream channels. This was done by adjusting the free spectral range of the grating demultiplexer. Measurements of the grating demultiplexer are shown in Figure 4.

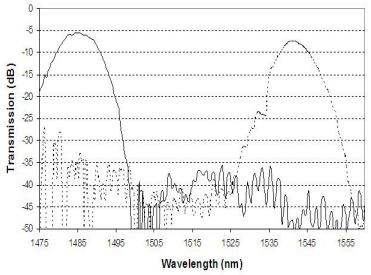

Figure 4: Transmission spectrum of the planar concave grating demultiplexer

The maxima of the transmission efficiencies are -5.4 dB for 1485 nm and -7.6 dB for 1542 nm and are limited by the Fresnel reflection at the Silicon/Air interface. The crosstalk at these maxima is about -30 dB and -40 dB respectively. Filtering of the 1310 nm channel is as good as -40 dB. Several techniques to reduce the insertion loss of this demultiplexer exist; for example with high reflectivity Bragg reflectors, as described in [5], the insertion loss can be reduced by 4 dB.

Conclusions

We have demonstrated how to couple, demultiplex and filter 1310 nm, 1490 nm and 1550 nm with the use of just 2 integrated optical components. A grating duplexer couples the light and splits the upstream/downstream bands. The PCG separates the 1490 nm and 1550 nm while filtering 1310 nm. In addition we have suggested how to increase the performance of these components and make the device polarisation independent. The proposed configuration contains all functionalities for the passive optical part of an SOI FTTH transceiver, while exploiting all advantages of the silicon-on-insulator platform. We believe that this proof of concept is a stepping stone for future low cost SOI fiber-to-the-home transceiver chips.

References

1. D. Taillaert et al IEEE Photonics Technology Letters, 15 (2003), pages 1249-1251
2. G. Roelkens et al Optics Express, 15 (2007), pages 10091-10096
3. J. Brouckaert et al Journal Of Lightwave Technology, 25 (2007), pages 1269-1275
4. G. Roelkens et al Applied Physics Letters, 92 (2008), page 131101
5. J. Brouckaert et al IEEE Photonics Technology Letters, 20 (2008), pages 309-311

Silicon-on-Insulator 1D Grating Couplers incorporating Polarization Splitting and Wavelength Duplexing

D. Vermeulen, *Member, IEEE*, D. Van Thourhout, *Member, IEEE*, G. Roelkens, *Member, IEEE*

Photonics Research Group, Department of Information Technology (INTEC)
Ghent University - imec, Sint-Pietersnieuwstraat 41, B-9000 Ghent, Belgium
e-mail: Diedrik.Vermeulen@intec.ugent.be
website: http://photonics.intec.ugent.be

This work was carried out in the framework of the Dutch Smartmix-Memphis project. D. Vermeulen thanks the Institute for the Promotion of Innovation by Science and Technology in Flanders (IWT) for a grant.

Abstract: The possible functionalities of a uniform 1-dimensional (1D) grating coupler are explored. Besides the main function of coupling light from fiber to chip, the grating can act as a polarization splitter or a wavelength demultiplexer. Experimental results are presented of a grating duplexer which couples and splits $1300\,\mathrm{nm}$ and $1520\,\mathrm{nm}$ with an efficiency of respectively $-6\,\mathrm{dB}$ and $-4\,\mathrm{dB}$. A polarization splitting grating coupler, coupling and splitting the orthogonal polarizations of $1300\,\mathrm{nm}$ with an efficiency of $-5.2\,\mathrm{dB}$ is demonstrated. A technique to minimize the polarization dependent loss (PDL) by varying the fiber angle and position is introduced, successfully compensating for polarization dependent loss in the test circuit. A more complicated 1D grating utilization incorporating both polarization splitting and wavelength duplexing is studied as a possible fiber-to-chip interface for Fiber-To-The-Home (FTTH) transceivers. Furthermore, simulation results are introduced of similar but more efficient 1D grating couplers using a silicon overlay to enhance the grating directionality.

Index Terms: Waveguides, Engineered photonic nanostructures, Fabrication and characterization, gratings, Silicon nanophotonics, Optical communications, Waveguide devices

1. Introduction

PHOTONIC integration is considered to be a key technology for future advancements in optical communication technologies. Scaling down the optical building blocks enables complex and ultra-compact photonic circuits at a fraction of the cost of conventional systems consisting out of discrete components. Choosing an appropriate platform for developing this miniaturization technology is guided by functionality, compatibility, performance, yield and cost. Regarding the last two issues, Silicon-on-Insulator (SOI) is by far the leading technology for low-cost and high-volume photonic integration since it can benefit from the processes developed in the mature electronics industry. Although the high refractive index contrast of SOI reduces the footprint of the integrated photonic devices considerably, it becomes more difficult to achieve a high-performance mode-size convertor between a single-mode optical fiber ($100\,\mu\mathrm{m}^2$) and an integrated optical waveguide ($0.1\,\mu\mathrm{m}^2$).

A possible solution is a lateral coupler using spot-size conversion with an inverted taper, in combination with a tapered/lensed fiber [1]. A recent method employing a thermal oxidation process to reduce the inverted tip width to less than $15\,\mathrm{nm}$ allows for highly efficient ($-0.5\,\mathrm{dB}$) and broadband optical coupling to both the transverse-magnetic (TM-) and transverse-electric (TE-) polarized modes [2]. Although unrivalled in terms of performance, lateral coupling requires a lot of post-processing such as cleaving and polishing the facets, making wafer-scale testing not feasible. Furthermore, the $1\,\mathrm{dB}$ misalignment tolerance is less than $1\,\mu\mathrm{m}$ and a misalignment of $2\,\mu\mathrm{m}$ introduces an insertion penalty of $5\,\mathrm{dB}$. These tolerances are not compatible for using a fiber array [3] which makes lateral coupling not attractive for a low-cost coupling method.
A more robust coupling technique is using periodic structured surfaces such as line gratings [4] or photonic crystals [5] to achieve out-of-plane coupling. They turn out to be an ideal candidate for the low-cost and high-volume oriented silicon photonics framework. The fact is that a relaxed $1\,\mathrm{dB}$ alignment sensitivity of $2\,\mu\mathrm{m}$ makes it possible to align several optical fibers at the same time with the use of fiber arrays for wafer-scale testing or packaging. They also are fully CMOS-compatible and don't need any post-processing. Today grating couplers are widely used in research environments to characterize SOI waveguide circuits and the coupling efficiency is approaching efficiencies required in practical optical communication applications [6], [7]. However, grating couplers are high index contrast wavelength dependent structures and thus exhibit strong polarization dependence and limited bandwidth. For example a conventional grating coupler, as reported in [8], couples TE-polarized light of one single wavelength band around $1550\,\mathrm{nm}$ with a peak efficiency of $-5\,\mathrm{dB}$. The $1\,\mathrm{dB}$ bandwidth is $30-50\,\mathrm{nm}$ and the $3\,\mathrm{dB}$ bandwidth is $70-100\,\mathrm{nm}$, corresponding to the full Conventional Band (C-Band). By changing the period of the grating one can easily change the central wavelength of the coupling spectrum and couple in other spectral bands. In this paper we will investigate 1D grating couplers with increased functionalities such as dual-band coupling/splitting and dual-polarization coupling/splitting.

2. Theoretical Outline

In this section we will explain the basic theory behind a grating coupler and the method to couple more than 1 wavelength band and/or polarization into the chip. Because discussing the different types of designs can become confusing quite easily, we will further introduce some rigorous short notation and transcribing method for 1D grating couplers.

2.1. Bragg Condition

The angle θ of the light diffracted from a grating structure with period Λ can be deduced from phase matching conditions. For a grating coupler these conditions are described by the projected Bragg condition [9] for the first order diffraction:

$$\vec{\beta} = \vec{k}_{in,z} + m\vec{K} \quad (m = \pm 1) \tag{1}$$

and

$$\begin{aligned} \beta &= \frac{2\pi}{\lambda} n_{eff} \\ k_{in,z} &= \frac{2\pi}{\lambda} n_{clad} \sin\theta \\ K &= \frac{2\pi}{\Lambda} \end{aligned}$$

with β the effective propagation constant of the grating mode, K the reciprocal lattice constant of the grating and $k_{in,z}$ the projected wave vector of the incident light. n_{clad} is the refractive index of the top cladding, n_{eff} is the effective refractive index of the grating mode and θ is the

angle between the optical fiber and the surface normal. [1] This condition will be only valid for one polarization since high index contrast waveguides and gratings are highly birefringent.

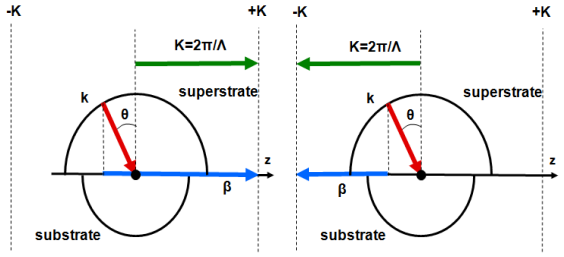

(a) F: Forward Coupling (m=+1) (b) B: Backward Coupling (m=-1)

Fig. 1: Schematic representations of the Bragg diagram for Forward and Backward coupling.

In Fig. 1 the Bragg condition is schematically presented in a Bragg diagram. If $m = 1$ both the effective propagation vector $\vec{\beta}$ and the projected wave vector $k_{in,z}$ will have the same direction. In this case we speak about Forward (F) coupling. If $m = -1$ the effective propagation vector $\vec{\beta}$ and $k_{in,z}$ will have opposite directions and we speak about Backward (B) coupling. From a mathematical point of view, one can say that for a certain grating and fiber angle θ the Bragg condition is always fulfilled for four wavelengths.[2] Two different wavelengths λ_1 and λ_2 which are respectively TE- and TM-polarized, will couple in the Forward direction. Two other wavelengths λ_3 and λ_4, respectively TE- and TM-polarized, will couple in the Backward direction. In order to reduce this tedious description of a grating coupler we will use a short notation and refer to it as the $F(\lambda_1 - TE, \lambda_2 - TM)\, B(\lambda_3 - TE, \lambda_4 - TM)$ grating coupler. Note that due to birefringence, it is impossible to couple the orthogonal polarizations of the same wavelength into the same direction F or B. Likewise, one cannot couple the same wavelength with the same polarization in opposite directions unless the optical fiber angle θ is exactly zero degrees and the grating will couple the same wavelengths equally Forward and Backward.[3] For high index contrast gratings, coupling a certain wavelength into the chip is accompanied by coupling a spectrum of wavelengths around this central wavelength. To emphasis this bandwidth, we will sometimes use the spectral bands (fully or partly coupled) instead of the wavelengths for the short notation of 1D grating couplers, e.g. $F(W - TE, X - TM)\, B(Y - TE, Z - TM)$ where W,X,Y and Z respectively refer to the W, X, Y and Z-bands. If the fiber angle θ is of importance, it will be placed at the end of the short notation: $F(\lambda_1 - TE, \lambda_2 - TM)\, B(\lambda_3 - TE, \lambda_4 - TM) - (\theta)$.

2.2. Fiber Coupling Efficiency Trade-Offs

Fulfillment of the Bragg condition for a certain grating with period Λ and for a certain wavelength λ_1 and angle θ, does not guarantee efficient fiber coupling. This depends strongly on all other grating parameters such as the refractive index contrast, mode confinement, grating width, duty cycle, number of periods, etch depth, chirping, grating height and entrance waveguide. Except for the number of periods, changing one of these grating parameters will alter the effective refractive index of the excited Bloch mode of the grating, especially in the case of high index contrast gratings.

[1] For low index contrast gratings, β can be approximated by the effective propagation constant of the waveguide. Dealing with high index contrast gratings is done by using the propagation constant of the excited Bloch mode of the periodic structure.

[2] We hereby assume that the effective refractive index n_{eff} is only slightly dependent on the wavelength.

[3] Perfect vertical coupling introduces a huge second order reflection back into the waveguide and is therefore avoided [10].

This in turn will have an effect on the Bragg condition (1) and thus the period Λ of the grating and angle θ of the optical fiber. Furthermore, for every grating the optimal position of the optical fiber needs to be optimized. Consider the example of a single wavelength and single polarization grating coupler $F(\lambda_1 - TE) - (\theta)$ wherefore the Bragg condition is fulfilled for λ_1 TE-polarized light and a fiber angle θ. Optimization of this type of grating coupler is explained in detail in [7]. There are 5 optimization factors which have to be taken into account in order to get almost perfect fiber coupling: Bragg condition, grating directionality, 2D fiber mode-matching (is subdivided in two 1D mode-matching conditions) and mode-matching between the waveguide mode and Bloch mode of the grating. All these optimization factors are connected by the effective refractive index n_{eff} of the grating Bloch mode and optimizing one factor will result in the deoptimization of the other factors. However, since the grating period Λ is an independent variable which only affects the Bragg condition, a deoptimization in the Bragg condition is easily counteracted by changing the period without influencing the other optimization factors. This greatly simplifies the optimization of a single wavelength single polarization type of grating coupler. Unfortunately, if we add a second wavelength (or equivalently a second polarization) to the grating functionality, this simplification is no longer valid since two coupled Bragg conditions fix the grating period and fiber angle thereby increasing the design complexity.

In section 2.1 we mentioned that the first optimization factor, i.e. the Bragg condition, can be fulfilled completely for as much as four wavelengths at the same. Since the Bragg condition has two design parameters, i.e. the grating period Λ and fiber angle θ, two wavelengths can be chosen randomly. The other two wavelengths wherefore the Bragg condition is fulfilled, are fixed and determined by the n_{eff}. Only by changing the n_{eff} itself it is possible to change the third and fourth wavelength. The grating directionality can be greatly enhanced by using a bottom mirror [11] or a silicon overlay [7]. However, these methods are inherently wavelength dependent and thus give rise to a coupling efficiency trade-off, unlike uni-wavelength uni-polarization grating couplers which can in theory almost achieve 100% coupling efficiency [8]. The grating with a silicon overlay has a very high (90%) directionality and broad bandwidth making it very suitable for multi-wavelength grating couplers. The bottom mirror approach can achieve full directionality for several wavelengths by choosing the right mirror/grating separation, but this will result in a narrower band coupling spectrum around the central wavelengths.

The most significant trade-off for a forward and backward coupling grating is the mode-matching in the z-direction [12]. The Gaussian fiber mode needs to be matched to the exponential decaying field of the grating. This is schematically shown in Fig. 2. For uni-directional gratings there is no restriction on the length, thereby assuring that all the light is diffracted and mode-matching is maximized. For a uniform grating coupler, the optimal mode-matching $\sim 80\%$ is obtained for a distance d between the optical fiber center and the grating edge approximately equal to the decoupling length $L_C = (2\alpha)^{(-1)}$ with 2α the coupling strength of the grating [13], [14], [15], [16]. For bi-directional uniform gratings optimal simultaneous forward and backward coupling is achieved for a grating length in the order of 2.5x the decoupling length L_C. This reduced length and non-optimal fiber position decreases the maximum obtainable mode overlap to 70%. Furthermore, when coupling light out of the chip, a certain amount of light will couple into the opposite waveguide resulting in crosstalk [12] (see Fig. 2). Depending on the application this crosstalk is unwanted and should be filtered.

By chirping or apodizing the grating strength, the electrical field profile from the grating can be matched to the Gaussian field profile of the fiber [17], [8]. However, optimizing the mode-matching for coupling in one direction worsens the mode-matching for coupling in the opposite direction. For bi-directional grating couplers it's thus impossible to achieve perfect mode-matching for both forward and backward coupling simultaneously. The same problem occurs if one tries to focus the coupled light by curving the grating [11], which will result in a defocusing for the opposite coupling direction.

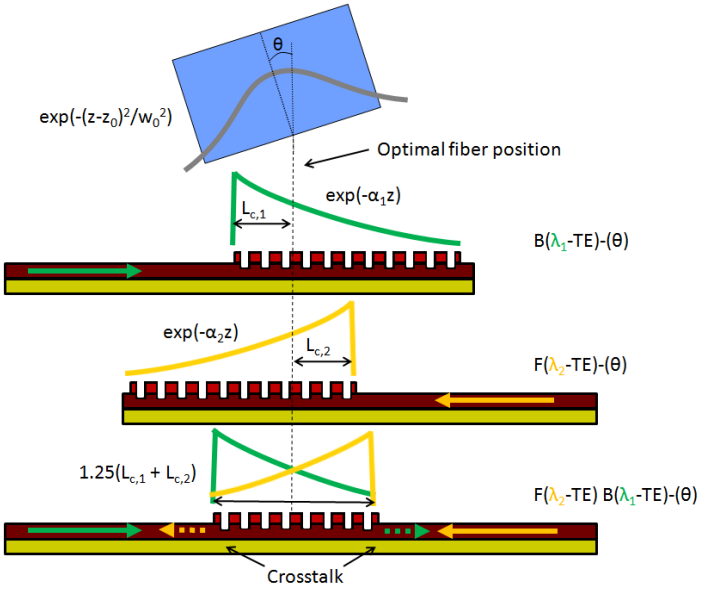

Fig. 2: Mode-matching for uni-directional and bi-directional grating couplers.

3. F(1310nm-TE) B(1520nm-TE)

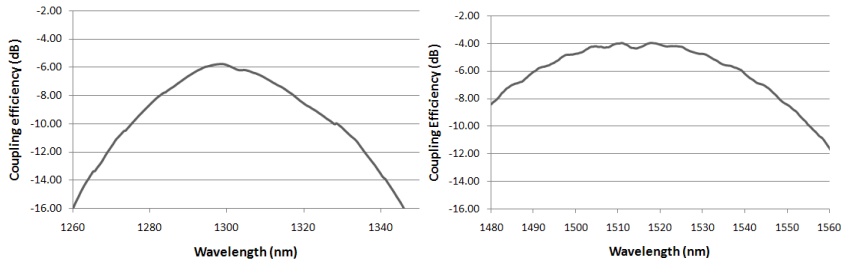

(a) $F(1310\,\mathrm{nm} - TE) - (10\,^\circ)$ (b) $B(1520\,\mathrm{nm} - TE) - (10\,^\circ)$

Fig. 3: Measured coupling efficiency of the $F(1310\,\mathrm{nm} - TE)\,B(1520\,\mathrm{nm} - TE) - (10\,^\circ)$ grating duplexer.

A grating duplexer, first reported in [12], is a 1D bi-directional grating coupler which couples two wavelengths in opposite directions, thereby acting as a coupler and splitter at the same time. In this section we will investigate the $F(1310\,\mathrm{nm} - TE)\,B(1520\,\mathrm{nm} - TE)$ grating duplexer. After solving the Bragg conditions CAMFR [18], a rigorous two-dimensional bidirectional mode expansion tool with perfectly matched layer absorbing boundary conditions, is used to optimize

the grating period, duty cycle, number of periods and optical fiber tilt angle by using a particle swarm optimization algorithm [19]. The period of the optimal grating is $520\,\mathrm{nm}$ and the duty cycle is 39%. The etch depth is $70\,\mathrm{nm}$. The number of grating periods is 20. The theoretical coupling efficiency is $-4\,\mathrm{dB}$ for both $1310\,\mathrm{nm}$ and $1520\,\mathrm{nm}$. The fabrication was performed on a $200\,\mathrm{mm}$ SOI wafer, consisting of a $220\,\mathrm{nm}$ silicon waveguide layer and a $2\,\mu\mathrm{m}$ buried oxide layer on a silicon substrate. $193\,\mathrm{nm}$ DUV lithography CMOS technology was used for fabrication. The measurement results of the grating duplexer are plotted in Fig. 3a and 3b. Index matching fluid was applied between the optical fiber facet and the grating duplexer to avoid reflections at the fiber facets and the fiber was tilted under an angle of $10\,^\circ$. The single-mode fiber had a mode field diameter ($1/e^2$ intensity width) of $10.4\,\mu\mathrm{m}$. TE-polarized light was used for the characterization of both wavelength bands. The position of the optical fiber was optimized only once, whereafter all measurements took place. The measured coupling efficiencies of the central wavelengths are $-6\,\mathrm{dB}$ for $1300\,\mathrm{nm}$ and $-4\,\mathrm{dB}$ for $1520\,\mathrm{nm}$. Decreasing these losses can be done by first depositing an extra silicon layer before defining the grating [7]. Simulations show that this overlay can boost efficiencies up to $-1.9\,\mathrm{dB}$ for both central wavelengths.

4. F(1310nm-TE) B(1310nm-TM)

An interesting subclass of bi-directional grating couplers couple in the orthogonal polarizations of the same wavelength in opposite directions [20], acting as both a coupler and polarization splitter for polarization diversity circuits [21]. In [22] a $F(1550\,\mathrm{nm}-TE)\,B(1550\,\mathrm{nm}-TM)-(15\,^\circ)$ grating coupler has been demonstrated with an efficiency of $-4.8\,\mathrm{dB}$ for the TE-polarization and $-3.6\,\mathrm{dB}$ for the TM-polarization. Using amorphous silicon and layers of Si/SiO2 as a dielectric Bragg mirror [23], these efficiencies could be increased to $-3\,\mathrm{dB}$ [24]. Here we will investigate the $F(1310\,\mathrm{nm}-TE)\,B(1310\,\mathrm{nm}-TM)$ grating coupler with and without silicon overlay to enhance the directionality. In depth analysis of the polarization dependent loss (PDL) will be given and finally the measurement results of this grating coupler without silicon overlay will be presented.

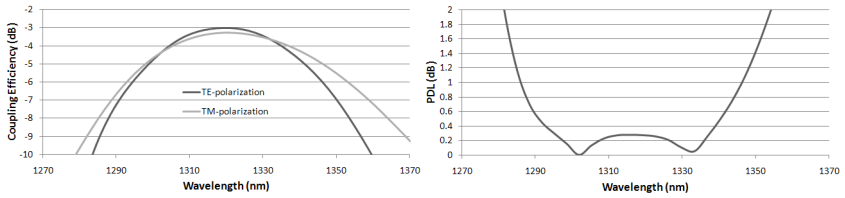

(a) Simulated coupling efficiency spectra (b) Polarization dependent loss (PDL) spectrum

Fig. 4: Simulations for the $F(1310\,\mathrm{nm}-TE)\,B(1310\,\mathrm{nm}-TM)-(9\,^\circ)$ grating using a silicon overlay.

The coupling spectra of the optimized grating coupler $F(1310\,\mathrm{nm}-TE)\,B(1310\,\mathrm{nm}-TM)$ with silicon overlay are plotted in Fig. 4a. First CAMFR was used to optimize the grating parameters by maximizing the product of the coupling efficiencies. Then, a second optimization of the fiber angle and position was done using 2D FDTD simulations in order to minimize the PDL over a broad wavelength range. This PDL minimization technique is shown in Fig. 5a. By varying the angle θ of the optical fiber, the central wavelengths of the coupling spectra can be changed such that they coincide. By varying the position z of the optical fiber, one can optimize the coupling efficiency for both polarizations such that the PDL is small over a broad wavelength range. The optimized parameters are summarized in Table Ia. The maximum theoretical coupling efficiency is $-3\,\mathrm{dB}$ for $1319\,\mathrm{nm}$, comparable to efficiencies obtained using a bottom DBR mirror. The PDL, plotted in Fig. 4b, is lower than $0.6\,\mathrm{dB}$ within the $-3\,\mathrm{dB}$ coupling efficiency bandwidth range of $50\,\mathrm{nm}$.

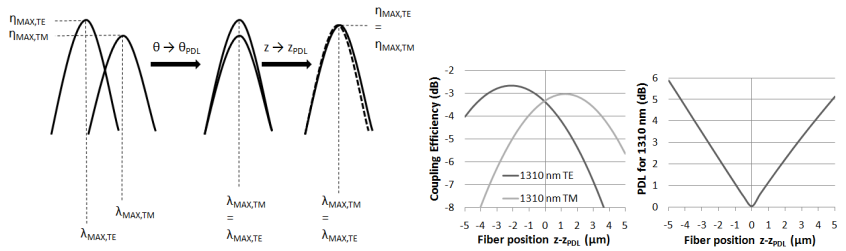

(a) PDL minimization technique (b) (c)

Fig. 5: PDL minimization technique and alignment sensitivity plots for the optimized $F(1310\,\mathrm{nm}-TE)\,B(1310\,\mathrm{nm}-TM)-(9\,^\circ)$ grating using a silicon overlay.

design	(a)	(b)
λ_1 (nm)	1310	1310
λ_2 (nm)	1520	1625
overlay thickness (μm)	0.13	0.0
etch depth (μm)	0.19	0.07
grating period (μm)	0.490	0.536
duty cycle (unetched)	0.55	0.48
fiber tilt θ ($^\circ$)	9.0	14.9
number of periods	18	18

TABLE I: Optimized $F(1310\,\mathrm{nm}-TE)\,B(1310\,\mathrm{nm}-TM)$ grating coupler designs with silicon overlay (a) and without silicon overlay (b). The fiber angle and position are optimized in order to have minimal PDL over a broad wavelength range.

In Table Ib the optimized parameters for the $F(1310\,\mathrm{nm}-TE)\,B(1310\,\mathrm{nm}-TM)$ grating coupler without silicon overlay are summarized. The simulated coupling spectra are plotted in Fig. 6a and 6b. The theoretical coupling efficiency is $-3.5\,\mathrm{dB}$ for $1310\,\mathrm{nm}$. The PDL for the $1310\,\mathrm{nm}$ wavelength band is lower than $0.6\,\mathrm{dB}$ within $45\,\mathrm{nm}$ of the $-3\,\mathrm{dB}$ coupling efficiency bandwidth range of $50\,\mathrm{nm}$. The grating coupler was measured in a loop test circuit shown in Fig. 7. A deterministic polarization scanning method was used for measuring the PDL as a function of the wavelength. By adjusting the fiber angle and position, as shown in Fig. 5a, the PDL could be minimized over a broad wavelength range. The optimal angle obtained with this PDL minimization technique is $14\,^\circ$, which differs from the theoretical fiber angle because of fabrication variations in the silicon waveguide thickness and etch depth of the grating. The measured transmission spectra, see Fig. 6a, shows $-5.2\,\mathrm{dB}$ coupling efficiency for $1300\,\mathrm{nm}$ with a $-1\,\mathrm{dB}$ optical bandwidth of $30\,\mathrm{nm}$. Index matching fluid was applied between the optical fiber facet and the fiber coupler to avoid reflections at the fiber facets. As shown in Figure 6b, from $1240\,\mathrm{nm}$ to $1312\,\mathrm{nm}$ the fiber-to-fiber PDL is lower than $1\,\mathrm{dB}$, which covers $42\,\mathrm{nm}$ within the $-3\,\mathrm{dB}$ coupling efficiency bandwidth of $50\,\mathrm{nm}$. The difference in coupling efficiency of $2\,\mathrm{dB}$ between simulations and experiment is mainly ascribed to a high bend loss for $1310\,\mathrm{nm}$ TM-polarized light in the $5\,\mu\mathrm{m}$ radius bends. This inherent PDL of the test circuit itself, however, is neutralized by moving the fiber position during the PDL minimization technique where the fiber and grating act as a tunable polarization and power splitter. In Fig. 5b and 5c the PDL is plotted as a function of the fiber position z. By moving the fiber one can control the PDL of the fiber coupling and thus counteract PDL created in the integrated circuit.

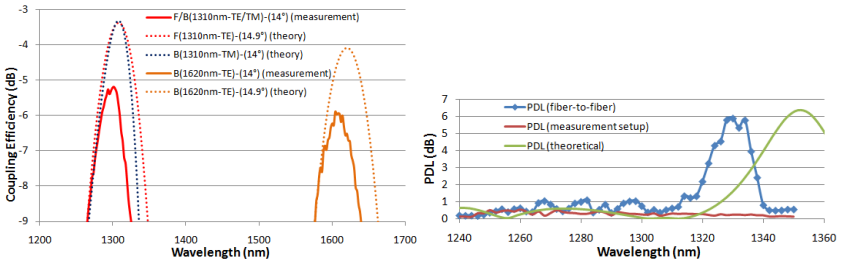

(a) (b)

Fig. 6: Theoretically and experimentally obtained fiber-to-waveguide coupling spectra (a) and PDL (b) for the $F(1310\,\mathrm{nm}-TE)\,B(1310\,\mathrm{nm}-TM)$ grating coupler design in Table Ib.

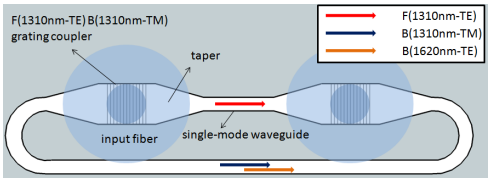

Fig. 7: Top view of the measured Silicon-on-Insulator polarization independent nanophotonic waveguide circuit.

5. F(1310nm-TE) B(1620nm-TE,1310nm-TM)

The measured $F(1310\,\mathrm{nm}-TE)\,B(1310\,\mathrm{nm}-TM)-(14\,^\circ)$ grating coupler from the previous section, also showed efficient backward coupling[4] for $1610\,\mathrm{nm}$ TE-polarized light with a coupling effiency of $-5.9\,\mathrm{dB}$ and a $-1\,\mathrm{dB}$ optical bandwidth of $35\,\mathrm{nm}$ (see Fig. 6a). As far as we know this is the first demonstration ever of a triple wavelength grating coupler. This type of grating coupler could be interesting for coupling a certain wavelength with unknown polarization (in this case $1310\,\mathrm{nm}$) into the chip and another wavelength, in this case $1610\,\mathrm{nm}$, with a fixed polarization out of the chip. One can for example use $1310\,\mathrm{nm}$ as pump light for an active component on the chip by coupling it in in a polarization independent way. Another application could be for example a Fiber-To-The-Home (FTTH) transceiver in the Central Office (CO) where the light for the upstream channels ($1490\,\mathrm{nm}$ and $1550\,\mathrm{nm}$) is provided by a laser of which the polarization is known and the polarization of the downstream wavelength ($1310\,\mathrm{nm}$) is unknown and can vary over time. We tried to optimize a grating coupler for $F(1310\,\mathrm{nm}-TE)\,B(1520\,\mathrm{nm}-TE, 1310\,\mathrm{nm}-TM)$ functionality, required for this FTTH transceiver. Without using a silicon overlay no solution was found. By introducing the silicon overlay, however, an extra degree of freedom was created to engineer the effective refractive index of the Bloch mode thereby enabling a highly efficient $F(1310\,\mathrm{nm}-TE)\,B(1520\,\mathrm{nm}-TE, 1310\,\mathrm{nm}-TM)$ grating coupler. For example, the silicon overlay grating with the optimized parameters from Table Ia shows a $-2.6\,\mathrm{dB}$ coupling for backward coupling of $1510\,\mathrm{nm}$ TE-polarized light besides the $-3\,\mathrm{dB}$ coupling efficiency for both orthogonal polarizations of $1310\,\mathrm{nm}$.

[4] for the same position of the optical fiber

6. Conclusion

We explored uniform 1D grating couplers on an SOI platform. A short notation for referring to more complicated 1D grating couplers was introduced. Three types of grating couplers were presented and experimentally verified: a $F(1310\,\mathrm{nm} - TE)\,B(1520\,\mathrm{nm} - TE)$ grating duplexer, a polarization splitting $F(1310\,\mathrm{nm} - TE)\,B(1310\,\mathrm{nm} - TM)$ grating coupler and a $F(1310\,\mathrm{nm} - TE)\,B(1610\,\mathrm{nm} - TE, 1310\,\mathrm{nm} - TM)$ triple wavelength grating coupler. Simulations show that by using a grating with silicon overlay, the effective refractive index of the grating can be engineered effectively to create a $F(1310\,\mathrm{nm} - TE)\,B(1520\,\mathrm{nm} - TE, 1310\,\mathrm{nm} - TM)$ grating coupler, which could have applications for FTTH transceivers. Recently, the second dimension of the grating has been explored using subwavelength structures to engineer the effective index of the Bloch modes in the grating [25], [26]. This extra degree of freedom could eventually lead to efficient quadruple wavelength engineered grating couplers.

References

[1] S. McNab, N. Moll, and Y. Vlasov, "Ultra-low loss photonic integrated circuit with membrane-type photonic crystal waveguides." *Optics express*, vol. 11, no. 22, pp. 2927–39, Nov. 2003. [Online]. Available: http://www.ncbi.nlm.nih.gov/pubmed/19471413

[2] M. Pu, L. Liu, H. Ou, K. Yvind, and J. r. M. Hvam, "Ultra-low-loss inverted taper coupler for silicon-on-insulator ridge waveguide," *Optics Communications*, vol. 283, no. 19, pp. 3678–3682, Oct. 2010. [Online]. Available: http://linkinghub.elsevier.com/retrieve/pii/S0030401810005018

[3] L. Zimmermann, H. Schröder, P. Dumon, W. Bogaerts, and T. Tekin, "ePIXpack - Advanced Smart Packaging Solutions for Silicon Photonics," in *ECIO*, Eindhoven, The Netherlands, 2008, pp. 33–36.

[4] D. Taillaert, W. Bogaerts, P. Bienstman, T. Krauss, P. Van Daele, I. Moerman, S. Verstuyft, K. De Mesel, and R. Baets, "An out-of-plane grating coupler for efficient butt-coupling between compact planar waveguides and single-mode fibers," *IEEE Journal of Quantum Electronics*, vol. 38, no. 7, pp. 949–955, Jul. 2002. [Online]. Available: http://ieeexplore.ieee.org/lpdocs/epic03/wrapper.htm?arnumber=1017613

[5] W. Bogaerts, D. Taillaert, P. Dumon, D. Van Thourhout, R. Baets, and E. Pluk, "A polarization-diversity wavelength duplexer circuit in silicon-on-insulator photonic wires." *Optics express*, vol. 15, no. 4, pp. 1567–78, Feb. 2007. [Online]. Available: http://www.ncbi.nlm.nih.gov/pubmed/19532389

[6] G. Roelkens, D. Vermeulen, D. Van Thourhout, R. Baets, S. Brision, P. Lyan, P. Gautier, and J.-M. Fedeli, "High efficiency diffractive grating couplers for interfacing a single mode optical fiber with a nanophotonic silicon-on-insulator waveguide circuit," *Applied Physics Letters*, vol. 92, no. 13, p. 131101, 2008. [Online]. Available: http://link.aip.org/link/APPLAB/v92/i13/p131101/s1&Agg=doi

[7] D. Vermeulen, S. Selvaraja, P. Verheyen, G. Lepage, W. Bogaerts, P. Absil, D. Van Thourhout, and G. Roelkens, "High-efficiency fiber-to-chip grating couplers realized using an advanced CMOS-compatible silicon-on-insulator platform." *Optics express*, vol. 18, no. 17, pp. 18 278–83, Aug. 2010. [Online]. Available: http://www.ncbi.nlm.nih.gov/pubmed/20721220

[8] D. Taillaert, F. Van Laere, M. Ayre, W. Bogaerts, D. Van Thourhout, P. Bienstman, and R. Baets, "Grating Couplers for Coupling between Optical Fibers and Nanophotonic Waveguides," *Japanese Journal of Applied Physics*, vol. 45, no. No. 8A, pp. 6071–6077, Aug. 2006. [Online]. Available: http://jjap.ipap.jp/link?JJAP/45/6071/

[9] Q. Huang and P. R. Ashley, "Holographic Bragg grating input-output couplers for polymer waveguides at an 850-nm wavelength." *Applied optics*, vol. 36, no. 6, pp. 1198–203, Feb. 1997. [Online]. Available: http://www.ncbi.nlm.nih.gov/pubmed/18250791

[10] D. Taillaert, P. Bienstman, and R. Baets, "Compact efficient broadband grating coupler for silicon-on-insulator waveguides." *Optics letters*, vol. 29, no. 23, pp. 2749–51, Dec. 2004. [Online]. Available: http://www.ncbi.nlm.nih.gov/pubmed/15605493

[11] F. Van Laere, G. Roelkens, M. Ayre, J. Schrauwen, D. Taillaert, D. Van Thourhout, T. F. Krauss, and R. Baets, "Compact and Highly Efficient Grating Couplers Between Optical Fiber and Nanophotonic Waveguides," *Journal of Lightwave Technology*, vol. 25, no. 1, pp. 151–156, Jan. 2007. [Online]. Available: http://ieeexplore.ieee.org/lpdocs/epic03/wrapper.htm?arnumber=4137620

[12] G. Roelkens, D. Van Thourhout, and R. Baets, "Silicon-on-insulator ultra-compact duplexer based on a diffractive grating structure." *Optics express*, vol. 15, no. 16, pp. 10 091–6, Aug. 2007. [Online]. Available: http://www.ncbi.nlm.nih.gov/pubmed/19547358

[13] J. Brazas and L. Li, "Analysis of input-grating couplers having finite lengths," *Applied Optics*, vol. 34, no. 19, pp. 3786–3792, 1995. [Online]. Available: http://www.opticsinfobase.org/abstract.cfm?URI=ao-34-19-3786

[14] D. Pascal, R. Orobtchouk, A. Layadi, A. Koster, and S. Laval, "Optimized coupling of a Gaussian beam into an optical waveguide with a grating coupler: comparison of experimental and theoretical results." *Applied optics*, vol. 36, no. 12, pp. 2443–7, Apr. 1997. [Online]. Available: http://www.ncbi.nlm.nih.gov/pubmed/18253224

[15] R. Orobtchouk, a. Layadi, H. Gualous, D. Pascal, a. Koster, and S. Laval, "High-Efficiency Light Coupling in a Submicrometric Silicon-on-Insulator Waveguide." *Applied optics*, vol. 39, no. 31, pp. 5773–7, Nov. 2000. [Online]. Available: http://www.ncbi.nlm.nih.gov/pubmed/18354577

[16] L. Vivien, D. Pascal, S. Lardenois, D. Marris-morini, E. Cassan, F. Grillot, A. Member, S. Laval, J.-m. Fédéli, and L. E. Melhaoui, "Light injection in SOI microwaveguides using high-efficiency grating couplers," *Journal of Lightwave Technology*, vol. 24, no. 10, pp. 3810–3815, Oct. 2006. [Online]. Available: http://ieeexplore.ieee.org/lpdocs/epic03/wrapper.htm?arnumber=1707847

[17] R. Waldhäusl, B. Schnabel, P. Dannberg, E. B. Kley, A. Bräuer, and W. Karthe, "Efficient coupling into polymer waveguides by gratings." *Applied optics*, vol. 36, no. 36, pp. 9383–90, Dec. 1997. [Online]. Available: http://www.ncbi.nlm.nih.gov/pubmed/18264498

[18] P. Bienstman and R. Baets, "Optical modelling of photonic crystals and VCSELs using eigenmode expansion and perfectly matched layers," *Optical and Quantum Electronics*, vol. 33, no. 4, pp. 327–341, 2001. [Online]. Available: http://www.springerlink.com/index/T6GR7M14164U64J0.pdf

[19] J. Kennedy, R. Eberhart, and Others, "Particle swarm optimization," in *Proceedings of IEEE international conference on neural networks*, vol. 4. Perth, Australia, 1995, pp. 1942–1948. [Online]. Available: http://www-com-serv.eng.cam.ac.uk/research/reading group/material/The Kalman Swarm.pdf

[20] Y. Tang, D. Dai, and S. He, "Proposal for a grating waveguide serving as both a polarization splitter and an efficient coupler for silicon-on-insulator nanophotonic circuits," *Photonics Technology Letters, IEEE*, vol. 21, no. 4, pp. 242–244, 2009. [Online]. Available: http://ieeexplore.ieee.org/xpls/abs_all.jsp?arnumber=4738359

[21] H. Fukuda, K. Yamada, T. Tsuchizawa, T. Watanabe, H. Shinojima, and S.-i. Itabashi, "Silicon photonic circuit with polarization diversity," *Quantum Electron*, vol. 16, no. 7, pp. 4872–4880, 2008. [Online]. Available: http://oe.osa.org/viewmedia.cfm?uri=oe-16-7-4872&seq=0

[22] Z. Wang, Y. Tang, N. Zhu, L. Wosinski, D. Dai, U. Westergren, and S. He, "Experimental demonstration of an ultracompact polarization beam splitter based on a bidirectional grating coupler," in *Communications and Photonics Conference and Exhibition (ACP)*, 2009, pp. 1–2. [Online]. Available: http://link.aip.org/link/PSISDG/v7631/i1/p763103/s1&Agg=doi

[23] S. Selvaraja, D. Vermeulen, M. Schaekers, E. Sleeckx, W. Bogaerts, G. Roelkens, P. Dumon, D. Van Thourhout, and R. Baets, "Highly efficient grating coupler between optical fiber and silicon photonic circuit," in *Lasers and Electro-Optics, 2009 and 2009 Conference on Quantum electronics and Laser Science Conference. CLEO/QELS 2009. Conference on*, vol. 1. IEEE, 2009, pp. 1–2. [Online]. Available: http://ieeexplore.ieee.org/xpls/abs_all.jsp?arnumber=5225319

[24] Z. Wang, Y. Tang, L. Wosinski, and S. He, "Experimental Demonstration of a High Efficiency Polarization Splitter based on a One-Dimensional Grating with a Bragg Reflector underneath," *Photonics Technology Letters, IEEE*, vol. 22, no. 21, pp. 1568–1570, 2010. [Online]. Available: http://ieeexplore.ieee.org/xpls/abs_all.jsp?arnumber=5559336

[25] L. Liu, M. Pu, K. Yvind, and J. M. Hvam, "High-efficiency, large-bandwidth silicon-on-insulator grating coupler based on a fully-etched photonic crystal structure," *Applied Physics Letters*, vol. 96, no. 5, p. 051126, 2010. [Online]. Available: http://link.aip.org/link/APPLAB/v96/i5/p051126/s1&Agg=doi

[26] X. Chen and H. Tsang, "Polarization-Independent Grating Couplers for Silicon-on-Insulator Nanophotonic Waveguides," *OPTICS LETTERS*, vol. 36, no. 6, pp. 796–798, 2011. [Online]. Available: http://www.opticsinfobase.org/ol/upcoming_pdf.cfm?id=139464

Efficient Tapering to the Fundamental Quasi-TM Mode in Asymmetrical Waveguides

D. Vermeulen, K. Van Acoleyen, S. Ghosh, S. Selvaraja, W.A.D. De Cort, N.A. Yebo, E. Hallynck, K. De Vos, P.P.P. Debackere, P. Dumon,W. Bogaerts, G. Roelkens, D. Van Thourhout and R. Baets
Photonics Research Group, Department of Information Technology (INTEC)
Ghent University - IMEC
Sint-Pietersnieuwstraat 41, 9000 Ghent, Belgium
Diedrik.Vermeulen@intec.ugent.be

Abstract—**The tapering problem of the fundamental quasi-TM mode in thin asymmetrical waveguides is investigated. Mode conversions are found to be at the origin of the failing adiabatic tapers. We propose and investigate three non-adiabatic taper solutions, a focusing grating coupler, a lensed taper and a discontinuous taper, which circumvent these mode conversions.**

Keywords-taper; quasi-TM; polarization; integrated photonics; asymmetrical waveguide; Silicon Photonics;

I. INTRODUCTION

Optical waveguides are the fundamental building blocks of integrated photonic devices. Besides waveguide loss, substrate loss, optical confinement and footprint one has to deal with polarization issues when designing a waveguide. In high index contrast platforms such as Silicon-On-Insulator (SOI), thin (subwavelength) waveguides are used resulting in quasi-polarized modes which differ substantially in effective refractive index (birefringence), optical confinement and waveguide loss. Besides the traditional optical communication application for integrated circuits where polarization diversity is required, interest in using the quasi-TM polarization is rising. One advantage is that because of a weaker optical confinement and because of a large evanescent field at the top of the waveguide, the quasi-TM mode is more suited for field interactions with deposited and bonded materials or for biosensing [1]. Another example is where the quasi-TM polarization is used to excite plasmons in a gold clad layer [2]. All these applications can result in highly asymmetrical waveguide structures. The problem is that asymmetrical waveguide circuits, unlike symmetrical ones, don't transmit any quasi-TM polarized light if adiabatic tapering from a multi-mode waveguide to a single-mode waveguide is present.

II. ADIABATIC MODE CONVERSIONS

All calculations have been performed for an SOI strip waveguide with a thickness of 220nm. When the top cladding of the waveguide is equal to the bottom cladding, we speak of a symmetrical waveguide. This vertical symmetry introduces a plane along which the mode is purely polarized, resulting in quasi-TE and quasi-TM modes. For waveguides where top and bottom cladding are different or in the case of a rib waveguide,

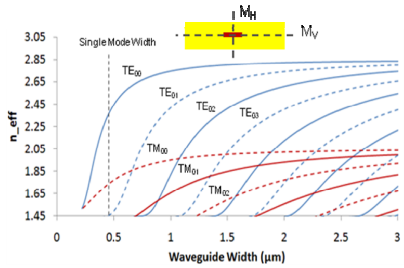

Figure 1. Adiabatic Mode Profile of a symmetric waveguide.

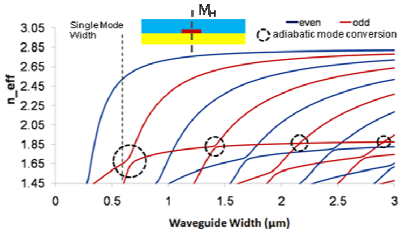

Figure 2. Adiabatic Mode Profile of an asymmetric waveguide.

the symmetry is broken and one cannot make a distinction between different quasi-polarized modes. As a convenience we shall use quasi-polarized mode naming in these asymmetrical waveguides referring to the quasi-polarized counterpart of the mode in the symmetrical case. Fig. 1 and 2 show the effective refractive index as a function of the waveguide width for all guided modes of respectively a symmetrical waveguide and asymmetrical waveguide. In a symmetrical waveguide two symmetry planes are present by which the modes can be

classified. Using the vertical symmetry (M_V), modes are split into quasi-TE and quasi-TM modes. The horizontal symmetry (M_H) subdivides these polarizations into even and odd modes. In an asymmetrical waveguide the symmetry plane for quasi-polarization classification disappears such that quasi-TE and quasi-TM modes can couple to each other in adiabatic tapers. The circles in Fig. 2 show the mode conversions from the fundamental quasi-TM mode to higher order quasi-TE modes. The latter are not guided in a single-mode waveguide what explains the breakdown of adiabatic tapering.

III. NON-ADIABATIC TAPERS

We will investigate different solutions which circumvent the mode conversion problem for tapering to the fundamental quasi-TM mode in an asymmetrical strip waveguide.

A. Focusing Fiber-To-Chip Grating Coupler

With a focusing grating coupler, see Fig. 3(a), one can couple and at the same time focus the light into a photonic wire [3]. This approach is experimentally verified and an efficiency of 13% is demonstrated for coupling from an optical fiber to the fundamental quasi-TM mode of a 220nm thick SOI single-mode photonic 500nm wire. The etch depth of the grating is 70nm and the top cladding is air, making the waveguide highly asymmetrical. The 1dB and 3dB bandwidth were respectively 45nm and 80nm.

B. Lensed Focusing Taper

Another way of avoiding the mode conversion problem due to adiabatic tapering is to use a focusing effect as is done in focusing grating couplers. This focusing effect can also be obtained by using in-plane lenses. These lenses can for example be fabricated in silicon using doping or by etching. The lenses considered here are made by etching 70nm of the 220nm high silicon area as shown in Fig. 3(b). Since the effective index of the etched area is smaller, a focusing lens has a concave shape. One can now design bi-concave and plano-concave lenses. From lensing theory it is known that the latter result in fewer aberrations when using them for focusing purposes. 2D effective index FDTD simulations were performed for focusing from a 10µm waveguide to a 450nm waveguide using bi-concave lenses. For a radius of curvature ranging from 5µm to 10µm, the focal length ranges from 9µm up to 23µm and the efficiency increases from 85% up to 90% respectively. The use of plano-concave lenses roughly doubles the focal distance but no significant improvement in efficiency was seen. The increase in efficiency for larger focal distances can be explained due to matching of the focused light to the diffraction of a 450nm waveguide. 3D-FDTD simulations were performed as well but these show a decrease in efficiency to about 30%. This is mainly due to the etch step which will scatter the light since the TM mode has the largest field intensity at the top and the bottom of the waveguide.

C. Discontinuous Taper

By avoiding the waveguide widths in a taper for which mode conversions take place, one can design a discontinuous taper as shown in Fig. 3(c). By optimizing the waveguide widths of the discontinuous sections of the taper with a 3D vectorial mode solver, 90% efficiency has been obtained for tapering from a 10µm waveguide to a 450nm waveguide of the fundamental quasi-TM mode.

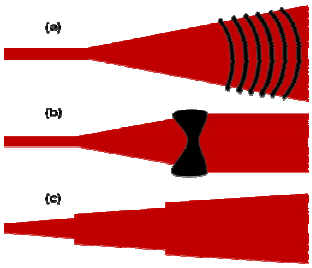

Figure 3. Non-Adiabatic tapers: (a) Focusing Grating Coupler (b) Lensed Focusing Taper (c) Discontinuous Taper

IV. CONCLUSION

We have found that asymmetrical adiabatic tapers exhibit a lot of mode conversions and are unsuitable for tapering of the fundamental quasi-TM mode. 13% coupling efficiency has been measured for a focusing grating coupler that couples and focus the light into a single-mode waveguide. 2D and 3D-FDTD simulations predict respectively 90% and 30% taper efficiency for a lensed focusing taper. According to 3D vectorial mode solving, an optimized discontinuous taper can have 90% taper efficiency. In symmetrical waveguides, process variations can break the symmetry resulting in mode conversions. In general one should avoid the waveguide widths near a mode conversion. For the same reason it is desirable to not make an adiabatic taper unnecessary long for symmetrical waveguides.

ACKNOWLEDGMENT

D. Vermeulen, W.A.D. De Cort and K. De Vos thank the Institute for the Promotion of Innovation by Science and Technology in Flanders (IWT) for a grant. K. Van Acoleyen, W. Bogaerts and G. Roelkens acknowledge the Research Foundation-Flanders (FWO-Vlaanderen) for a research grant.

REFERENCES

[1] A. Densmore, D. X. Xu, P. Waldron, S. Janz, P. Cheben, J. Lapointe, A. Delge, B. Lamontagne, J. H. Schmid, and E. Post, "A silicon-on-insulator photonic wire based evanescent field sensor," IEEE Photonics Technology Letters, 18:23 (2006), 2520-2522.

[2] P. Debackere, R. Baets, and P. Bienstman, "Bulk sensing experiments using a surface-plasmon interferometer," Optics letters, 34:18 (2009), 2858-2860.

[3] F. Van Laere, T. Claes, J. Schrauwen, S. Scheerlinck, W. Bogaerts, D. Taillaert, L. O'Faolain, D. Van Thourhout, and R. Baets, "Compact focusing grating couplers for silicon-on-insulator integrated circuits," IEEE Photonics Technology Letters, 19:23 (2007), 1919-1921.

III-V/Silicon-on-Insulator Photonic Integrated Circuit for Fiber-to-the-Home Central Office Transceivers in a Point-to-Point Network Configuration

D. Vermeulen[(1)], T. Spuesens[(1)], P. De Heyn[(1)], P. Mechet[(1)], R. Nötzel[(2)], S. Verstuyft[(1)], D. Van Thourhout[(1)], G. Roelkens[(1)]

[(1)] Photonics Research Group, Ghent University/IMEC, Sint-Pietersnieuwstraat 41, B-9000 Ghent, Belgium, diedrik.vermeulen@intec.ugent.be

[(2)] Photonics and Semiconductor Nanophysics, Eindhoven University of Technology, The Netherlands

Abstract *We describe the realization of III-V/silicon-on-insulator photonic integrated circuits for Fiber-to-the-Home transceivers in the central office. Above 0.4A/W responsivity is obtained in the 1310nm band (with polarization dependent loss below 0.5dB). Crosstalk from the 1490nm/1550nm wavelength channel is below -20dB.*

Introduction

In the Fiber-to-the-Home (FTTH) market, two technologies are competing: passive optical networks (PON) and Ethernet-based point-to point networks. The European market is mostly choosing Ethernet-based point-to-point. The Japanese and - to a lesser extent - the US markets are working with PON. Ethernet point-to-point has considerable advantages over PON: Ethernet is an open standard, upgrading is easier and the network is future-proof. However, PON has a strong advantage as well: since PON networks are shared between end-users, the space and power consumption required for the central office is much smaller. In addition, the cost of the PON central office equipment is less than for point-to-point access switches. Reducing the size, power consumption and cost of Ethernet-based central office equipment, which consists of an individual transceiver per user, would therefore take away important drawbacks of point-to-point networks.

Photonic integrated circuits allow integrating multiple optical components on a single chip, thereby realizing the required reduction in size, cost and power consumption for the central office equipment. Contrary to traditional platforms for photonic integration such as III-V monolithic integration, which requires expensive regrowth techniques, or silica-on-silicon, which is not compatible with a compact form-factor, the silicon platform seems the only one which is truly compatible with large scale integration. This is due to the high refractive index contrast that is available in so called silicon photonic wires, allowing for wavelength scale routing and handling of light on the SOI chip. Wafer-level processing using CMOS fabrication tools and wafer level testing will enable low cost levels.

Using high index contrast photonic integrated circuits for communication applications however also brings along considerable challenges, especially regarding the efficient fiber-to-chip coupling and polarization independent operation of the photonic integrated circuit. Especially since the photonic integrated circuit needs to be able to handle widely spaced wavelength bands. Efficient optical coupling (-1.6dB) from a single mode fiber to a silicon photonic wire was demonstrated[1] using a diffractive grating structure for a single polarization in the optical fiber. The 1dB optical bandwidth is limited to 50nm however. In order to address the polarization sensitivity of the grating coupler, a polarization diversity approach was presented[2] using two-dimensional grating couplers to couple both orthogonal polarizations to the silicon chip. While this allows reducing the polarization dependent loss, it also only works over a limited wavelength range, insufficient for Fiber-to-the-Home transceiver applications, where a 100nm wavelength band needs to be covered in the 1310nm wavelength range). Moreover, the two-dimensional grating approach introduces a decrease in fiber-to-chip coupling efficiency.

Since the FTTH transceivers require photodetection and light emission on the photonic integrated circuit, other materials need to be integrated in order to perform these functions. Ge-based photodetectors are a good option given their direct compatibility with the CMOS compatible processing of the silicon photonic integrated circuit. In this paper however we focus on a novel photodetector configuration based on a heterogeneously integrated III-V semiconductor photodetector. This approach has the advantage that it also allows the

integration of III-V light sources and III-V modulators on the same photonic integrated circuit.

Transceiver configuration

The layout of the considered device is schematically depicted in figure 1. The III-V semiconductor layer stack consists of an InP/InGaAsP p-i-n structure with an absorption layer with a band gap wavelength of 1.37µm. This bandgap wavelength allows the 1310nm wavelength band to be efficiently absorbed, while the absorption layer is transparent for the 1490nm-1550nm wavelength channels. In order for the detector to be completely transparent for these wavelength channels, the III-V layer stack thicknesses have been optimized for transparency at the central wavelength of 1520nm. The III-V heterostructure is transferred on top of a silicon grating coupler structure using DVS-BCB adhesive wafer bonding[3]. After layer transfer, the III-V photodetector is processed, lithographically aligned to the underlying silicon-on-insulator waveguide circuit. The main idea underlying this configuration is that it allows efficient detection with low polarization dependent loss over the full 1260nm-1360nm wavelength band, since this light is not coupled to the silicon waveguide layer. On the other hand, the 1490nm/1550nm wavelength channels (which are generated on chip and therefore have controlled polarization and better controlled emission wavelength) can be efficiently coupled from the silicon waveguide layer to the optical fiber using a one-dimensional diffractive structure (operating for a single polarization)[1].

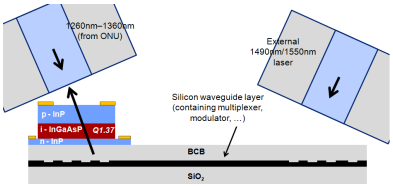

Fig. 1: Schematic cross-section of the III-V/SOI transceiver

A microscope image of a prototype device is depicted in figure 2. The III-V photodetector was processed on top of a silicon-on-insulator waveguide circuit consisting of a planar concave grating capable of multiplexing a 1490nm-band data signal and a 1550nm-band data signal in a single output waveguide. The devices were fabricated using standard CMOS fabrication tools on an 8inch SOI wafer consisting of a 220nm silicon waveguide layer and 2µm buried oxide layer thickness (through the multi-project wafer shuttle run service ePIXfab).

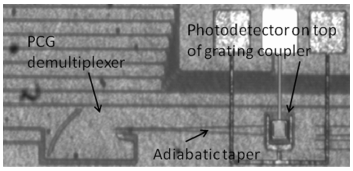

Fig. 2: Microscope image of the fabricated III-V/SOI transceiver circuit

This serves as a proof-of-principle that the silicon waveguide circuit can contain functional elements that handle 1490nm and 1550nm wavelength bands. In the future we will extend the functionality on the silicon platform by adding integrated power splitters, arrays of 1490nm and 1550nm modulators and wavelength multiplexers to realize integrated transceiver arrays (e.g. 8 channels) for central office equipment with a single CW external light source (VCSEL or DFB laser) per wavelength band, as shown in figure 3.

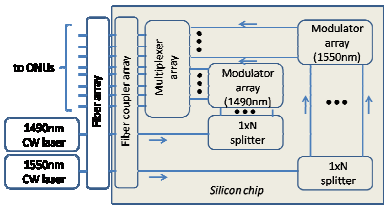

Fig. 3: Envisioned device configuration for integrated transceiver arrays for FTTH central office equipment

Transceiver characterization

The fabricated devices were characterized in the 1310nm and 1490-1550nm wavelength band. For this proof-of-principle device, a standard silicon diffractive grating structure was used with a known fiber-to-chip coupling efficiency of -6dB. The implementation of advanced fiber-to-chip couplers[1] with a fiber-to-chip coupling efficiency of -1.6dB is expected not to affect the operation principle of the proposed device. The optical fiber is tilted 10 degrees off vertical in order to avoid second order Bragg reflection from the silicon grating. Figure 4a shows the responsivity of the photodetector for the 1310nm wavelength band. It varies around 0.4A/W. The polarization dependent loss is plotted in figure 4b, showing excellent behaviour (<0.5dB PDL) over the full wavelength range.

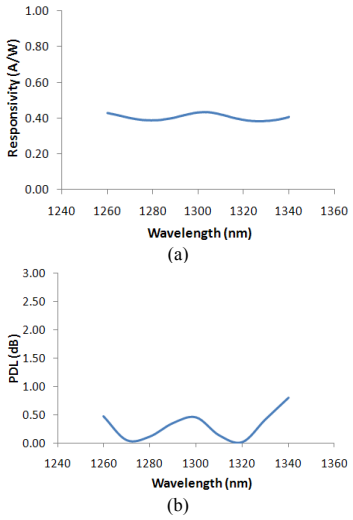

Fig. 4: Photodetector responsivity (a) in the 1310nm wavelength band and the associated polarization dependent loss (PDL) (b)

This would have been very hard to obtain when the 1310nm channel had to be coupled to the silicon waveguide circuit and demultiplexed from the 1490nm/1550nm signal prior to photodetection. Assuming an external laser source for the 1490nm/1550nm upstream channel (from the viewpoint of the central office equipment), the fiber-to-fiber transmission of the fabricated photonic IC (using two identical grating couplers of which one is covered by the heterogeneously integrated photodetector) was measured. -12dB peak transmission, consistent with the -6dB fiber-to-chip coupling efficiency of a single grating, was obtained. This shows that the integration of the photodetector on top of the fiber coupler doesn't aversely affect its performance in the 1490nm/1550nm wavelength range.

In order to assess if the integrated photodetector is truly transparent for the 1490nm/1550nm wavelength channel and doesn't introduce a significant electrical crosstalk in the photodetector, the device responsivity was also characterized in the 1490nm/1550nm wavelength band. This crosstalk, here defined as the ratio between the responsivity at a wavelength in the 1490nm/1550nm wavelength range to a typical responsivity of 0.4A/W in the 1310nm wavelength range is shown in figure 5, and is below -30dB. Therefore, even a significant difference in optical power between the point-to-point downstream 1310nm wavelength channel and the upstream 1490nm/1550nm wavelength channel of 10dB will still lead to better than -20dB crosstalk in the photodetector, thereby showing the feasibility of this approach. The planar concave grating, used to multiplex the 1490nm and 1550nm wavelength channels works as expected after photodetector integration (although with a higher insertion loss due to the cladding of the device with DVS-BCB, which reduced the power reflection at the silicon grating facets, but this can be accounted for in the design).

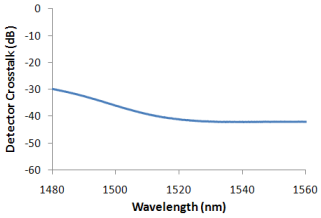

Fig. 5: Photodetector cross-talk due to the transmission of the 1490nm/1550nm data signal

At the conference, more data will be presented regarding the dynamic performance of the photodetector using modulated data signals.

Conclusions

This paper shows for the first time that a heterogeneous III-V/silicon photonic integrated circuit can be used to realize integrated transceiver arrays for Fiber-to-the-Home central office equipment in point-to-point networks. The concept is limited to operation in the central office, but there, the need for integration – in order to reduce the floor space and power consumption in the central office – is the most obvious.

Acknowledgements

This work was carried out in the framework of the Dutch Smartmix-Memphis project. D. Vermeulen and T. Spuesens thank the Institute for the Promotion of Innovation by Science and Technology in Flanders (IWT) for a grant. G. Roelkens acknowledges the Fund for Scientific Research Vlaanderen (FWO) for a postdoctoral grant.

References

1 D. Vermeulen et al., Proc. Group IV Photonics p. FPD1 (2009)
2 R. Halir et al,. Proc. OFC'10, p. OWJ1 (2010)
3 G. Roelkens et al., Jorn. Electrochem. Soc. p. G1015-G1019 (2006)

3

Polarization-Multiplexed (PM) Differential Quadrature Phase Shift Keying (DQPSK) Receiver

3.1 Introduction

For mid-reach and long-reach telecommunication networks, the optical link becomes very expensive and wavelength demultiplexing (WDM) is employed to scale the fiber capacity. This can be CWDM (with a coarse wavelength grid of typically 20 nm) or DWDM (with a dense wavelength grid of 0.8 nm or smaller). The typical frequency spacing used in DWDM networks is 100 GHz, 50 GHz or even 25 GHz. The low-loss C and L band of an optical fiber contain 100 channels with a 100 GHz spacing. Modulation by on-off keying (OOK) is simple to implement and commonly used for data or short-reach telecom applications, but for longer reach telecom applications the spectral efficiency is insufficient. Improving the spectral efficiency (bit/s/Hz) can be done by transmitting multiple magnitude levels, using the optical phase and/or using both polarizations [1]. Such an advanced modulation format is quadrature phase shift keying (QPSK) which provides two bits per symbol instead of one bit per symbol for standard OOK. The symbol diagrams of different formats are shown in Fig. 3.1. Four bits per symbol can be achieved if QPSK is combined with two magnitude levels. This

modulation format is called 16-QAM. However, going to multiple magnitude levels such as 16-QAM gives an optical signal-to-noise ratio (OSNR) penalty of about 4 dB with respect to QPSK for a constant bit rate and bit error rate (BER) of 10^{-3} . As an alternative, by using both orthogonal fiber polarizations the spectral efficiency can be doubled. This is called polarization multiplexing (PM) and together with QPSK a four bits per symbol modulation format can be achieved called PM-QPSK.
Advanced demodulation typically requires differential encoding to avoid the problem of cycle slips (any jump in phase will result in the loss of the absolute phase reference point). Differential encoding has the drawback of doubling the BER for QPSK [2]. A local laser, generally called local oscillator (LO), is used as a fixed CW light source to interfere with the incoming signal such that the optical phase can be extracted. This LO also amplifies the signal, increasing the sensitivity theoretically with 3 dB. Furthermore, digital signal processing (DSP) can compensate for many fiber impairments. The alternative to using a LO is a self-coherent receiver in which every symbol interferes with the previous one. This has the advantage of not needing a LO in the receiver. Furthermore, since the system is self-coherent the laser linewidth specifications are more relaxed. This self-coherent detection in combination with QPSK is called differential QPSK (DQPSK).
Transmitters and receivers using advanced modulation formats are very complex and need multiple optical components and electrical inputs/outputs. Because of this complexity such transceivers are perfect candidates for optical integration. Especially when the phase and optical delay between different optical components has to be controlled accurately, lithographic alignment achieved through optical integration is a key advantage with respect to the splicing or board assembly of multiple optical components. In this chapter I will focus on integrating a receiver for DPSK, DQPSK and PM-DPQSK modulation formats.

3.2 Single polarization DQPSK receiver

The first challenge is to make a DQPSK receiver which works for one polarization. This device can be used in a system where the polarization is controlled or as a subcircuit in a PM-DQPSK receiver.

3.2.1 Differential phase shift keying (DPSK) circuit fabricated by means of e-beam lithography

A first circuit was fabricated by means of e-beam lithography at the Valencia Nanophotonics Technology Center in cooperation with DAS photonics. E-beam lithography provides a quick prototyping method for integrated circuits with

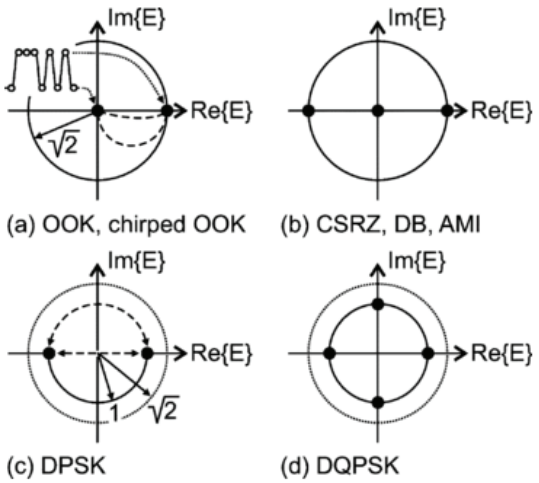

Figure 3.1: Modulation formats symbol diagrams: On-Off Keying (a) , Duobinary (b), Differential Phase Shift Keying (C) and Differential Quadrature Phase Shift Keying (d). (Courtasy of Peter Winzer [1])

respect to optical lithography through a CMOS fab which can easily take a few months. However, since it is a serial writing technique, there are some drawbacks in making large integrated photonic circuits. The typical writing field of an e-beam is 100 μm by 100 μm and stitching errors due to misalignment occur at the intersection of the writing fields. A waveguide passing at a writing field intersection thus has to be avoided as much as possible since it introduces waveguide loss and will backscatter the light. Another design issue that needs to be taken into account is a fixed drift of the writing field of about 60 nm per hour in the case there are no re-alignment procedures used. This drift will introduce a stitching error.

A silicon photonics DPSK demodulator was fabricated using e-beam lithography for 5 GHz, 10 GHz, 20 GHz and 40 GHz symbol rates. The main advantage of silicon photonics with respect to III/V based circuits is that the passive optical loss is typically much smaller and consistent and on the order of 0.5 dB/cm to 2 dB/cm, depending on the waveguide cross section and fabrication process. A delay line for 5 GHz symbol rate is 1.8 cm long, thus introducing a 1 dB to 4 dB loss. The received light needs to be split and one part is delayed by exactly one symbol period. I use a variable optical splitter to compensate for the optical loss in the delay line such that the interfering symbols are power balanced. This variable optical splitter is implemented using an MZI where at least one arm has an optical phase shift modulator based on the thermo-optic effect (further

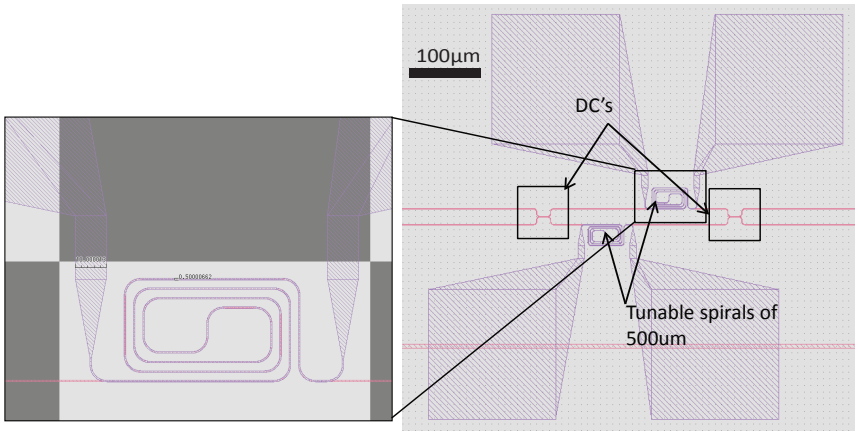

Figure 3.2: Mask design of a tunable MZI splitter optimized for e-beam lithography.

called heater). The waveguide with heater is 500 μm long an rolled up in a spiral such that it only occupies one e-beam writing field, as can be seen in Fig. 3.2. In Fig. 3.3 and 3.4 the design and fabricated device with a tunable splitter, delay line and 180° hybrid[1] interferer are shown. The hybrid is a tunable MZI. The delay line is 0.9 cm long and is divided in four spirals which each fit exactly in one writing field. The total number of writing field intersections for the delay line is thus four, minimizing the optical loss due to stitching errors. Light is coupled into and out of the chip by means of horizontal coupling to a 3 μm broad silicon waveguide. Static measurements showed the principle of the delay interferometer and compensation of the delay line loss with the variable optical splitter. High-speed measurement of a similar device can be found in [3].

3.2.2 90 degree hybrid

A 4-port 3 dB splitter such as a two by two MMI will interfere the two inputs in a balanced way and with a relative phase of ±90°, achieving a 180° hybrid. With a combination of 3 dB splitters and optical phase shifters one can easily form a 90° hybrid. However, a non-tunable 90° hybrid is preferred. One such component is a 6-port two by four MMI as reported in [4, 5]. The MMI design is shown in Fig. 3.5. It uses a shallowly etched multimode region to reduce the phase errors, in combination with deeply etched input and output waveguides. A Common Mode Rejection Ratio (CMMR) better than −20 dBe can be achieved together with phase errors better than ±5° in a ~ 50nm optical bandwidth.

[1] 90°/180° hybrids are the special case of a two/four-port directional coupler that is designed for a 3dB (equal) power split.

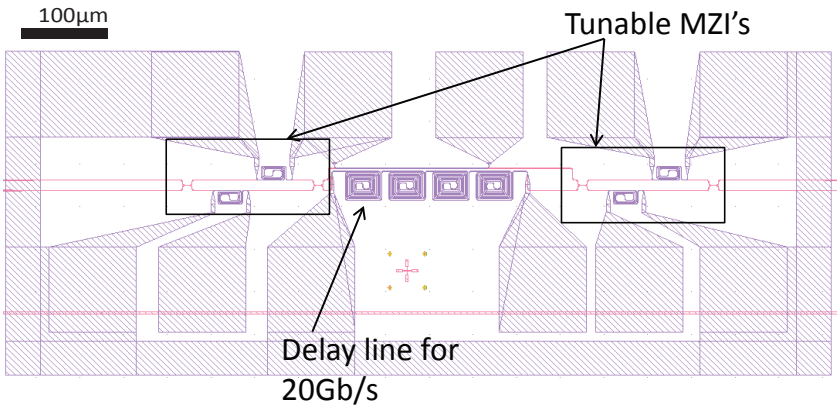

Figure 3.3: Mask design of a DPSK receiver with tunable MZI splitter and combiner for e-beam lithography. The delay line is sectionized such that the number of writing field intersections is minimized.

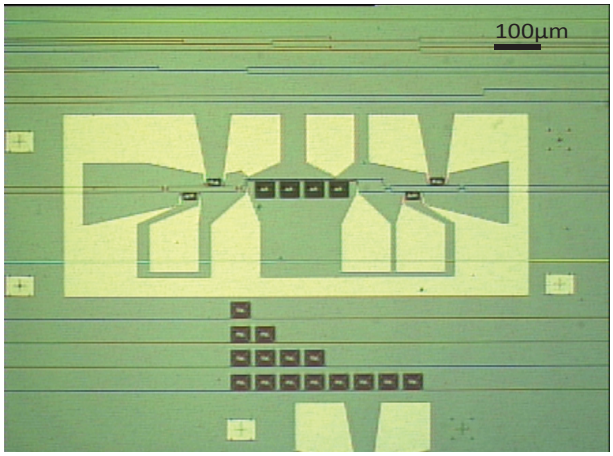

Figure 3.4: Microscope picture of a fabricated DPSK receiver with e-beam lithography.

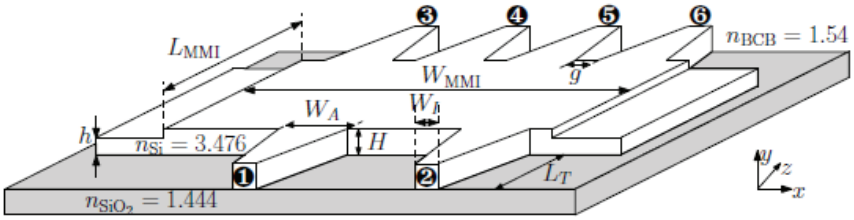

Figure 3.5: Schematic drawing 90° hybrid MMI geometry. Refractive indices are given at $\lambda = 1.55\mu$m. (courtesy of Rober Halir)

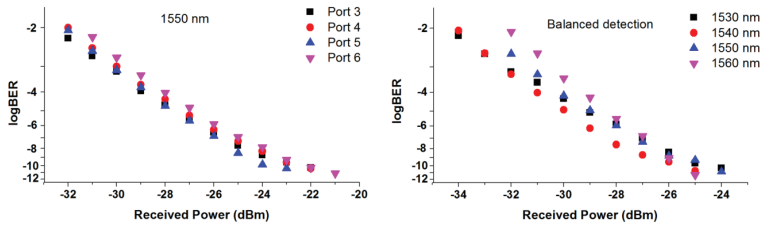

(a) 4 output ports (single-ended detection) (b) 4 wavelengths (balanced detection)

Figure 3.6: BER vs. received power measurements. (courtesy of Nikolaos Sotiropoulos)

A demodulator based on this 90° hybrid MMI has been characterized in [6]. The performance of the demodulator is evaluated for a number of operating wavelengths, with results indicating good uniformity and low wavelength dependency. BER measurements as a function of the received power for every output of the device, with single-ended detection, for a number of wavelengths were performed. The BER curves for 1550 nm are shown in Fig. 3.6(a), obtained using a pattern length of $2^{31} - 1$ in the experiments. From the results it can be seen that there is good uniformity between all the outputs of the device. As far as wavelength dependency is concerned, optimal performance is observed for the 1535 nm – 1550 nm range. This is in agreement with the CW measurements, which indicated optimum performance up to a wavelength of 1560 nm. Experiments involving balanced detection of a pair of outputs were performed. The results of balanced detection for outputs 3 and 6 for a PRBS of $2^7 - 1$ and for a number of wavelengths can be seen in Fig. 3.6(b). An improvement over the single-ended case, as expected, together with a small wavelength dependency of around 1 dB can be observed.

3.2.3 DQPSK receiver demonstrator with zero biased balanced photodetectors

The next step is to co-integrate the photodetectors. To have a 3 dB increase in sensitivity of the receiver, balanced detection can be used instead of single-ended detection. We demonstrated within the context of the Helios project, a 2-port balanced germanium photodetector which is laterally doped in a zero-biased pinpin configuration [7]. This photodetector was designed by the Institut d'Electronique Fondamentale (IEF). The generated currents are automatically subtracted and hence achieving balanced detection. The Balanced PhotoDetector (BPD) works at zero bias. This lateral pinpin germanium balanced photodetector is only 10μm long and is selectively grown at the end of silicon waveguides.
The balanced photodetectors were characterized using a DQPSK receiver and the results published in [7]. This paper is attached at the end of this chapter page 3-18. The layout of this receiver is shown in Fig. 3.7 and a microscope picture of the design fabricated at LETI is shown in Fig. 3.8. It includes a variable optical MZI power splitter, a delay line of 100 ps (for 10 GHz symbol rate or 20 Gb/s bitrate in the case of a 2 bits per symbol modulation format such as DQPSK), a 90° hybrid MMI and a pair of balanced photodetectors. The length of the waveguide pairs connecting two corresponding output ports of the 90° hybrid to a balanced photodetector are equal. However, the length of both pairs is not equal, introducing a (controlled) skew between the quadrature signals. The DC contact pads of the heaters and the RF contact pads of the balanced photodetectors are placed in the north and east quadrant respectively and at a fixed pitch for easy probing with probe arrays.
To test the high speed behavior of the receiver an optical data stream was generated using a Lithium Niobate (LN) dual-drive modulator generating a DQPSK signal. Measurements were carried out by the Universidad Politecnica de Valencia, DAS photonics and the Technical university of Eindhoven. The bit streams used were two decorrelated pseudorandom binary sequences (PRBS) with a pattern length of $2^{23}-1$ at 10 Gbps and 20 Gbps, generated by a bit pattern generator (SHF BPG 44E). The eye and symbol diagram of the input signal are shown in Fig. 3.9. At the output of the chip, the signal was extracted directly from the photodiodes using a GSGSG probe and fed to a Communication Analyzer. Fig. 3.10 and Fig. 3.11 show the open eye-diagrams and symbol diagrams at 10 Gbps and 20 Gbps operation respectively after offline processing. These results show the feasibility of Silicon Photonics for coherent detection applications. More details about the experiment can be found on page 3-24.

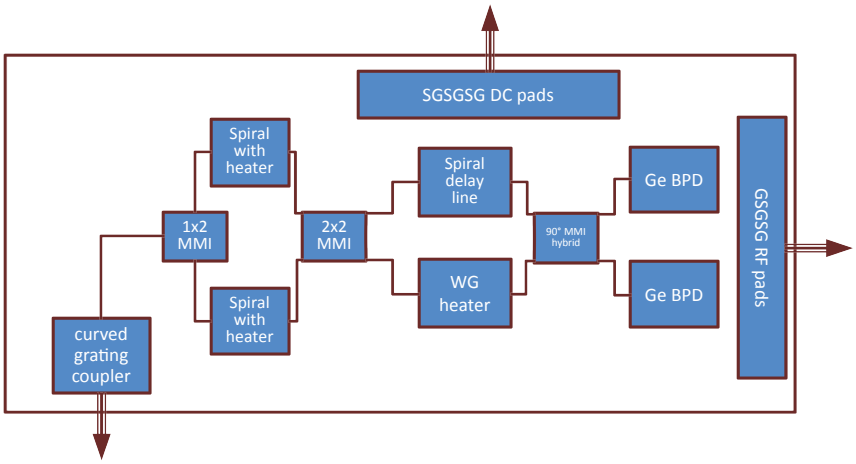

Figure 3.7: DQPSK receiver Silicon Photonics circuit layout. The arrows are the probing direction of a component.

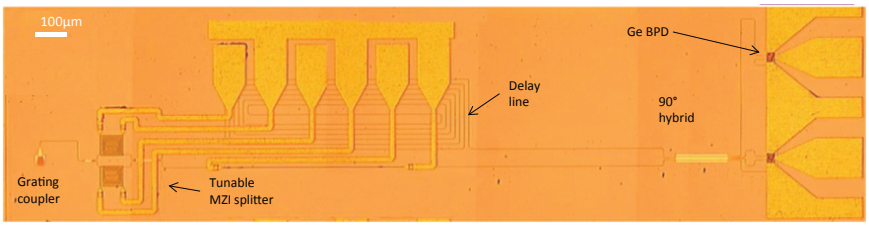

Figure 3.8: DQPSK receiver demonstrator with balanced Ge photodetectors.

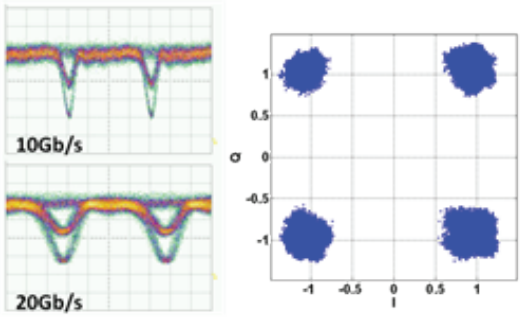

Figure 3.9: Eye diagrams and symbol diagram for the DQPSK transmitted signal.

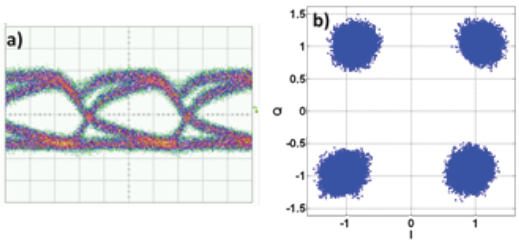

Figure 3.10: DQPSK eye diagram (a) and symbol diagram (b) measured for the 10 Gbps *differential receiver with a received power of* −19 dBm.

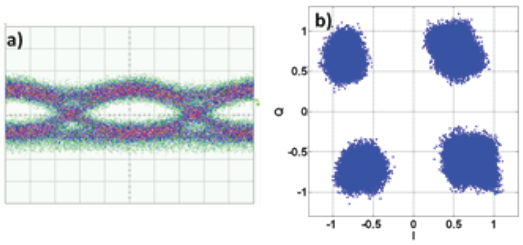

Figure 3.11: DQPSK eye diagram (a) and symbol diagram (b) measured for the 20 Gbps *differential receiver with a received power of* −12 dBm.

3.3 Polarization-multiplexed DQPSK receiver

The bitrate can be doubled by using orthogonal polarizations in a single-mode fiber. This is called polarization multiplexing (PM) and can be combined with for example DQPSK to achieve a 4 bits per symbol modulation format. For polarization multiplexing at the transmitter one needs to double the amount of single-polarization transmitters, rotate the modulated signal of one circuit and combine them into the fiber. Polarization demultiplexing at the receiver is more difficult since the polarization rotation in the optical fiber is random and varies with time. There exist a number of solutions to this problem. I have explored the feasibility of a polarization tracking receiver for PM-DQPSK [8] using Silicon Photonics by demonstrating all necessary subcomponents.

3.3.1 Polarization splitter and filter

High-index waveguide cross sections are highly birefringent and the on-chip light is mainly manipulated while being in the TE-polarization state in the waveguide. However, the TM mode is sometimes used if low backscattering or high top surface sensitivity is required. For a receiver which employs horizontal fiber-to-chip coupling, the orthogonal polarized modes in the fiber will excite the

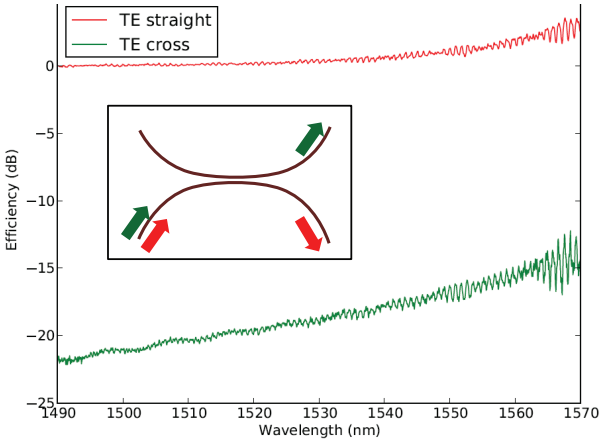

Figure 3.12: Measured efficiency for the polarization splitting directional coupler when the TE-polarized mode is launched.

corresponding TE and TM mode in a single-mode waveguide. In order to process both polarizations, the orthogonal polarized modes have to be split on the chip. We have demonstrated a polarization splitter by using a deeply etched directional coupler. The splitting principle makes use of the difference in confinement and effective refractive index between the TE and TM mode for single-mode waveguides with 220 nm x 500 nm dimensions. The TM mode is much less confined than the TE mode and will couple very efficiently to the adjacent waveguide while the TE mode does not couple at all. The optimal waveguide spacing is found to be 400 nm. The measurements of a polarization splitter of length 9.8μm are shown in Fig. 3.12 and Fig. 3.13. These measurements were performed by means of grating couplers. A drawback of grating couplers is that the exact coupling spectrum is dependent on the fiber position. A small shift in the spectrum is introduced due to small misalignments, although the spectral shape and center efficiency stay quasi constant. This is the reason why some un-physical, i.e. no power conservation, effects are measured at the edge of the spectrum. The TE to TM crosstalk (TE cross) is about −20 dB. The TM to TE crosstalk (TM straight) ranges from −10 dB to −40 dB.

This polarization splitter can be used as a polarization filter. A broadband polarization filter with better than −40 dB crosstalk can be designed by cascading a series of polarization filters with different crosstalk minima. Alternatively, one could use a waveguide cross section which does not guide the TM mode or a sharp waveguide bend which exhibits high TM loss.

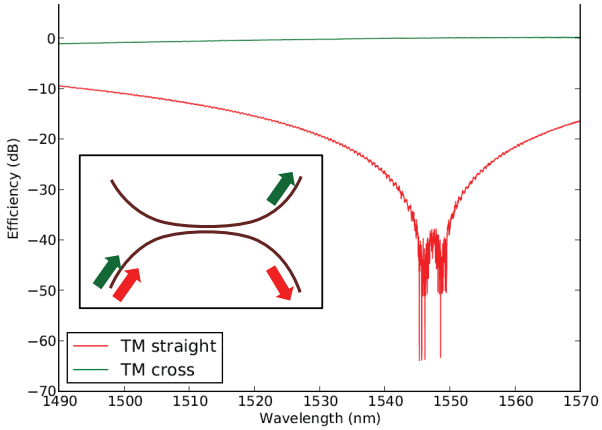

Figure 3.13: Measured efficiency for the polarization splitting directional coupler when the TM-polarized mode is launched.

3.3.2 Polarization rotator

A polarization rotator has long been a missing component in silicon PICs. It requires to specifically break the vertical symmetry of the system which is typically not easy in a planar fabrication process flow while fulfilling all design rules. I have demonstrated a polarization rotator in [9], attached at the end of this chapter page 3-21, based on the advanced *imec* process flow with silicon overlay as shown in Fig. 2.13. Fig. 3.14 shows a schematic picture of the polarization rotator together with a high-efficiency grating coupler. The SEM image bird's eye view of a realized polarization rotator is shown in Fig. 3.15. The polarization rotator design is based on symmetry breaking of a waveguide with an almost square waveguide profile. The figure accompanying the explanation is Fig. 3.16. The waveguide cross sections of the polarization rotator are shown from left to right. First the waveguide is tapered to an almost square cross section using an inverted taper. Then a part of the waveguide is shallow etched, introducing a new symmetry plane which is 45° rotated. A TE mode or TM mode which are eigenmodes of the vertical symmetry waveguide will thus excite the two hybrid modes in the partly shallowly etched waveguide. For a fill factor of 75% for the silicon overlay, a TE or TM polarized fundamental mode couples equally to both 50% TE/TM polarized hybrid modes of the asymmetrical waveguide at the symmetric-asymmetric waveguide interface. After propagation over a certain length, both asymmetrical hybridly polarized waveguide modes will couple to the fundamental TM mode in the output waveguide when a TE mode is launched (and vice versa when a TM mode is launched) at the asymmetric-symmetric waveguide interface, thereby obtaining polarization conversion. The measurement results and robustness

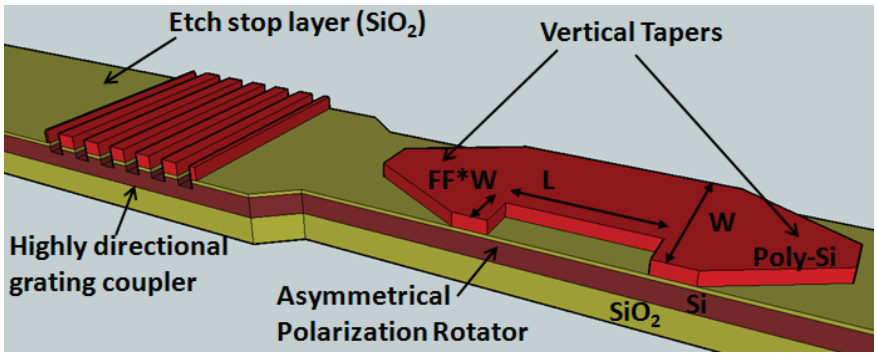

Figure 3.14: Artist's impression of a highly directional fiber coupler and asymmetrical polarization rotator fabricated within the same process flow. (Dimensions are not to scale)

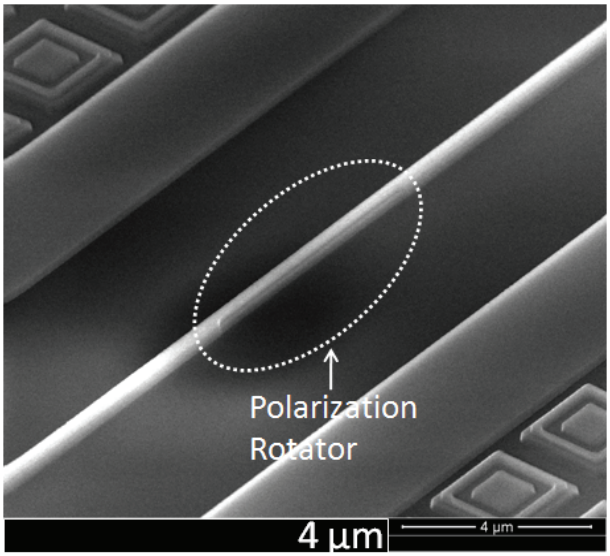

Figure 3.15: Bird's eye view SEM image of a fabricated polarization rotator.

studies are presented in [9] (see page 3-21). A polarization conversion efficiency of −0.51 dB over a bandwidth of 80 nm was measured. I have shown that the design has −0.5 dB Polarization Conversion Efficiency (PCE) tolerances making it compatible with standard CMOS fabrication tolerances. The crosstalk is −9.55 dB and could be easily improved by using a polarization splitter or filter, e.g. the polarization filter from section 3.3.1.

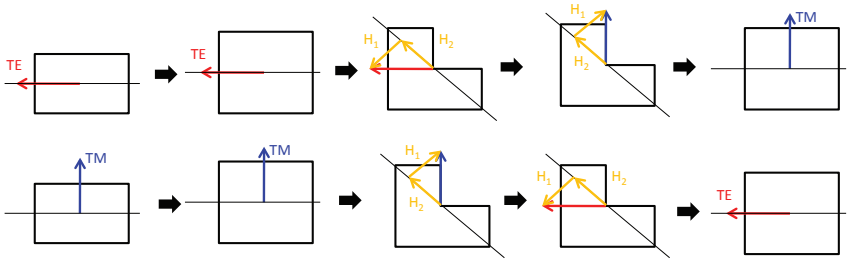

Figure 3.16: Polarization rotator principle explanation using the waveguide cross sections and electrical fields of the modes.

3.3.3 Polarization tracking demonstrator

In the previous sections of this chapter I have demonstrated all necessary components to design a PM-DQPSK receiver. Such a design is shown in Fig. 3.17. This design has been fabricated but not characterized and is not optimal for short wirebonding to a TIA chip for packaging. Nonetheless, all subcomponents and subcircuits were demonstrated. It uses a 2D polarization splitting grating coupler which acts as a coupling, polarization splitting and rotating device at the same time [10, 11]. The drawback is that it is relatively narrow band. Alternatively, an inverted taper as horizontal coupler in combination with a polarization splitter and rotator can be used. This configuration can easily achieve a 100 nm optical bandwidth. The polarization splitter on the chip will in general not split the corresponding polarizations which contain the quadrature signals. One could add a discrete polarization rotator before the chip which tracks the polarization rotation. However, this is quite expensive and bulky. In the design in Fig. 3.17 I have chosen a polarization tracking circuit configuration similar to the one presented in [8]. Since the orthogonal fiber polarizations are coupled to the same on-chip polarization they can be interfered. Besides interfering a symbol with the previous symbol of a certain polarization, one can also interfere a symbol of polarization TE_1 with the previous symbol of polarization TE_2 and vice versa. Doing this it is possible to obtain all polarization information after digital processing. A consequence of this architecture is that the number of balanced photodetectors is doubled. This PM-DQPSK circuit is an excellent example of the integration possibilities that Silicon Photonics offers. The size of the whole circuit in Fig. 3.17 is only 1.4 mm × 2.4 mm. This means that we could get about 10000 devices out of one 200 mm SOI wafer.

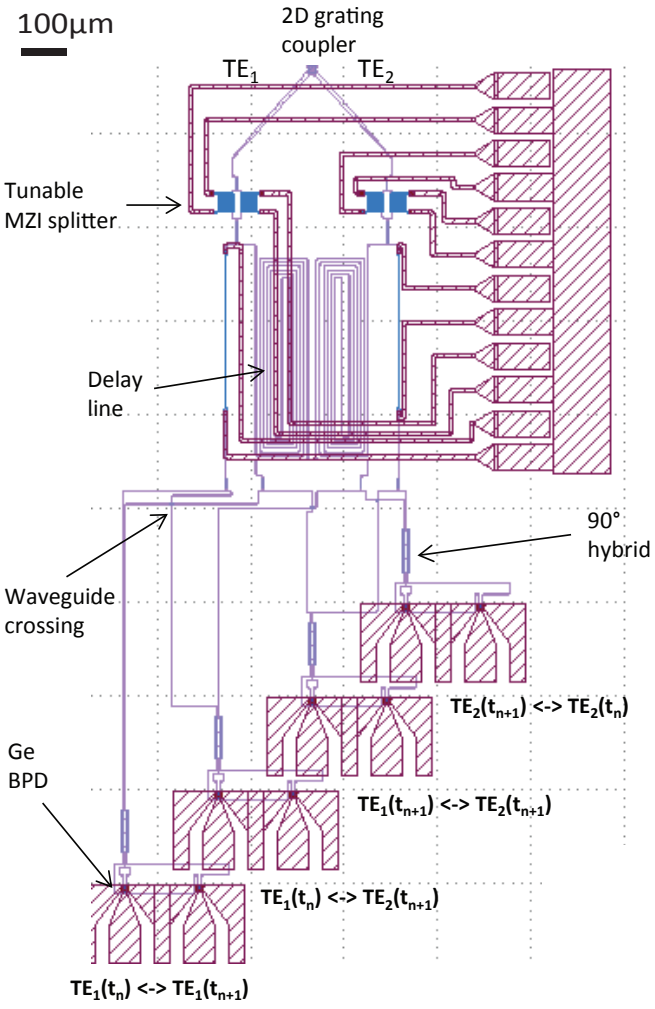

Figure 3.17: Mask design of a PM-DQPSK receiver using a polarization tracking architecture.

3.4 Conclusion

Silicon photonics is shown to be an excellent platform for recievers in applications requiring high spectral efficiency modulation formats. I primarily focused on a proof-of-principle demonstrator of fully integrated DPSK, DQPSK and PM-DQPSK receivers. In a first stage I focused on the most crucial components such as a tunable splitter and delay line and used e-beam lithography as rapid prototyping technique to achieve a DPSK receiver. In a second stage I employed DUV lithography including Ge photodetector integration to realize a DPQSK receiver. This circuit requires a 90° hybrid and balanced photodetectors. Successful operation at 10 Gb/s and 20 Gb/s was achieved. Finally I investigated and designed a PM-DQPSK receiver using a 2D polarization splitting grating coupler to couple, split and rotate the polarizations. Alternatively one could couple horizontally with an inverted taper. For this method I demonstrated a polarization splitter and polarization rotator to handle the polarizations.

References

[1] P. J. Winzer and RJ Essiambre. *Advanced Optical Modulation Formats.* Proceedings of the IEEE, 94(5):952–985, 2006.

[2] J. M. Kahn and K. P. Ho. *Spectral Efficiency Limits and Modulation/Detection Techniques for DWDM Systems.* IEEE Journal of Selected Topics in Quantum Electronics, 10(2):259–272, 2004.

[3] M. Aamer, A. Griol, A. Brimont, A. M. Gutierrez, P. Sanchis, and A. Hakansson. *Increased sensitivity through maximizing the extinction ratio of SOI delay-interferometer receiver for 10G DPSK.* Optics express, 20(13):14698–704, 2012.

[4] R. Halir, G. Roelkens, A. Ortega-Moñux, and J. G. Wangüemert-Pérez. *High-performance 90 degree hybrid based on a silicon-on-insulator multimode interference coupler.* Optics letters, 36(2):178–80, 2011.

[5] Karsten Voigt, Lars Zimmermann, Georg Winzer, and Klaus Petermann. *SOI based 2ÃŮ2 and 4ÃŮ4 waveguide couplers - Evolution from DPSK to DQPSK.* In Group IV Photonics, pages 209–211, 2008.

[6] N. Sotiropoulos, H. De Waardt, A. M. J. Koonen, D. Vermeulen, and G. Roelkens. *Performance of 80 Gb/s MMI-Based DQPSK Demodulator on SOI.* In 6th European Conference on Integrated Optics (ECIO), Barcelona, Spain, 2012.

[7] A. Hakansson, M. Aamer, N. Sotiropoulos, Antoine Brimont, Pablo Sanchis, J. M. Fedeli, Delphine Marris-Morini, Eric Cassan, L. Vivien, Karen Gilbert, Philippe Grosse, Jean Michel Hartmann, D. Vermeulen, and G. Roelkens. *Compact silicon differential receiver with integrated zero biased balanced detection.* The 9th International Conference on Group IV Photonics (GFP), 6:165–167, 2012.

[8] R. Nagarajan, M. Kato, J. Pleumeekers, D. Lambert, V. Lal, A. Dentai, M. Kuntz, J. Rahn, H.-S. Tsai, R. Malendevich, G. Goldfarb, J. Tang, J. Zhang, T. Butrie, M. Raburn, B.E. Little, A. Nilsson, M. Reffle, F. Kish, and D. Welch. *10 Channel, 45.6 Gb/s per Channel, Polarization-Multiplexed DQPSK, InP Receiver Photonic Integrated Circuit.* Lightwave Technology, Journal of, 29(4):386–395, 2010.

[9] D. Vermeulen, S.K. Selvaraja, P. Verheyen, P. Absil, W. Bogaerts, D. Van Thourhout, and G. Roelkens. *Silicon-on-Insulator Polarization Rotator Based on a Symmetry Breaking Silicon Overlay.* IEEE Photonics Technology Letters, 24(6):482–484, 2012.

[10] D. Taillaert, P.I. Borel, L.H. Frandsen, R.M. De La Rue, and R. Baets. *A compact two-dimensional grating coupler used as a polarization splitter*. IEEE Photonics Technology Letters, 15(9):1249–1251, 2003.

[11] W. Bogaerts, D. Taillaert, P. Dumon, D. Van Thourhout, R. Baets, and E. Pluk. *A polarization-diversity wavelength duplexer circuit in silicon-on-insulator photonic wires.* Optics express, 15(4):1567–78, 2007.

Compact Silicon Differential Receiver with Integrated Zero Biased Balanced Detection

Andreas Hakansson, Mariam Aamer, Nikolaos Sotiropoulos, Antoine Brimont, Pablo Sanchis, Jean-Marc Fedeli, Delphine Marris-Morini, Eric Cassan, Laurent Vivien, Karen Gilbert, Philippe Grosse, Jean Michel Hartmann, Diedrik Vermeulen and Gunther Roelkens

***Abstract*— We present an optimized differential receiver in silicon with a minimized footprint and balanced zero biased Ge photodiodes. The receiver integrates a delay-line with a 2x4 MMI 90 degree hybrid and two balanced photo diodes for DQPSK demodulation. Also a tunable power splitter is included for better balancing. Two receivers were tested, for 10Gbps and 20Gbps operation, and well opened eye-diagrams were measured.**

***Index Terms*— silicon photonics; coherent receiver; balanced detectors**

I. INTRODUCTION

THE differential-phase-shift-keyed (DPSK) modulation format exhibits several advantageous qualities [1]. It enables 3-dB improved receiver sensitivity with balanced detection, and has higher tolerance to nonlinear degradation compared with on-off keying (OOK). The detection of the phase at the receiver can either be implemented using coherent or differential (non-coherent) detection. A coherent receiver uses carrier tracking by phase-locked loops to estimate the absolute phase, while in differential encoded DPSK the information is in the phase transition and can be demodulated using a passive delay-interferometer. The simplicity of the differential detection and the elimination of a local oscillator (LO) and digital signal processor (DSP) makes differential detection advantageous for low cost links.

Mainly two designs of differential silicon receivers have been addressed in the literature, either using more standard Mach-Zehnder Delay-Line Interferometer MZDI [2-4] or by using micro ring-resonators [5]. Even though the size of the ring-resonator can be very compact the optimal performance is reached for an optimized Q-factor and at the same time maximized extinction ratio, which usually requires adding some tuning mechanism as in [6] and therefore increases power consumption and complexity of the receiver. The MZDI still seems to be the most used implementation in more complete systems such as presented in [2,4].

In this paper we demonstrate 5GBaud (10Gbit/s) and 10GBaud (20Gbit/s) operation using a very compact differential receiver for DQPSK demodulation. The receiver includes a tunable power splitter, a delay-line spiral, a compact 2x4 MMI 90 degree hybrid and two balanced germanium PDs.

II. DESIGN AND OPTIMIZATION

The principle of operation of a differential demodulator using a MZDI is to superpose two adjacent bits using a delay-line (DL) and the intensity of the superposed signal can then directly be photo-detected converting the differential bit-transition into an intensity variation of the signal. In DQPSK modulation the four bits are coded as four different orthogonal phases.

The layout of the proposed structure is depicted in Figure 1, including a thermo-optically tunable MZI power splitter in series with a MZDI and a 90 degree hybrid. At the output the in-phase and quadrature signal are detected using two balanced PDs in *pinpin* configuration. In the following sections the implementation and optimization of each of these elements will be described.

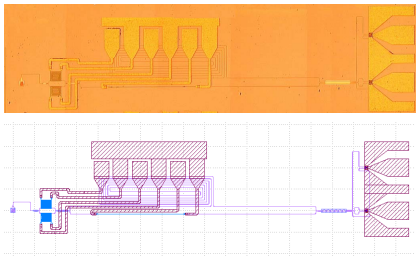

Fig. 1. Design of the differential receiver for DQPSK and 10G symbol rate; (upper) optical photograph of fabricated device, (lower) gds design. The receiver is assembled using 5 componentes, from left to right in the figure: Curved grating coupler, MZI tunable power splitter, delay-line interferometer, 90-degree hybrid and two balanced photo detectors.

The research leading to these results has partially received funding from the European Community's Seventh Framework Program under grant agreement no. 224312 HELIOS. ANR project call MICROS is also acknowledged.

A. Hakansson is with DAS Photonics S.L, Camino de Vera s/n Ed 8F 2a, Ciudad Politecnica de la Inovacion, Valencia, Spain (e-mail: ahakansson@dasphotonics.com).

M. Aamer, A Brimont and P Sanchis are with Nanotechnology Center Valencia, Universidad Politécnica Valencia, Valencia, Spain

N. Sotiropoulos is with COBRA Research Institute, Eindhoven University of Technology, Eindhoven, the Netherlands

J-M. Fedeli, K. Gilbert, P. Grosse, J. M Hartmann are with CEA, LETI, Minatec Campus, 17 rue des Martyrs, GRENOBLE, France

D. Marris-Morinie, E. Cassan and L. Vivien are with Institut d'Electronique Fondamentale, Univ. Paris-Sud, CNRS, Bât. 220, F-91405 ORSAY cedex – France

D. Vermeulen and G. Roelkens are with Photonics Research Group, INTEC, Ghent University / imec, Sint-Pieters, Belgium. (D.V currently address is at Acacia Communications)

A. Curved grating couplers

The grating couplers are standard curved gratings [7]. Curved gratings are used in order to minimize the size of the chip since there will be no need to include spot size converters.

B. MZI tunable power splitter

To maximize the sensitivity of the receiver the output of the MZDI has to be balanced. To deal with the (potentially varying from run to run) loss in the delay-line, resulting in unbalanced behavior, we include a tunable power splitter at the input of the MZDI. If needed, we can now use micro-heaters to actively tune the input power, the propagation loss can then be compensated for by directing more optical power into the delay-line arm in order to have perfect balance at the output. The MZI switch is designed using two identical spirals which will optimize the footprint and the bandwidth of the device.

C. MZDI

Two different receivers with different delay-lines lengths were tested, including 5G and 10G symbol rates. The length for the 5G and 10G delay-lines are approximately 1.8cm and 0.9cm, respectively. On the one hand, we want to fold these delay-lines into spirals to have a maximum compactness of the receiver, on the other hand we want to minimize propagation losses. Even though 5 micron bend radius is considered close to loss-less we wanted to make sure no extra loss was introduced in the spirals. By using adiabatic bendings there is a smooth transition to the tight curvature and no loss is expected [8]. The 18 mm and 9 mm spirals have been folded to a minimal footprint occupying only 1.1 mm × 0.1 mm and 0.6 mm × 0.1 mm, respectively.

D. 90 degree hybrid

Instead of the more standard implementation of a DQPSK receiver with two parallel MZDI, each coupled to a 180 degree hybrid, here a single MZDI is used coupled to a 90 degree hybrid. This will both minimize the chip area by almost a factor of two as well as the number of active controls needed for tuning.

Here we use a 2x4 MMI design with shallowly etched multimode region. The device has a footprint of only 0.1 mm × 0.1 mm and exhibits a common mode rejection ratio (CMRR) better than −20 dBe and phase errors better than ±5 degrees in a 50 nm bandwidth [9].

E. Balanced Photodetectors

To have a 3dB increase in sensitivity of the receiver, balanced detection is used instead of single detection. We here use zero bias balanced detection and we can hence scale down the complexity and size of the receiver by excluding the need of a decoupling capacitor. Also, by using one single detector in a *pinpin* configuration, additional wire bonding or metal connections are eliminated since the signal is directly extracted from one single central pad. Here a lateral *pinpin* germanium balanced photodetector, only 10 µm long, is selectively grown at the end of silicon waveguides. The photodiodes used are comparable to the ones having a bandwidth above 10GHz for any negative voltage bias [10] , which clearly is sufficient for our application. The responsivity is measured to 1 A/W at 1550 nm using 0 to -2V bias with a dark current of 10nA.

III. SIMULATIONS

Figure 2 shows the simulated spectral response of the MZDI and the two balanced photodiodes using the transfer matrix method [11]. On the x-axis is the differential phase with respect to the two adjacent bits. The two curves are shifted exactly 90 degrees with respect to each other in order to obtain the four different states on the DQPSK modulation format. The states are marked in the figure as dotted vertical lines at the four different orthogonal phases at, -90, 0, +90, and +180 degrees.

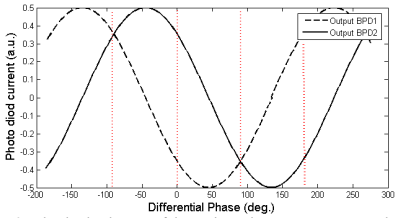

Fig. 2. The simulated output of the receiver. The two curves represent how the in-phase and quadrature detected current from the two diodes varies with the differential phase. The four different two-bits states are marked as dotted lines at -90, 0, 90, and 180 degrees, corresponding to [+1 +1], [-1 +1], [-1 -1], and [+1 -1], respectively.

IV. FABRICATION

On SOITEC optical SOI with 220nm Si on 2µm BOX, the process starts with the deposition of 100nm High Temperature Oxide (HTO) on top of the silicon layer. The gratings and the waveguide arms are first patterned, followed by RIE silica etching with C_4F_8, which defines a hardmask. The silicon is then partially etched (65nm) with HBr and controlled by ellipsometry in order to define precisely the grating teeth depth. In the second lithography step, the gratings are protected by the resist and the remaining hardmask serves for the waveguides in a self-alignment process. Then a full silicon etch down to the box completes the waveguide fabrication. We then defined cavities for the selective epitaxial growth of Germanium. This is achieved by deposition of a silica layer which is etched at the end of waveguides. In order to achieve direct coupling, the silicon part of the cavities is etched down to 50nm on top of the BOX. Germanium was then selectivity grown in the cavities and CMP used to adjust the thickness around 300nm. The doped regions (N and P) of the lateral Ge photodetector are defined sequentially by ion implantation of Phosphorus and Boron. A 400nm thick SiO2 was deposited and a deposition and etching of 100nm of Ti/TiN defined the heaters. Then after deposition of 500nm of SiO_2 and two-step openings, the electrodes were defined by Ti/TiN/AlCu metal

stack deposition and Cl2 etching.

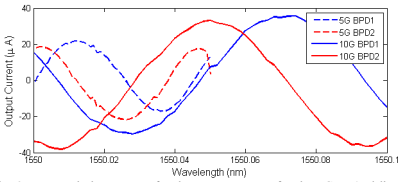

Fig. 3. Transmission spectra for the output current for the 5GHz (red lines) and 10GHz (blue lines) symbol-rate receiver. The solid and the dashed lines corresponds to the quadrature and in-phase outputs

V. MEASUREMENTS AND EXPERIMENTAL RESULTS

Continuous-wave light was generated by an external cavity tunable laser. The light was coupled to the chip through the curved grating coupler using manual micro-positioners. A GSGSG probe with a 100μm pitch was used to measure the output current of the photo diodes. Figure 3 shows the measured transmission spectra for -3dBm input power. The spectra have excellent agreement with the expected behavior for a DQPSK receiver shown in Figure 2. For both the 5G and 10G receiver, the two outputs are perfectly 90 degree phase shifted with respect to each other. The lower output current from the 5G receiver is expected due to the longer delay-line.

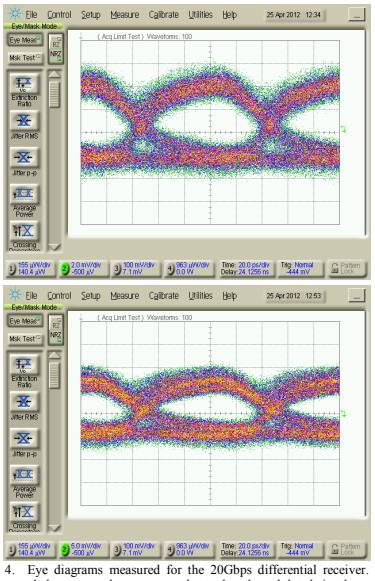

Fig. 4. Eye diagrams measured for the 20Gbps differential receiver. The upper and lower graphs correspond to the demodulated in-phase and quadrature signal.

To test the high speed behavior of the receiver an optical data stream was generated using a Lithium Niobate dual-drive modulator generating a DQPSK signal. The bit streams used were two decorrelated pseudorandom binary sequences (PRBS) with a pattern length of 2^{23}-1 at 10Gbps, generated by a bit pattern generator (SHF BPG 44E). At the output of the chip, the signal was extracted directly from the photodiodes using a GSGSG probe and fed to a Communication Analyzer (Infinium DCA-J 86100C). For an input power of 5.5dBm, Figure 4 shows well opened eye-diagrams of the two demodulated I and Q signals for 20Gbps operation.

VI. CONCLUSION

An optimized receiver for DQPSK transmission was demonstrated with a minimum footprint and with zero biased photo detectors. Each building block of the receiver is optimized for high performance, low loss and maximum compactness. The results demonstrate the compactness and high performance of a silicon DQPSK receiver.

REFERENCES

[1] A. H. Gnauck and P. J. Winzer, "Optical phase-shift-keyed transmission," J. Lightwave Technol., vol. 23, pp. 115-130, 2005.
[2] C. R. Doerr, L. Chen, B. Labs, and H. Road, "Monolithic PDM-DQPSK receiver in silicon," 36th European conference and Exhibition on Optical Communication (ECOC), p1-3, 2010.
[3] K. Voigt et al., "Performance of 40-Gb/s DPSK Demodulator in SOI-Technology," IEEE Photonics Technology Letters, vol. 20, no. 8, pp. 614-616, Apr. 2008.
[4] K. Suzuki, H. C. Nguyen, T. Tamanuki, F. Shinobu, Y. Sakai, and T. Baba, "Slow-light-based variable symbol-rate silicon photonics DQPSK receiver," Optics Express, vol. 20, no. 4, pp. 4796-4804, 2012.
[5] L. Xu, C. Li, C. Y. Wong, and H. K. Tsang, "DQPSK demodulation using integrated silicon microring resonators," Optics Communications, vol. 284, no. 1, pp. 172-175, Jan. 2011.
[6] L. Chen, N. Sherwood-droz, and M. Lipson, "Compact bandwidth-tunable microring resonators," Optics Letters, vol. 32, no. 22, pp. 3361-3363, 2007.
[7] F. Van Laere, T. Claes, J. Schrauwen, S. Scheerlinck, W. Bogaerts, D. Taillaert, L. O'Faolain, D. Van Thourhout, R. Baets, "Compact Focusing Grating Couplers for Silicon-on-Insulator Integrated Circuits", IEEE Photonics Technology Letters, vol. 19, no. 23, pp.1919-1921, 2007.
[8] S. Selvaraja, W. Bogaerts, P. Absil, D. Van Thourhout and R. Baets , "Record Low-Loss Hybrid Rib/Wire Waveguides for Silicon Photonic Circuits", Group IV Photonics International Conference, China, 2010
[9] R. Halir, G. Roelkens, A. Ortega-Moñux, and J. G. Wangüemert-Pérez , "High-performance 90° hybrid based on a silicon-on-insulator multimode interference coupler", Optics Letters, vol. 36, no. 2, pp. 178-180, 2011.
[10] L. Vivien, A. Polzer, D. Marris-Morini, J. Osmond, J. Hartmann, P. Crozat, E. Cassan, C. Kopp, H. Zimmermann, and J. Fédéli, "Zero-bias 40Gbit/s germanium waveguide photodetector on silicon," Opt. Express, vol. 20, pp. 1096-1101, 2012.
[11] J. Poon, J. Scheuer, S. Mookherjea, G. Paloczi, Y. Huang, and A. Yariv, "Matrix analysis of microring coupled-resonator optical waveguides," Opt. Express, vol. 12, pp. 90-103, 2004.

Silicon-on-Insulator Polarization Rotator Based on a Symmetry Breaking Silicon Overlay

Diedrik Vermeulen, *Student Member, IEEE*, Shankar Selvaraja, *Member, IEEE*, Peter Verheyen, Philippe Absil, Wim Bogaerts, *Member, IEEE*, Dries Van Thourhout, *Member, IEEE*, and Gunther Roelkens, *Member, IEEE*

***Abstract*— We demonstrate a polarization rotator fabricated using a 4 etch-step complementary metal–oxide–semiconductor (CMOS)-compatible process including layer depositions on a silicon-on-insulator wafer. The measured polarization rotation efficiency is −0.51 dB over a wavelength range of 80 nm. A robustness investigation shows that the design is compatible with CMOS fabrication capabilities.**

***Index Terms*— Polarization rotator, silicon-on-insulator (SOI).**

I. Introduction

SILICON-ON-INSULATOR (SOI) photonic integrated circuits (PICs) are rapidly becoming a key technology for low-cost and high-volume oriented photonic applications. By organizing Multi Project Wafer (MPW) shuttles silicon PIC prototyping can be realized at an affordable cost while at the same time guaranteeing specifications comparable to Complementary Metal Oxide Semiconductor (CMOS) circuits. This fabless model also allows the research community to focus on device and application ideas, design and characterization. In the first stage of the Silicon Photonics era much research was focused on proof-of-concept circuits, solving the most stringent problems like fiber coupling and mimicking photonic devices developed on other platforms such as InP and polymer waveguide circuits. Nowadays, researchers are focusing on methods to optimize existing photonic components and on expanding the set of photonic functionalities. Polarization independent functionalities are in most cases not an option due to the highly birefringent waveguides in high index contrast SOI waveguides. Polarization diversity on the other hand requires a broadband and efficient polarization rotator which remained until recently a missing link.

An early polarization diversity circuit [1] made use of 2-dimensional grating fiber couplers which act as a fiber coupler, polarization splitter and polarization rotator at the same time. Unfortunately, their efficiency is rather low, around −7 dB, and their 1-dB bandwidth is only 20 nm. Another polarization diversity circuit [2] uses an off-axis double core structure of a small silicon wire and large SiN wire ($0.84\,\mu\text{m} \times 0.84\,\mu\text{m}$) as polarization rotator. Achieving such a thick high quality SiN in a CMOS environment using Low Pressure Chemical Vapor Deposition (LPCVD) is not obvious. Furthermore, if the PIC contains electro-optic components or photodetectors, the implementation of such a structure is non-trivial. A mode-evolution-based polarization rotator was successfully demonstrated in [3], but with insertion losses up to 5 dB. Large core waveguides ($\sim 2\,\mu$m) with angled sidewalls were investigated in [4]. An interesting development are polarization rotators based on asymmetrical directional couplers ([5], [6]). These structures are very simple and require only a single etch step. However, the waveguide structure needs to be vertically asymmetrical to achieve coupling between both polarizations. In [7] a compact polarization rotator was proposed using a straight asymmetric shallow etch in a square strip waveguide configuration. In what follows we will elaborate on this report by experimentally demonstrating a slightly modified polarization rotator configuration and investigate the robustness of this structure. Furthermore, the fabrication process is exactly the same as for the highly efficient grating couplers reported in [8], thereby permitting cointegration of both polarization rotators and high-efficiency grating couplers.

II. Design and Fabrication Process

The complete fabrication process is done in a CMOS pilot line with 193 nm deep ultraviolet (DUV) lithography. First a 5 nm silicon oxide layer is thermally grown on a 200 mm SOI wafer with a buried oxide layer thickness of 2 μm and a crystalline silicon layer thickness of 220 nm. In a second step an amorphous silicon layer of 160 nm is deposited and a deep etch is performed through the amorphous silicon and oxide layer reaching 70 nm into the crystalline silicon layer. This is used to define the slits of the high efficiency grating couplers. Next, the amorphous silicon is removed where necessary and the thermally grown oxide layer in the first step will now act as an etch stop layer in order to not affect the underlying crystalline silicon. A shallow etch of 70 nm in the 220 nm crystalline silicon layer is introduced to achieve low loss and robust spectral filter components. Finally, the waveguide trenches are defined by a 220 nm etch and the amorphous silicon is annealed after which it becomes polycrystalline silicon.

This work was supported in part by the Dutch Smartmix-Memphis Project and in part by the European Union in the FP7-ICT-HELIOS Project. The work of D. Vermeulen was supported in part by a grant from the Institute for the Promotion of Innovation by Science and Technology, Flanders (IWT).

D. Vermeulen, S. Selvaraja, W. Bogaerts, D. Van Thourhout, and G. Roelkens are with the Department of Information Technology, Photonics Research Group, Ghent University-IMEC, Gent B-9000, Belgium (e-mail: diedrik.vermeulen@intec.ugent.be; shankar@intec.ugent.be; wim.bogaerts@intec.ugent.be; dries.vanthourhout@intec.ugent.be; gunther.roelkens@intec.ugent.be).

P. Verheyen and P. Absil are with IMEC, Leuven 3001, Belgium (e-mail: verheyen@imec.be; absilp@imec.be).

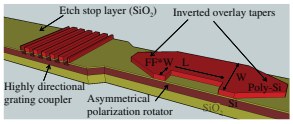

Fig. 1. Artist's impression of a highly directional fiber coupler and asymmetrical polarization rotator fabricated within the same process flow. (Dimensions are not to scale)

In Fig. 1 an artist's impression is shown of a high-efficiency grating coupler and a polarization rotator, both compatible with the aforementioned process flow. The polarization rotator design is based on symmetry breaking of a waveguide with an almost square waveguide profile. An inverted taper, defined in the silicon overlay, is used as an adiabatic transition between a 450 nm wide *Si* waveguide with a height of 220 nm and an equally wide waveguide with a silicon overlay. This double patterned strip waveguide has a combined thickness of 380 nm and is formed by 220 nm crystalline silicon and a 160 nm polycrystalline silicon with 5 nm thermally grown silicon oxide in between. According to simulations the 100 nm wide tip of the inverted taper would introduce no loss and a 0.4 dB loss for TE- (Transverse Electric) and TM-polarized (Transverse Magnetic) light respectively. The actual polarization rotator is formed by a 405 nm wide waveguide with an asymmetrical overlay. For a fill factor of 75 % for the silicon overlay, a TE or TM polarized fundamental mode couples equally to both 50 % TE/TM polarized hybrid modes of the asymmetrical waveguide at the symmetric-asymmetric waveguide interface. After propagation over 7.6 μm, both asymmetrical hybridly polarized waveguide modes will couple to the fundamental TM mode in the output waveguide when a TE mode is launched (and vice versa when a TM mode is launched) at the asymmetric-symmetric waveguide interface, thereby obtaining polarization conversion, see Fig. 2. The short conversion length is a consequence of the large difference in propagation constants of the two beating modes ($\beta_{H1} - \beta_{H2} = 10.12\,\mu\text{m}^{-1} - 9.70\,\mu\text{m}^{-1} = 0.42\,\mu\text{m}^{-1}$) in the asymmetric waveguide and results in a large (> 100 nm from simulation) polarization conversion optical bandwidth. SEM pictures of the fabricated polarization rotator are shown in Fig. 3(a) and 3(b).

III. MEASUREMENTS

The polarization rotators were characterized by means of grating couplers. These are highly polarization dependent structures and act as polarization filtering couplers with an extinction ratio of around 50 dB. The periods of the grating couplers were 630 nm and 1040 nm for coupling respectively TE- and TM-polarized light. First the inverted overlay tapers with a designed tip width of 100 nm were characterized by measuring the TE and TM insertion loss of a waveguide which is tapered to a strip waveguide with silicon overlay and back. The measured insertion loss for the inverted taper is smaller than 0.1 dB for both TE- and TM- polarized light which is explained by the reduced tip width of 50 nm of the fabricated

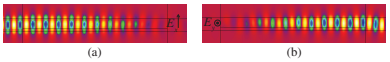

Fig. 2. Top view field plots of the polarization rotator, obtained using a fully vectorial eigenmode expansion tool. (a) E_x field (TE polarization). (b) E_y field (TM polarization).

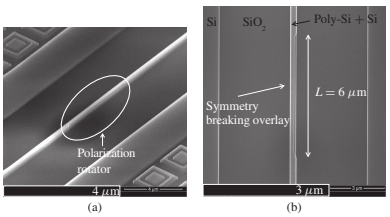

Fig. 3. SEM images of the fabricated polarization rotator. (a) Bird's eye view of a realized polarization rotator. (b) Top view: a poly-Si overlay breaks the symmetry of the waveguide such that after a propagation over L of 6 μm, almost total polarization conversion is achieved.

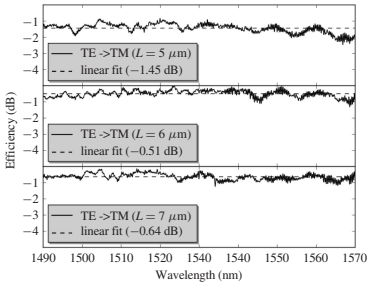

Fig. 4. Measurements of the polarization rotator ($W = 405$ nm, $FF = 75\,\%$) TE to TM insertion loss for different rotator lengths L.

device. The polarization rotators are characterized by measuring the TE to TM transmission $T_{TE->TM}$, normalized with the reference measurements of the grating couplers. The TE to TM insertion loss is the sum of the intrinsic loss of the polarization rotator and the TE to TE transmission $T_{TE->TE}$ (crosstalk). Simulations show that the insertion loss is very low, so we can assume that $T_{TE->TE} = 1 - T_{TE->TM}$ and that the polarization conversion efficiency (PCE), defined by $PCE = T_{TE->TM}/(T_{TE->TE} + T_{TE->TM})$, equals $T_{TE->TM}$. The measurement results of polarization rotators with a width W of 405 nm and fill factor FF of 75 % are plotted in Fig. 4. The optimal structure has a length L between 6 μm and 7 μm, which is in relatively good agreement with our simulations where we found that the optimal lenght is 7.6 μm. The highest measured PCE is −0.51 dB for a rotator length of 6 μm.

Furthermore, the high PCE was measured over a broad wavelength range of 80 nm, equal to the 3-dB bandwidth of the

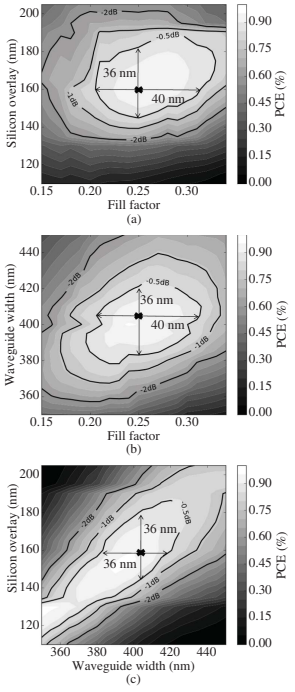

Fig. 5. Polarization rotator robustness investigation as a function of the critical parameters. The contour lines are the PCE penalties with respect to the highest PCE of the device. (a) PCE as a function of the silicon overlay thickness and fill factor. (b) PCE as a function of the waveguide width W and fill factor FF. (c) PCE as a function of the waveguide width W and silicon overlay thickness.

grating coupler. The upper limit for the crosstalk ($T_{TE->TE} < 1 - T_{TE->TM}$) is -9.55 dB. For practical applications, this residual crosstalk can be easily removed by implementing a polarization filter or polarization splitter such as a directional coupler, multi-mode interferometer (MMI) or sharp bend.

IV. Robustness

The robustness was assessed by scanning the critical parameter space of the fabricated polarization rotator ($W = 405$ nm, $FF = 75\,\%$, $L = 7\,\mu$m) where the rotator length L is kept constant. The cross in the robustness figures indicates the parameters of the fabricated polarization rotator with a simulated PCE of 95 % or -0.22 dB. In Fig. 5(a) the PCE is plotted versus the fill factor FF and silicon overlay thickness. For a -0.5dB PCE penalty, the duty cycle may vary $\pm 5\,\%$ which translates into to a mask alignment tolerance of ± 20 nm. The silicon overlay thickness -0.5 dB PCE tolerance is $+21$ nm and -15 nm. Note that the etch depth is fixed in our case at exactly the silicon overlay thickness due to the SiO_2 etch stop layer (see Fig. 1) which attributes to the overall robustness of our component. Nonetheless, it introduces and extra 0.2 dB PCE penalty for a 5 nm thick silicon oxide etch stop layer. The PCE is plotted as a function of the waveguide width and fill factor in Fig. 5(b) and as a function of the overlay thickness and waveguide width in Fig. 5(c). The -0.5 dB PCE tolerance is $+15$ nm and -21 nm for the waveguide width. These robustness specifications are compatible with CMOS fabrication capabilities.

V. Conclusion

We have experimentally realized a high efficiency and broadband integrated polarization rotator with a polarization conversion efficiency of -0.51 dB over a bandwidth of 80 nm. An advanced passive SOI 4 etch-step process flow was used for the fabrication. With this process, 4 different layer thicknesses can be resolved and high-efficiency grating couplers using a silicon overlay could be integrated on the same optical chip. Furthermore, the accompanied extra design freedom offers an excellent tool to optimize other optical integrated components such as splitters, filters and optical interconnects. Additionally, we investigated the robustness and have shown that the design has -0.5 dB PCE tolerances which are compatible with standard CMOS fabrication tolerances. The crosstalk is -9.55 dB and could be easily improved by using a polarization splitter or filter, e.g. a directional coupler, MMI or sharp bend.

References

[1] W. Bogaerts, D. Taillaert, P. Dumon, D. Van Thourhout, R. Baets, and E. Pluk, "A polarization-diversity wavelength duplexer circuit in silicon-on-insulator photonic wires," *Opt. Express*, vol. 15, no. 4, pp. 1567–1578, 2007.

[2] H. Fukuda, K. Yamada, T. Tsuchizawa, T. Watanabe, H. Shinojima, and S.-I. Itabashi, "Silicon photonic circuit with polarization diversity," *Opt. Express*, vol. 16, no. 7, pp. 4872–4880, 2008.

[3] J. Zhang, M. Yu, G.-Q. Lo, and D.-L. Kwong, "Silicon-waveguide-based mode evolution polarization rotator," *IEEE J. Sel. Topics Quantum Electron.*, vol. 16, no. 1, pp. 53–60, Jan./Feb. 2010.

[4] H. Deng, D. O. Yevick, C. Brooks, and P. E. Jessop, "Fabrication tolerance of asymmetric silicon-on-insulator polarization rotators," *J. Opt. Soc. Amer. A, Opt., Image Sci., Vis.*, vol. 23, no. 7, pp. 1741–1745, 2006.

[5] L. Liu, Y. Ding, K. Yvind, and J. R. M. Hvam, "Silicon-on-insulator polarization splitting and rotating device for polarization diversity circuits," *Opt. Express*, vol. 19, no. 13, pp. 12646–12651, 2011.

[6] D. Dai and J. E. Bowers, "Novel concept for ultracompact polarization splitter-rotator based on silicon nanowires," *Opt. Express*, vol. 19, no. 11, pp. 10940–10949, 2011.

[7] Z. Wang and D. Dai, "Ultrasmall Si-nanowire-based polarization rotator," *J. Opt. Soc. Amer. B*, vol. 25, no. 5, pp. 747–753, 2008.

[8] D. Vermeulen, *et al.*, "High-efficiency fiber-to-chip grating couplers realized using an advanced CMOS-compatible silicon-on-insulator platform," *Opt. Express*, vol. 18, no. 17, pp. 18278–18283, 2010.

A Silicon Differential Receiver with Zero Biased Balanced Detection for Access Networks [1]

Mariam Aamer, Nikos Sotiropoulos, Andreas Hakansson, Antoine Brimont, Jean-Marc Fedeli, Delphine Marris-Morini, Eric Cassan, Laurent Vivien, Karen Gilbert, Philippe Grosse, Jean Michel Hartmann, Diedrik Vermeulen, Gunther Roelkens and Pablo Sanchis

***Abstract*—We present an optimized differential receiver in silicon with a minimized footprint and balanced zero biased Ge photodiodes. The receiver integrates a delay-line with a 2x4 multimode interferometer (MMI) 90 degree hybrid and two balanced photodiodes for differential quadrature phase-shift keying (DQPSK) demodulation. Also a tunable power splitter is included for better balancing. Two receivers were tested, for 10Gbps and 20Gbps operation, and well opened eye-diagrams were obtained, as well as error vector magnitude (EVM) values around 12.5% and 19.57% respectively.**

***Index Terms*— Integrated optics, silicon photonics, balanced detectors, phase-shift keying.**

I. INTRODUCTION

An ever growing amount of access network bandwidth is required by end users. The deployment of passive optical network has already begun to address this demand. But network operators demand solutions based on reusing the existing infrastructure developed for 10Gbit/s links. This scaling of the bit rate can be achieved using advanced modulation formats while keeping the 10Gbit/s infrastructure.

Differential-phase-shift-keying (DPSK) offers several advantages over an on-off keying modulation format because of its nonlinearity tolerance, 3-dB receiver sensitivity improvement when used with balanced detection and the possibility to operate at lower symbol rates for a given bit rate [1]. The detection of the phase at the receiver can be implemented either by using coherent or non-coherent differential detection. The coherent detection provides an improvement of the optical signal to noise ratio by mixing a local oscillator (LO) signal with the transmitted signal and effectively compensates for signal degradations due to chromatic dispersion and polarization mode dispersion on the transmission line. However, a digital signal processing (DSP) unit is necessary, which implies higher costs and electric power consumption. In the differential encoded DPSK, the information is in the phase transition and can be demodulated using a passive delay-interferometer, which allows the elimination of the LO and the DSP, making differential detection advantageous for low cost links.

Different approaches have been proposed for differential silicon receivers, mainly based on the use of standard Mach-Zehnder delay interferometers (MZDI) [2-4] or using microring resonators [5, 6]. While the ring resonator approach allows a very compact implementation, optimal performance usually requires a tuning mechanism [7], increasing the complexity of the receiver and the power consumption. Accordingly, the MZDI design appears to be the most suitable to be used in more complete systems [4, 8].

In this paper we demonstrate 5GBaud (10Gbit/s) and 10GBaud (20Gbit/s) operation using a very compact differential receiver for DQPSK demodulation with zero biased balanced detection and using a compact 2x4 MMI 90 degree hybrid instead of the standard implementation with two 180 degree hybrids. 10Gbit/s and 20Gbit/s constellations were obtained, as well as its error vector magnitude (EVM) and bit error rate (BER).

II. SILICON DQPSK RECEIVER STRUCTURE

The principle of operation of a differential demodulator using a MZDI is to interfere two adjacent symbols using a delay-line (DL). The intensity of the resulting signal can then directly be photodetected converting the differential bit-transition into an intensity variation of the signal. In DQPSK modulation the four bits are encoded as four different orthogonal phases.

The schematic of the proposed receiver is depicted in Fig. 1. A thermo-optically tunable Mach-Zehnder interferometer (MZI) power splitter is placed in series with a MZDI and a 2x4 MMI acting as 90 degree hybrid. At the output the in-phase and quadrature signals are detected using two balanced photodetectors (PDs) in *pinpin* configuration. In the following lines the implementation and optimization of each of these elements is described.

The research leading to these results has partially received funding from the European Community's Seventh Framework Program under grant agreement no. 224312 HELIOS. ANR project call MICROS is also acknowledged.

M. Aamer, A. Brimont and P. Sanchis are with Nanotechnology Center Valencia (NTC), Universitat Politecnica Valencia, 46022 Spain (e-mail: maaa@ntc.upv.es; abrimont@ntc.upv.es; pabsanki@ ntc.upv.es).

N. Sotiropoulos is with Eindhoven University of Technology.

A. Hakansson is with DAS Photonics S.L, Camino de Vera s/n Ed 8F 2a, Ciudad Politecnica de la Inovacion, Valencia, Spain.

N. Sotiropoulos is with Eindhoven University of Technology

J-M. Fedeli, K. Gilbert, P. Grosse, J. M Hartmann are with CEA, LETI, Minatec Campus, 17 rue des Martyrs, GRENOBLE, France

D. Marris-Morinie, E. Cassan and L. Vivien are with Institut d'Electronique Fondamentale, Univ. Paris-Sud, CNRS, Bât. 220, F-91405 ORSAY cedex – France

D. Vermeulen and G. Roelkens are with Photonics Research Group, INTEC, Ghent University / imec, Sint-Pietersnieuwstraat 41, 9000 Ghent, Belgium. (D.V. his current affiliation in Acacia Communications)

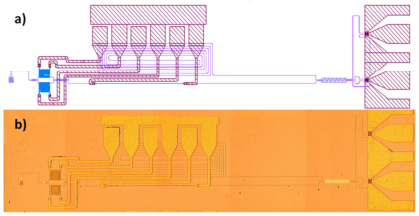

Fig. 1. DQPSK differential receiver. (a) GDS design and (b) optical photograph of fabricated device. The receiver is assembled using 5 components, from left to right in the figure: curved grating coupler, MZI tunable power splitter, delay line interferometer, 90-degree hybrid and two balanced PDs.

The proposed device was fabricated on a SOITEC wafer with a silicon device layer thickness of 220nm and a buried oxide of 2µm, covered by a 1µm-thick silica overcladding. To couple light from the input fiber to the receiver, and in order to minimize the size of the chip, curved gratings [9] were used. The next element of our receiver is a tunable MZI power splitter. In case of unbalanced behavior at the output of the MZDI due to excess loss in the delay line, micro-heaters can be used to actively tune the power at the MZDI input, resulting in an increase in the extinction ratio of the MZDI [10], and consequently in the sensitivity of the receiver.

At the output of the power splitter, a MZDI was placed. Compact spirals were used in order to minimize the size of the structure. A waveguide length of XXmm and XXmm was chosen for 5Gbaud/s and 10Gbaud/s operation respectively, leading to an insertion loss of XX dB and XX dB respectively. The MZDI outputs were coupled to the 2x4 MMI inputs. This MMI will act as a 90 degree hybrid [11] instead of the standard implementation of a DQPSK receiver with two parallel MZDI coupled to a 180 degree hybrid, in accordance with the intention of minimizing the chip area, as well as the number of active controls needed for tuning. In order to have a 3dB increase in the sensitivity of the receiver and minimize power consumption, zero bias balanced detection was used based on a Ge photodetector pair in lateral *pinpin* configuration. Hence, the photodetected signal is directly extracted from one single central pad avoiding additional wire bonding or metal connections. The 10µm-length balanced Ge-PD was selectively grown at the end of silicon waveguides, and it is comparable to the ones used in [12], which satisfies the application requirements.

III. EXPERIMENTAL RESULTS

The setup used to test the high speed behavior of the receiver is shown in Fig. 2, where a DQPSK signal was generated using a dual-drive Lithium Niobate commercial modulator, biased at minimum, using a $2V_\pi$ driving voltage and driven by the outputs of the pulse pattern generator, appropriately decorrelated, aligned and amplified. The generated DQPSK signal passes through a variable optical attenuator, which is the reference point for the receiver power, and is amplified by an erbium doped fiber amplifier (EDFA) set at a constant output power of +16 dBm. Such high input power was necessary, since the detected signals were only amplified off-chip. At the output of the chip, the electrical signals were extracted directly from the photodiodes using RF probes in a GSGSG configuration, and were transferred to two amplifiers, and then were sampled by the digital phosphor oscilloscope for further processing off-line.

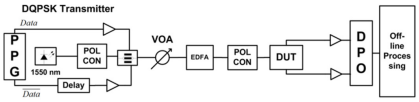

Fig. 2. Experimental setup for characterizing the DQPSK receiver.

The DQPSK transmitted eyes at 10 and 20Gbit/s are shown in Fig. 3, as well as the reference constellation obtained by using a discrete receiver described in [13].

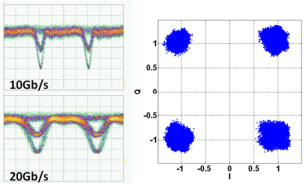

Fig. 3. 10Gbit/s and 20Gbit/s Transmitted DQPSK eyes, and reference constellation measured by a discrete receiver.

For the 10Gbit/s integrated receiver, well opened eye-diagrams and remarkably good constellation diagrams were obtained, as shown in Fig. 4 for a received power of -19dBm. The EVM as a function of the received power was then characterized. Fig. 5(a) shows the measured results.

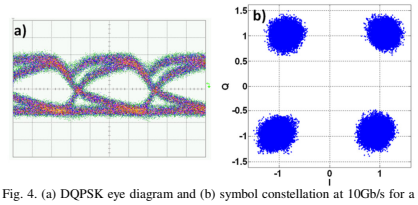

Fig. 4. (a) DQPSK eye diagram and (b) symbol constellation at 10Gb/s for a received power of -19dBm.

The BER was also characterized. However, as the quality of the received signal was quite good so that no significant amount of errors were recorded in the captured length of the data, which was 100k symbols, the EVM of the signal was used to estimate the BER for received powers above -23 dBm, as shown in Fig. 5(b). BER was estimated using the following equation taken from [15]

$$BER \approx \frac{2\left(1-\frac{1}{L}\right)}{\log_2 L} Q\left[\sqrt{\left[\frac{3\log_2 L}{L^2-1}\right]\frac{2}{EVM^2 \log_2 M}}\right] \quad (1)$$

where L is the number of signal levels per quadrature, M is the order of the modulation and Q indicates the Q-function. For QPSK modulation, L is 2 and M is 4.

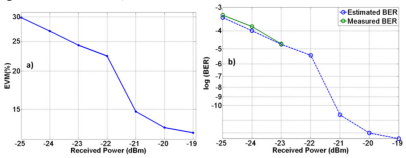

Fig. 5. (a) EVM versus received power. (b) Measured (green curve) and estimated (blue curve) BER versus received power, for the 10Gbit/s differential receiver.

Examining the EVM results shown in Fig. 5(a), a very satisfactory floor value around 12.5% is observed. It can also be seen that there is a sharp decline in EVM, which is also translated into the BER curve shown in Fig. 5(b). The reason is that for input powers lower than -21 dBm, the EDFA can no longer amplify the signal to the aforementioned +16 dBm, and lower powers reaches the balanced photodiodes. On the other hand, looking at the BER results depicted in Fig. 5(b), it can be seen that the error floor is around 10^{-15}. Furthermore, even at -25 dBm received power, the BER is lower than the Forward Error Correction (FEC) threshold. It is also important to notice that the measured BER values, from -25 to -23 dBm received power, are in good agreement with the estimated values using Eq. (1).

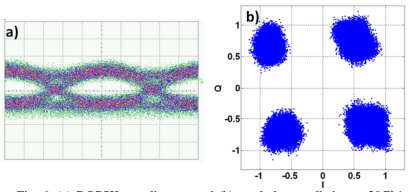

Fig. 6. (a) DQPSK eye diagram and (b) symbol constellation at 20Gb/s for a received power of -12dBm.

For the 20 Gbit/s DQPSK receiver, opened eyes and good constellation diagram were also measured, as shown in Fig. 6 for a received power of -12 dBm. Comparing the obtained constellation diagram with the reference one shown in Fig. 3, it can be seen that some additional noise appears in the symbols of the constellations. Nevertheless, the EVM of the obtained constellation was measured to be 19.57% and the corresponding BER was estimated by using Eq. (1) in $1.7 \cdot 10^{-7}$.

IV. CONCLUSION

A minimum footprint differential receiver for DQPSK transmission with zero biased detection for access networks has been demonstrated at 10 and 20 Gbit/s. Each building block of the receiver was optimized for high performance, low loss and maximum compactness. The results indicate the potential of integrated silicon receivers to become key building blocks for future passive optical networks based on advanced modulation formats. Since the receivers were not packaged with transimpedance amplifiers, its sensitivity was reduced. DQPSK was used to evaluate the receiver. However, higher-order modulation formats can be supported due to the low EVM values achieved. For instance, for an EVM of 12.5%, translated into BER for D8PSK, results into a BER lower than 10^{-5} [14].

ACKNOWLEDGMENT

The authors acknowledge funding by the European Commission under project HELIOS (pHotonics Electronics functional Integration on CMOS), FP7-224312. The authors would also like to thank Dr. Javier Herrera and Dr. Rakesh Sambaraju for fruitful discussions.

REFERENCES

[1] A. H. Gnauck and P. J. Winzer, "Optical phase-shift-keyed transmission," *J. Lightw. Technol.*, vol. 23, no. 1, pp. 115-130, Jan. 2005.

[2] M. Kroh, L. Zimmermann, H.-G. Bach, K. Voigt, A. Beling, M.L. Nielsen, R. Ludwig, J. Bruns, and G. Unterbörsch, "Integrated receivers on silicon-on-insulator for advanced modulation formats," *Optoelectronics, IET* , vol.5, no.5, pp.211-217, October 2011.

[3] S. Faralli, K. N. Nguyen, J. D. Peters, D. T. Spencer, D. J. Blumenthal, and J. E. Bowers, "Integrated hybrid Si/InGaAs 50 Gb/s DQPSK receiver", *Opt. Exp.*, vol. 20, no. 18, pp. 19726-19734 (2012).

[4] C.R. Doerr, N.K. Fontaine, and L.L. Buhl, "PDM-DQPSK Silicon Receiver With Integrated Monitor and Minimum Number of Controls," *IEEE Photonics Technol. Lett.*, vol. 24, no. 8, pp. 697-699, Apr. 2012.

[5] L. Xu, C. Li, C. Y. Wong, and H. K. Tsang, "DQPSK demodulation using integrated silicon microring resonators," *Opt. Commun.*, vol. 284, no. 1, pp. 172-175, Jan. 2011.

[6] Y. Ding, J. Xu, C. Peucheret, M. Pu, L. Liu, J. Seoane, H. Ou, X. Zhang, and D. Huang, "Multi-Channel 40 Gbit/s NRZ-DPSK Demodulation Using a Single Silicon Microring Resonator," *J. Lightw. Technol.*, vol. 29, no. 5, pp. 677-684, Mar. 2011.

[7] L. Chen, N. Sherwood-droz, and M. Lipson, "Compact bandwidth-tunable microring resonators," *Opt. Lett.*, vol. 32, no. 22, pp. 3361-3363, Nov. 2007.

[8] K. Suzuki, H. C. Nguyen, T. Tamanuki, F. Shinobu, Y. Sakai, and T. Baba, "Slow-light-based variable symbol-rate silicon photonics DQPSK receiver," *Opt. Exp.*, vol. 20, no. 4, pp. 4796-4804, Feb. 2012.

[9] F. Van Laere, T. Claes, J. Schrauwen, S. Scheerlinck, W. Bogaerts, D. Taillaert, L. O'Faolain, D. Van Thourhout, R. Baets, "Compact Focusing Grating Couplers for Silicon-on-Insulator Integrated Circuits", *IEEE Photonics Technol. Lett.*, vol. 19, no. 23, pp.1919-1921, Feb. 2007.

[10] M. Aamer, A. Griol, A. Brimont, A. Gutierrez, P. Sanchis, and A. Håkansson, "Increased sensitivity through maximizing the extinction ratio of SOI delay-interferometer receiver for 10G DPSK," *Opt. Exp.*, vol. 20, no. 13, pp. 14698-14704, Jun. 2012.

[11] R. Halir, G. Roelkens, A. Ortega-Moñux, and J. G. Wangüemert-Pérez , "High-performance 90° hybrid based on a silicon-on-insulator multimode interference coupler", *Opt. Lett.*, vol. 36, no. 2, pp. 178-180, Jan. 2011.

[12] L. Vivien, A. Polzer, D. Marris-Morini, J. Osmond, J. Hartmann, P. Crozat, E. Cassan, C. Kopp, H. Zimmermann, and J. Fédéli, "Zero-bias 40Gbit/s germanium waveguide photodetector on silicon," *Opt. Exp.*, vol. 20, no. 2, pp. 1096-1101, Jan. 2012.

[13] N. Sotiropoulos, T. Koonen, and H. de Waardt, "TDM-PON with 30 Gb/s D8PSK downstream and 10 Gb/s OOK upstream based on a digital incoherent receiver," *Opt. Exp.*, vol. 20, no. 27, pp. 29096-29104, Dec. 2012.

[14] R. Schmogrow, B. Nebendahl, M. Winter, A. Josten, D. Hillerkuss, S. Koenig, J. Meyer, M. Dreschmann, M. Huebner, C. Koos, J. Becker, W. Freude and J. Leuthold, "Error Vector Magnitude as a Performance Measure for Advanced Modulation Formats," *IEEE Photonics. Technol. Lett.*, vol. 24, no. 1, pp. 61-63, Jan. 2012.

4 FlexPON router

4.1 Introduction

In this chapter I will discuss an integrated wavelength router for Fiber-To-The-Home/Business/Premises/Curb (FTTx) using a Flexible Passive Optical Network (FlexPON) technology. This work was performed in cooperation with Genexis and in the framework of the Dutch Smartmix-Memphis project. FlexPON is a new concept for FTTx based on Dense Wavelength Demultiplexing (DWDM) developed to increase the bandwidth of the network [1]. Furthermore, it increases the dynamic re-configurability and resilience of the network. In Fig. 4.1 a schematic drawing of a FlexPON network is shown. Single-mode fibers (SMF) connect the Central Office (CO) to a number of Remote Nodes (RNs) in the field. Several Home Users, called Optical Network Units (ONUs), are served by a common RN. The CO transmits a set of downstream (DS) data signals and a complementary set of continious waveform (CW) signals to a RN. A DS-signal and the complementary CW-signal from a wavelength pair and are dropped at the RN to an ONU. In order to be able to use commercial lasers at the CO, all wavelengths are on the ITU-T wavelength grid of the C-band. The CW signal makes it possible to replace an expensive temperature controlled laser at the ONU by a low-cost and broadband Reflective Semiconductor Optical Amplifier (RSOA) which amplifies, reflects and modulates the CW-signal into an upstream signal. The broadband photodector and broadband RSOA make the transceiver at the ONU colorless

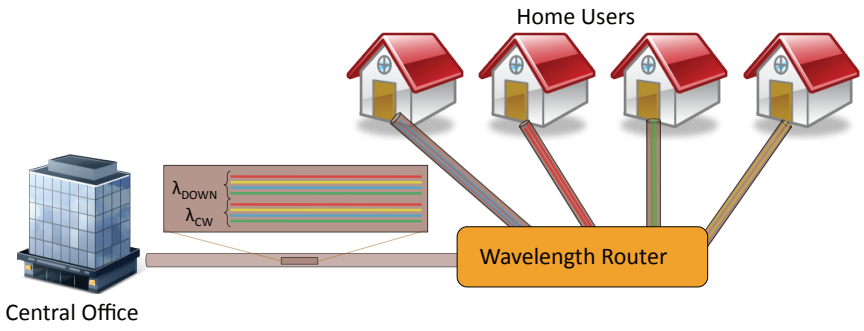

Figure 4.1: Schematic drawing of a FlexPON newtork. A reconfigurable wavelength router (part of the RN) drops wavelength pairs from the Central Office to the Home Users or ONU.

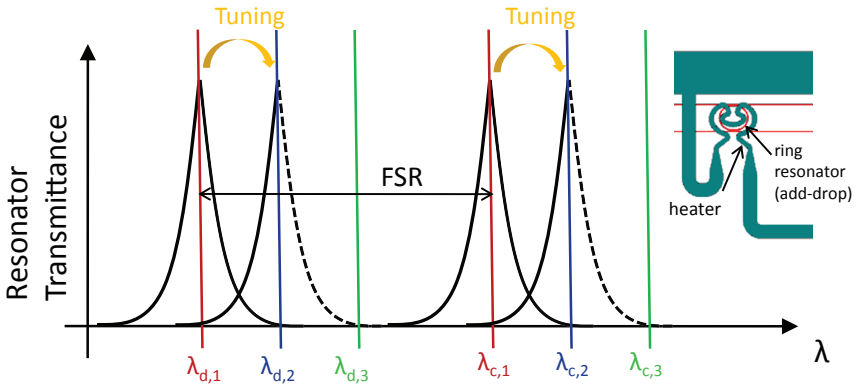

Figure 4.2: The spectrum before and after tuning of a microring resonator. The Free Spectral Range (FSR) coincides with the wavelength spacing between the Downstream (DS) and Continuous Wave (CW) wavelength pairs.

such that wavelength channels can be reconfigured over time.
The enabling component of the RN is a Wavelength Router (WR). I will investigate the feasibility of realizing a WR based on an SOI integrated photonics chip employing microring resonators which are thermally tuned with heaters. These microring resonators are particularly interesting since they can filter and thus drop multiple wavelengths at the same time, spaced by the Free Spectral Range (FSR) of the resonator. The principle is shown in Fig. 4.2. By tuning the ring resonator, a pair of wavelengths of choice can be dropped to one or multiple users.

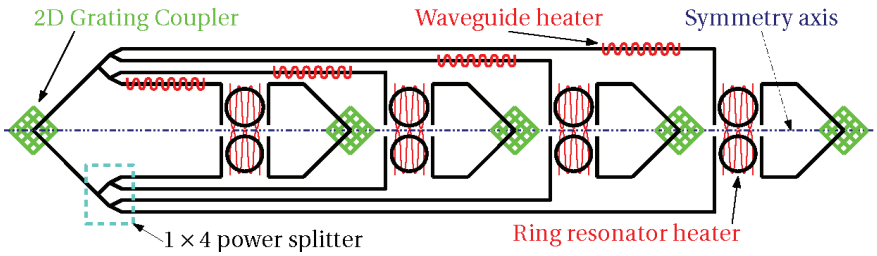

Figure 4.3: Polaization diversity implementation of a FlexPON WR. 2D grating couplers are used as in and out coupling elements. The upper circuit introduces a π phase shift using thermally tunable waveguide heaters for PDL minimization.

4.2 2D grating PDL compensation

In order to integrate the WR on SOI, we need to develop the appropriate on-chip components. In Fig. 4.3 an integration scheme for a FlexPON WR is shown. Due to the waveguide birefringence, I chose a polarization diversity scheme and thus process both orthogonal polarizations separately using an identical circuit of splitters and ring resonators. Fabrication variations can be compensated for by thermally tuning the ring resonators individually thereby obtaining an identical transfer function for both polarizations. The fiber-to-chip coupling is done by means of near vertical fiber 2D grating couplers [2]. This 2D grating is a big contributor to the polarization dependent loss (PDL).
In [3] (see attached paper on page 4-15) we explain and solve the 2D grating PDL problem for a fiber-to-fiber integrated circuit such as a WR. By introducing a relative phase shift of π in one of the polarization diversity circuits, the PDL introduced by the 2D grating used as incoupling element can be compensated for by the PDL introduced by the 2D grating used as outcoupling element. The PDL of the 2D grating itself is thus not removed, but the total PDL of the fiber-to-fiber circuit is annihilated. We introduce the π phase shift with a waveguide heater (see Fig. 4.3). A microscope picture of the fabricated FlexPON WR is shown in Fig. 4.4. By tuning the ring resonators and using the heaters to introduce a π phase shift the PDL can be reduced to 0.15 dB, well below the required PDL specification of 0.5 dB. These PDL measurments are plotted in Fig. 4.5 for 1556.5 nm and 1560 nm.

4.3 Ring resonators

Integrated ring resonators are a key building blocks for our FlexPON wavelength router. Typical ring resonators in silicon single-mode strip waveguides (fully etched) do not have high performance. This is attributed to the high in-

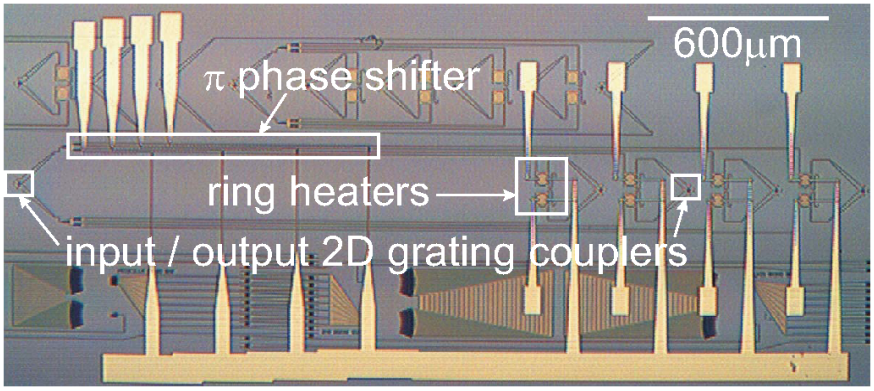

Figure 4.4: Microscope picture of a fabricated FlexPON WR SOI chip.

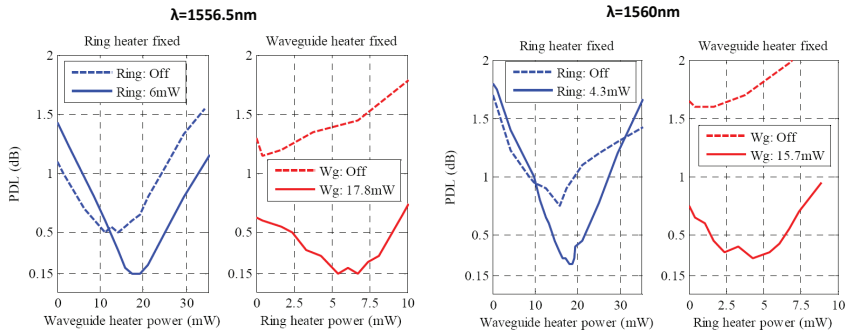

Figure 4.5: PDL measurements of the FlexPON WR chip as a function of the waveguide and ring heater power for two different wavelengths. (see [3] on page 4-15)

dex contrast of the waveguide which introduces high waveguide bend losses and backscattering due to surface roughness of the waveguide sidewalls. The backscattered light will excite a counter-propagating mode of the ring resonator [4] causing a resonance splitting. Although deeply etched SOI waveguides using DUV lithography can achieve < 2 dB/cm loss for TE polarized light [5], typical achieved Q factors in ring resonators are 10 000, corresponding to a waveguide loss of around 10 dB/cm.

4.3.1 Ring resonator using TM polarization

Reducing the waveguide bend loss and side-wall (back-) scattering loss is key to enhance the performance of a ring resonator. We employed this principle by exciting the TM mode instead of the TE mode in a ring resonator. The TM mode is less confined and will thus have a smaller overlap with the sidewalls. Furthermore, the electrical field is vertical such that the field discontinuities occur at the top and bottom interfaces of the waveguide instead of the sidewalls which exhibit the most roughness from etching. The results were published in [6]. We achieved an intrinsic Q (Q_i) of up to 340 000, which is roughly 4 times more than Q's obtained with TE-polarized light. This corresponds with a resonator waveguide loss of 1.94 dB/cm. Another advantage of using the TM mode is that it exhibits a lower effective refractive index, such that the ring resonator fabrication tolerances are more relaxed. This can be verified from the ring resonator spectra which showed excellent response over the whole C-band.
A drawback of using the TM mode is that the lower effective refractive index restricts us to make low-loss bends with a small bend radius. The TM ring resonators need typically a bend radius of at least 15 μm to achieve a Q_i of more than 100 000. This translates in a maximum FSR of 8 nm, restricting the number of channels for our FlexPON application with wavelength spacing of 200 GHz (about 1.6 nm) to 4 channels. The tuning range of a ring resonator is typically limited and on the order of 5 nm to 10 nm (600 GHz-1.2 THz). This is in essence the main contributer to the reconfigurable channel limit.
In most applications TE-polarized light is preferred for fiber-to-chip coupling and waveguide routing. Both horizontal and vertical fiber-to-chip coupling methods have lower losses for the TE mode. Furthermore, the high confinement of the TE mode allows for tight waveguide routing. To avoid the need for a polarization rotator, which converts the TE mode in the TM mode on chip, we investigated if it is possible to excite the TM mode in the ring resonator with a TE mode in the bus waveguide. The results can be found in [7] at the end of the chapter page 4-18. We used an asymmetrical coupling section such that the TE mode in the bus waveguide is phase matched to the TM mode in the ring resonator. We achieved a mean Q of 326 600 and mean finesse of 88 for a critically coupled

all-pass ring resonator. The ER was better than 16 dB over a 40 nm wavelength range and no peak-splitting was observed. We call this kind of ring resonator a polarization rotating ring resonator.[1]
More detail and a deeper investigation of polarization rotating ring resonator was published in [8]. This study was performed using a rigorous fully-vectorial eigenmode expansion and propagation tool. There are two required levels of asymmetry in the directional coupler exciting the ring resonator: 1) a different waveguide width for the bus and the ring and 2) an asymmetrical cladding. The study reveals that besides the fundamental TM mode also the fundamental TE mode and higher order modes are excited in the ring resonator. The ideal coupling section coincides with a maximized coupling to the TM mode and minimal coupling to the other modes. We also found that certain designs couple equally to the TM and TE mode, thus creating a double resonance. This double resonating ring resonator was for example used in a biosensing application [9].

4.3.2 Ring resonator based on a rib waveguide

Our quest to achieve record-high Q's led us to a ring resonator employing shallow etched rib waveguides. A shallow rib waveguide mode has almost all light in Si and has a very low overlap with the thin sidewalls. The results of all-pass ring resonators were published in [10]. The measurements for the mean Q's and mean finesses as a function of the gap distance between bus and ring waveguide are shown in Fig. 4.6 and Fig. 4.7 for different waveguide widths and ring radiuses. For large gap widths, the Q asymptotically converges to the intrinsic Q of the ring resonator. For certain geometries of the waveguide, i.e. 700 nm waveguide width and ring radius of 50 μm, the measured Q's were ultra-high and on the order of 500 000. Furthermore, the finesse was determined to be 1000. This means that the ring resonator waveguide loss decreased to a mere 0.81 dB/cm. In Fig. 4.8 the resonance spectrum of two ring resonators are plotted. Ring 1 is critically coupled with an extinction ratio of 17 dB while having a Q of 417 000 and ultra-high finesse of 1100. Similar results have been published in [11]. This record finesse could enable a whole new set of applications such as reduced threshold in Raman lasers, ultra-dense WDM applications, sensing and delay lines.

4.4 XPON/FlexPON

The XPON/FlexPON network is a hybrid architecture where the downstream data follows the FlexPON principle as shown in Fig. 4.9 and has been explained earlier in Chapter 4.1. It is a flexible PON network where redistribution of the

[1] This work has been done in close cooperation with Peter De Heyn.

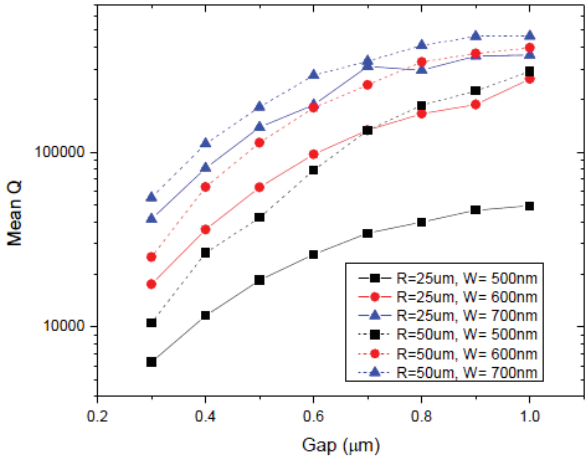

Figure 4.6: The mean Q_i (1520 nm – 1560 nm) of shallow rib waveguide based ring resonators as a function of gap for varying waveguide width (W) and ring radius (R). (Courtasy of Peter De Heyn [10])

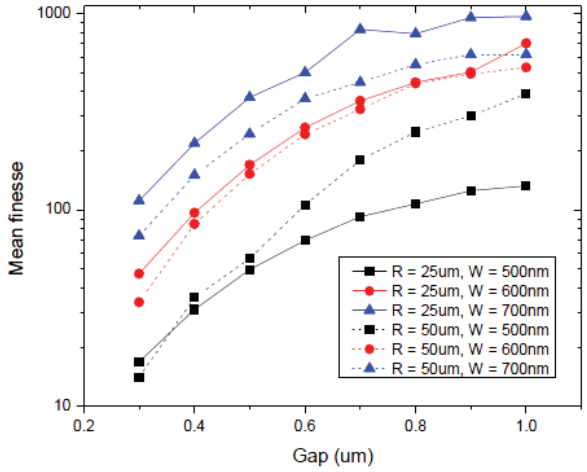

Figure 4.7: The mean finesse (1520nm-1560nm) over all resonances per ring as a function of gap for varying waveguide width (W) and radius (R). (Courtasy of Peter De Heyn [10])

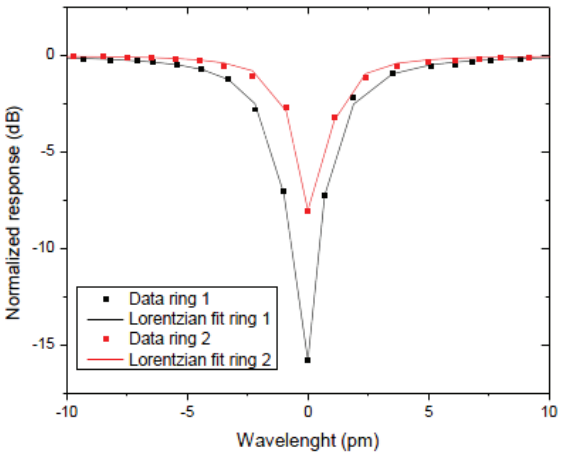

Figure 4.8: Illustration of two critically coupled microring resonators with a Lorentzian fit. Ring 1: R = 25 μm, gap = 0.7 μm, width = 0.7 μm, *around* 1550nm. *Ring 2:* R = 50 μm, gap = 0.7 μm, width = 0.7 μm, *around* 1530 nm. *(Courtasy of Peter De Heyn [10])*

downstream data takes place by means of wavelength switching. For example, users demanding temporarily high bandwidth can be appointed a dedicated wavelength or a wavelength that is shared with a smaller number of users. The upstream data transmission in PON networks is typically done by means of electrical time division multiplexing schemes. In the XPON or switchPON concept, the Time Division Multiplexing (TDM) is done in the optical domain using wavelength switching. This has the advantage that the optical power is not splitted among all the ONUs, and that the transceiver at the ONU does not have to have any TDM awareness. Furthermore, multiple wavelengths can be used to increase the upstream bandwidth and/or facilitate large bandwidth demanding ONUs. As was the case in the FlexPON architecture, the XPON also works with CW signals transmitted at the CO which are reflected, modulated and amplified at the ONU. The XPON principle is schematically shown in Fig. 4.10 and Fig. 4.11.
With all the previous building blocks that I have demonstrated we are able to build the wavelength router needed to enable this XPON/FlexPON network architecture. The mask design of the wavelength router circuit is shown in Fig. 4.12. The colors correspond to the same wavelengths as in Fig. 4.9 to 4.11. The wavelength router is designed for two downstream wavelengths (red and blue) in the L-band and two upstream wavelengths wavelengths in the C-band. The wavelengths are on the ITU-T wavelength grid and have a wavelength spacing of 200 GHz. The left input grating coupler provides the fiber-to-chip interface with the fiber connected to the CO. The four grating couplers on the right con-

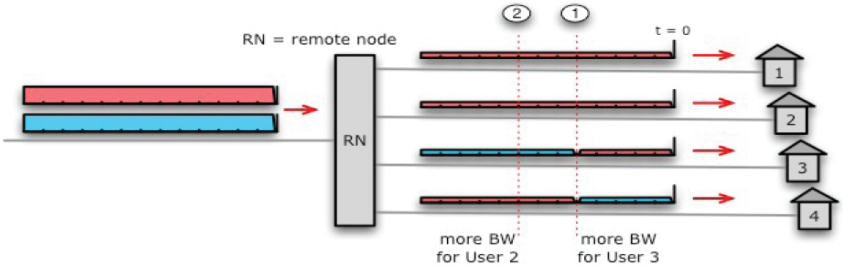

Figure 4.9: Downstream data following the FlexPON principle.

nect 4 ONUs to the wavelength router. The grating couplers are 2-dimensional and couple the orthogonal polarizations upwards and downwards in separate waveguides. The on-chip circuit handles the coupled orthogonal polarizations separately (polarization diversity). The light from the CO is then broadband splitted with a Mach-Zehnder-Interferometer (MZI) into the C-band and L-band, corresponding to the upstream wavelength and downstream wavelength bands respectively. The downstream wavelengths are passively split in four with a 1×2 MMI splitting tree. The circuit contains a ring resonator for each user and each downstream/upstream wavelength. The resonance wavelength of the ring resonators is controlled by low-loss thermal tuning. Each ring resonator is tuned such that its resonant wavelength is slightly smaller than the corresponding downstream/upstream wavelength. This allows for a tuning or switching delay smaller than 1 ms as specified for downstream wavelength tuning.
Although I solved a great deal of issues for realizing a wavelength router that fulfills the FlexPON/XPON specifications, an important number of issues are not completely solved or demonstrated. For the upstream wavelength switching, a delay of not more than 1 μs is allowed which is very challenging to achieve by thermal tuning. This could be solved by using the plasma dispersion effect to attenuate the ring resonator while it is cooling down. However, the biggest problem remains the power budget and specifically the fiber-to-chip coupling loss. This cannot exceed 1.5 dB over a wavelength range of 50 nm (part of C-band and L-band) which can't be achieved with a fully optimized 2D grating coupler. Therefore, a horizontal coupling approach with polarization rotator as was demonstrated in Chapter 3 would be better suited. Alternatively, one could integrate semiconductor optical amplifiers (SOA) using for example heterogeneous III/V BCB bonding to compensate for the higher grating coupler losses.

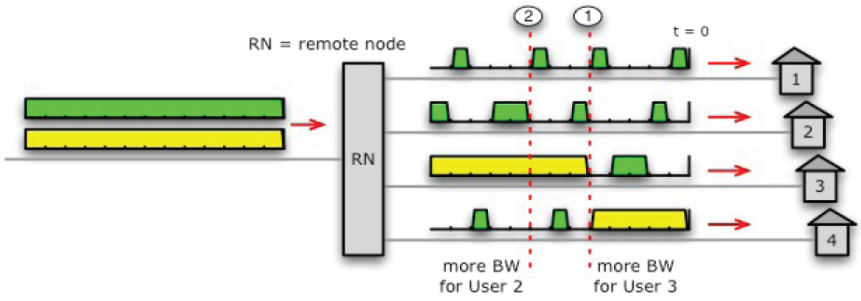

Figure 4.10: Continuous wave signal for upstream modulation distributed to ONUs.

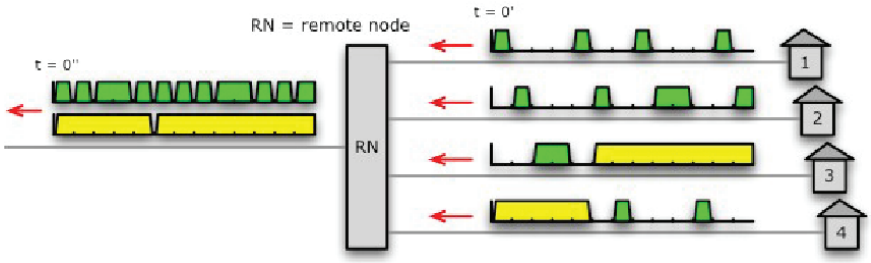

Figure 4.11: Modulated upstream signals combined at remote note.

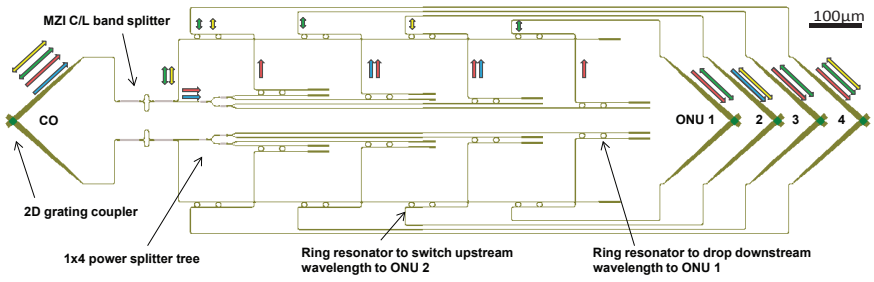

Figure 4.12: Mask design of a wavelength router enabling a XPON/FlexPON network architecture. The ring and waveguide heaters are not shown for clarity.

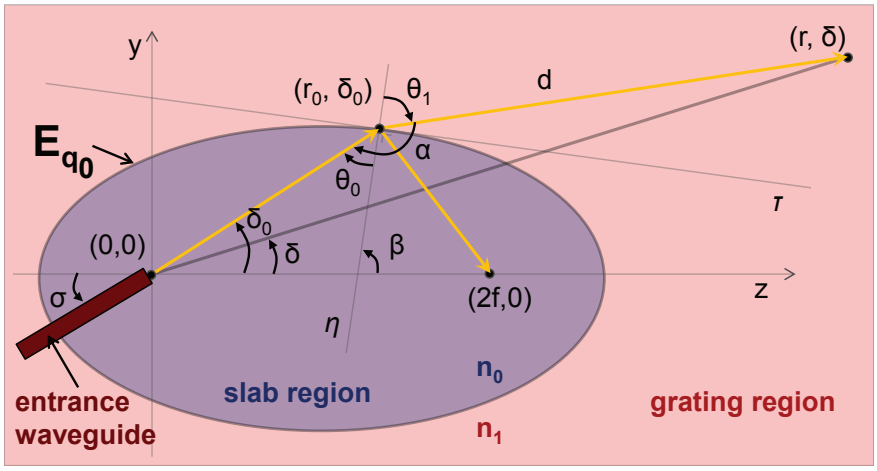

Figure 4.13: Focusing grating coupler geometry parameters. The light (yellow arrows) is refracted and reflected at the first grating ellipse E_{q_0}. τ and η are the tangent and normal line respectively of ellipse E_{q0} at point (r_0, δ_0).

4.5 Reflectionless grating coupler

The specified return loss for a wavelength router is 45 dB or better. PICs with integrated lasers or SOA's are ultra-sensitive to on-chip reflections. An elegant and low-loss Silicon Photonics isolator is yet to be demonstrated. Due to the high index contrast in SOI integrated circuits, special care has to be taken to minimize on-chip reflections. For example, MMI power splitters can be optimized for minimal return loss by angling all waveguide interfaces [12]. Grating couplers are typical sources of high return loss. More specifically, the grating reflection back into the waveguide is problematic for a lot of PIC applications which contain amplifiers. This back reflection is mainly dependent on the exact grating cross section. Back reflections from −10 dB to −25 dB have been reported. I demonstrated a grating coupler design which reduces the back reflection to −40 dB, the typical reflection performance of an optical fiber connector. The principle, design rules and 3D FDTD simulations have been published in [13] (see attached paper on page 4-20). The measurement results were published in [14] and the improved grating couplers showed a 10 dB lower return loss without introducing an IL penalty. This reflectionless grating coupler design is based on a focusing grating coupler design [15]. The grating is curved such that a plane wavefront originating from the tilted optical fiber is diffracted to the TE-polarized mode of a broad SOI waveguide, so that the wavefront is curved cylindrically and focusing occurs in the center of curvature of the wavefront. The easiest way to describe this system is to use a polar coordinate system (r, δ) with the origin

placed at the exit point of the entrance waveguide (see Fig. 4.13). The phase matching condition for the position of the grating scattering holes or trenches is the collection of points p that will give constructive interference between a point at the origin (waveguide ending) and the family of planes V, tilted under an angle ϕ (the fiber tilt angle):

$$2\pi q = \beta r + kd(p,V) \tag{4.1}$$

with β the propagation constant in the silicon slab, k the upper cladding propagation constant and q an integer number. V is the plane family $x + \tan\phi z + cst = 0$ and p is a scatter grating point $(r\cos\delta, r\sin\delta)$. The distance between a scatter point and plane V is given by

$$d(p,V) = \frac{\vec{n}.\vec{p}}{|\vec{n}|} = r\cos\delta\sin\phi \tag{4.2}$$

which results together with Eq. (4.1) in Eq. (1) of [13] (see page 4-20):

$$q\lambda_0 = r n_s - r n_c \cos\delta\sin\phi \tag{4.3}$$

with λ_0 the wavelength in vacuum, n_s the effective refractive slab index and n_c the refractive index of the top cladding. This is the basic formula on which a curved and reflectionless grating coupler is based. I improved this formula by taking into account the difference in effective refractive index between the slab and grating region and by taking into account the diffraction at the slab/grating interface (see [13] page 4-20 for more details).

4.6 Conclusion

FlexPON or the XPON/FlexPON variant are new concepts for FTTx based on Dense Wavelength Demultiplexing (DWDM) developed to increase the bandwidth of the network. This concept requires a wavelength router (WR) in a remote node that reconfigures the network in the optical domain. Integrated photonics and in particular Silicon Photonics is an enabling technology for realizing such a highly complex WR. I investigated the necessary subcomponents and optimized them such that the WR specs can be reached. A PDL compensation method in the case of fiber-to-chip coupling by means of 2D grating couplers has been demonstrated achieving a PDL as low as 0.15 dB. Ring resonators, serving as the main component for wavelength switching, have been improved to achieve ultra-high Q's of one million. Furthermore, the return loss of grating couplers have been improved up to 45 dB.

References

[1] M. M. De Laat, R. L. Duijn, E. G. C. Pluk, G. N. Van Den Hoven, P. J. Urban, and H. De Waardt. *FlexPON : a Hybrid TDM / WDM Network enabling Dynamic Bandwidth Reconfiguration using Wavelength Routing.* In ECOC, number 1, page 1.6.3, 2009.

[2] D. Taillaert, P.I. Borel, L.H. Frandsen, R.M. De La Rue, and R. Baets. *A compact two-dimensional grating coupler used as a polarization splitter.* IEEE Photonics Technology Letters, 15(9):1249–1251, 2003.

[3] R. Halir, D. Vermeulen, and G. Roelkens. *Reducing Polarization-Dependent Loss of Silicon-on-Insulator Fiber to Chip Grating Couplers.* IEEE Photonics Technology Letters, 22(6):389–391, 2010.

[4] B E Little, J P Laine, and S T Chu. *Surface-roughness-induced contradirectional coupling in ring and disk resonators.* Optics letters, 22(1):4–6, 1997.

[5] S.K. Selvaraja, W. Bogaerts, P. Absil, D. Van Thourhout, and R. Baets. *Record Low-Loss Hybrid Rib / Wire Waveguides for Silicon Photonic Circuits.* Group IV Photonics, 2010.

[6] P. De Heyn, B. Kuyken, D. Vermeulen, W. Bogaerts, and D. Van Thourhout. *High-Performance Low-Loss Silicon-on-Insulator Microring Resonators using TM-polarized Light.* In The Optical Fiber Communication Conference and Exposition (OFC) and The National Fiber Optic Engineers Conference (NFOEC), Los Angeles, United States, 2011.

[7] D. Vermeulen, P. De Heyn, T. Van Vaerenbergh, W. Bogaerts, and G. Roelkens. *Silicon-on-Insulator polarization rotating micro-ring resonator.* In IEEE Photonics Conference (IPC), volume 4, pages 875–876, Arlington, United States, 2011.

[8] P. De Heyn, D. Vermeulen, D. Van Thourhout, and G. Roelkens. *Silicon-on-Insulator All-Pass Microring Resonators Using a Polarization Rotating Coupling Section.* IEEE Photonics Technology Letters, 24(14):1176–1178, 2012.

[9] T. Claes, D. Vermeulen, P. De Heyn, K. De Vos, G. Roelkens, D. Van Thourhout, and P. Bienstman. *Towards a silicon dual polarization ring resonator sensor for multiplexed and label-free structural analysis of molecular interactions.* page 159, Barcelona, Spain, 2012.

[10] P. De Heyn, D. Vermeulen, T. Van Vaerenbergh, B. Kuyken, and D. Van Thourhout. *Ultra-high Q and finesse all-pass microring resonators on Silicon-on-Insulator using rib waveguides.* In 16th European Conference on Integrated Optics, Barcelona, Spain, 2012.

[11] D. Adams, G. Madejski, and S. Preble. *High-Q shallow etch silicon micro resonators for optical delay.* In IEEE Photonic Society 24th Annual Meeting, volume 2, pages 871–872, 2011.

[12] Y. Li and R. Baets. *Improved multi-mode interferometers (MMIs) on silicon-on-insulator with the optimized return loss and isolation.* In 16th Annual Symposium of the IEEE Photononics Benelux Chapter, volume 2, 2011.

[13] D. Vermeulen, Y. De Koninck, Y. Li, E. Lambert, W. Bogaerts, R. Baets, and G. Roelkens. *Reflectionless grating couplers for Silicon-on-Insulator photonic integrated circuits.* Optics Express, 20(20):22278, 2012.

[14] Y. Li, D. Vermeulen, Y. De Koninck, G. Yurtsever, G. Roelkens, and R. Baets. *Fiber couplers for silicon-on-insulator photonic IC's with optimized on-chip return loss.* In Optical Fiber Communication Conference (OFC), volume 1, page JTh2A.8, 2012.

[15] F. Van Laere, G. Roelkens, M. Ayre, J. Schrauwen, D. Taillaert, D. Van Thourhout, Thomas F. Krauss, and R. Baets. *Compact and Highly Efficient Grating Couplers Between Optical Fiber and Nanophotonic Waveguides.* Journal of Lightwave Technology, 25(1):151–156, 2007.

Reducing Polarization-Dependent Loss of Silicon-on-Insulator Fiber to Chip Grating Couplers

Robert Halir, Diedrik Vermeulen, and Günther Roelkens

***Abstract*—For many telecommunication applications, low polarization-dependent loss (PDL) operation is mandatory. On the silicon-on-insulator photonic wire platform, this can be achieved using polarization diversity configurations. However, as we show here, when using two-dimensional grating couplers for near vertical fiber input and output, the low PDL bandwidth is limited. We propose and demonstrate the use of a π phase shifter in one of the arms of the polarization diversity circuit to effectively reduce PDL (0.15-dB PDL is shown) and increase the low PDL bandwidth.**

***Index Terms*—Grating coupler, polarization-dependent loss (PDL), polarization diversity, silicon-on-insulator.**

I. Introduction

SILICON-ON-INSULATOR photonic wire technology allows for a substantial scaling in the size of photonic integrated circuits due to the high refractive index contrast that is available. Silicon waveguides with dimensions on the order of 500 nm by 200 nm allow for single-mode propagation and tight optical confinement. The high refractive index contrast makes the waveguide structures very polarization-dependent, which is, however, an issue in many practical applications. Therefore, polarization diversity schemes are being proposed to tackle this problem. In one approach, a polarization splitter and rotator is being integrated on the chip, such that the two arms of the polarization diversity circuit are processing the same polarization state. This resulted in relatively low polarization-dependent loss (PDL) (about 1 dB) [1], [2]. In [3], it was proposed to use a two-dimensional (2-D) grating structure, which at the same time fulfills the role of optical fiber interface, polarization splitter, and rotator, all on a 100-μm^2 area. Taking into account the full bandwidth of the grating coupler spectrum, still quite substantial PDL can be observed in the experiment (1- to 2-dB PDL in the fiber to fiber coupling 1-dB bandwidth). In this letter, we show that, by introducing a π phase shifter in one arm of the polarization diversity circuit, a substantial PDL reduction can be obtained.

This work was carried out in the framework of the Dutch Smartmix-Memphis project. The work of R. Halir was supported by the Spanish Ministerio de Educación under a FPU scholarship with reference AP-2006-03355. The work of D. Vermeulen was supported by the Institute for the Promotion of Innovation by Science and Technology in Flanders (IWT) under a grant. The work of G. Roelkens was supported by the Fund for Scientific Research Vlaanderen (FWO) under a postdoctoral grant.

R. Halir is with the Departamento de Ingeniería de Comunicaciones, ETSI Telecomunicación, Universidad de Málaga, 29010 Málaga, Spain (e-mail: robert.halir@ic.uma.es).

D. Vermeulen and G. Roelkens are with the Department of Information Technology (INTEC), Ghent University – Interuniversity Microelectronics Center (IMEC), B-9000Gent, Belgium (e-mail: gunther.roelkens@intec.ugent.be)

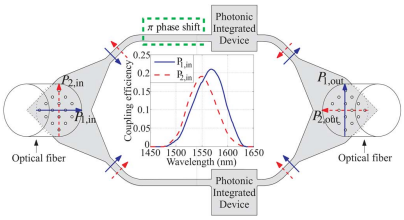

Fig. 1. Schematic illustration of a polarization diversity circuit with 2-D gratings. The inset shows the simulated coupling efficiency of a 2-D grating for polarizations $P_{1,\mathrm{in}}$ and $P_{2,\mathrm{in}}$.

II. Causes and Reduction of PDL

In a polarization diversity scheme like the one shown in Fig. 1, light is coupled in and out of the circuit with fibers positioned over the 2-D grating couplers [3], [4]. These couplers convert any polarization state in the fiber to transverse-electric (TE) polarized light in both arms of the polarization diversity circuit. In order to avoid strong back reflections from the gratings, the fibers have to be slightly tilted, typically at $\sim 10^\circ$ with respect to the vertical. In both arms the light is then directed to the integrated photonic device that performs the desired functionality and is finally coupled into the output fiber using an identical 2-D grating coupler. In such a polarization diversity configuration, there are three main sources of PDL.

First, if the input and output fibers are not positioned along the diagonal of the 2-D grating couplers, symmetry is lost and some polarization states will couple more efficiently to and from the integrated waveguides than others. This contribution to PDL can be minimized with proper fiber alignment, as detailed in Section III. Second, due to fluctuations during fabrication, the devices in either arm may not behave identically, thus introducing a different amount of loss. Trimming or tuning of the devices may be used to cancel this effect. In some device configurations, the same device can be used for both arms of the polarization diversity circuit, by propagation in opposite directions [5]. Finally, the grating couplers themselves also introduce PDL. This is best understood considering the two linear polarizations at 0° and 90°, $P_{1,\mathrm{in}}$ and $P_{2,\mathrm{in}}$, shown in Fig. 1. Due to the near vertical coupling, $P_{1,\mathrm{in}}$ is slightly tilted out of the grating plane, while $P_{2,\mathrm{in}}$ lies in the same plane as the grating coupler. Consequently, $P_{1,\mathrm{in}}$ and $P_{2,\mathrm{in}}$ will not exhibit the same coupling efficiency. The different coupling efficiencies are shown in the inset

of Fig. 1. They were obtained with three-dimensional (3-D) finite-difference time-domain simulations of a 19×19 array of circular holes with a diameter of 400 nm and a 605-nm pitch. The outgoing waveguides form an 83.8° angle to account for the effect of the tilted fiber (see [4]). Since the coupling efficiency of both polarizations only coincides at a specific wavelength, the grating coupler will generally introduce PDL. The reduction of this type of PDL is the main contribution of this letter and will be discussed in more detail in the following.

From symmetry considerations it is clear that if polarization state $P_{1,\text{in}}$ is aligned along the grating bisection line, it will couple symmetrically to the upper and lower arm of the polarization diversity circuit. This is schematically illustrated with the solid arrows on the left side of Fig. 1. On the other hand, polarization state $P_{2,\text{in}}$ will couple antisymmetrically, i.e., with a 180° phase shift between the upper and the lower arm, as shown with the dashed arrows on the left side of Fig. 1. If the optical signals in both arms experience the same phase shift when propagating through the photonic device, the output grating will restore the original input polarization state. That means that when light with either polarization $P_{1,\text{in}}$ or $P_{2,\text{in}}$ is coupled in, it will experience the same coupling efficiency curve (see inset of Fig. 1) twice, thus increasing PDL.

Here we propose to introduce a π phase shift in one of the arms of the polarization diversity circuit. As illustrated on the right side of Fig. 1, this will cause the polarization states $P_{1,\text{in}}$ and $P_{2,\text{in}}$ to interchange their orientation at the output grating coupler. Consequently, either of these states will experience both coupling efficiency curves (one at the input, and the other one at the output), so that the overall input to output coupling is identical for both, and PDL vanishes. Naturally, complete PDL compensation requires almost identical input and output coupling efficiencies. This can be achieved because the grating couplers are close together and are defined by state-of-the-art 193-nm deep ultraviolet lithography, so that they are virtually identical, and highly symmetric fiber alignment is possible using one-dimensional grating couplers as polarization references (see Section III).

III. Device and Measurement Setup

To demonstrate the PDL reduction concept we use a polarization diversity circuit, as shown in Fig. 1, with the generic device substituted by a ring resonator (see inset of Fig. 2). The final purpose of the circuit is to act as tunable wavelength router for fiber-to-the-home applications. As such, in this prototype, it has to deliver two wavelengths to the home user, one with the downstream data ($\lambda_{\text{down},1,2}$), and a continuous wave ($\lambda_{\text{cw},1,2}$) that can be modulated at the user end. Both of these wavelengths must be routed with low PDL. Furthermore, wavelengths intended for other users should be suppressed, but PDL is less critical at these wavelengths. The component operates with the downstream data and continuous-wave wavelengths at two consecutive transmission peaks of the ring resonators, while wavelengths of other users are located at transmission minima. The recorded transmission spectrum is plotted in Fig. 2. An insertion loss of 21 dB is obtained, which is due to the limited efficiency of the grating couplers (approximately 7-dB loss per coupler) and the 1×4 splitter implemented in the circuit. The efficiency of the grating couplers can be improved, however, by using a silicon overlay, as shown in [6]. This, however, does not change the concept of PDL reduction. The free spectral range of the rings is ∼4.5 nm, while their extinction ratio will still be optimized.

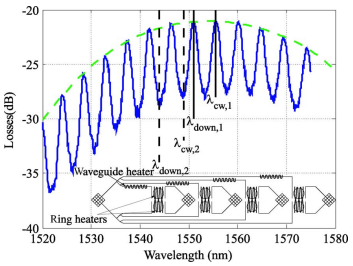

Fig. 2. Measured spectral response of the wavelength router with all heaters turned OFF. The dashed envelope indicates the overall efficiency of the two 2-D grating couplers. A schematic of the device is shown in the inset.

Fig. 3. Microscope image of the wavelength router with waveguide heaters (phase shifters) and ring heaters.

The device was fabricated on a silicon-on-insulator wafer with a silicon thickness of 220 nm using deep UV lithography and a two etch depth process. A 70-nm etch depth was used for the grating couplers, whereas the photonic wires were completely etched. After cladding the device with divinylsiloxane-bis-benzocyclobutene, titanium heaters were defined on top of both ring resonators to allow for wavelength tuning as well as matching the devices in both arms. The π phase shifter was also implemented with a heater on top of one of the arms of the polarization diversity circuit. A microscope image of a wavelength router for four users is shown in Fig. 3.

To reduce fiber-misalignment-induced PDL, the fibers were first aligned to a reference waveguide with one-dimensional grating couplers. The high polarization dependence of these couplers was used to adjust the input polarization to the $P_{2,\text{in}}$ state shown in Fig. 1, using a polarization controller. The fibers were then aligned for maximum transmission on the 2-D gratings. Since the fiber coupling efficiency is relatively position tolerant (typically ∼2 μm for a 1-dB variation), this effectively minimizes PDL due to asymmetric power coupling. However, a slight misalignment, that does not produce significant coupling asymmetry, may still result in an unwanted phase shift between both arms. Current was supplied independently to the π phase shifter and the ring heaters. For PDL characterization, a tunable laser source and the Fiberpro "PL 2000" PDL meter[1] were employed. The latter employs the polarization scanning method to determine PDL and allows for simultaneous insertion loss measurements.

IV. Results

For device characterization, the transmission spectrum of the device was first recorded with the fixed $P_{2,\text{in}}$ polarization state

[1]Available: http://www.fiberpro.com/products/ofc_pl2000.asp

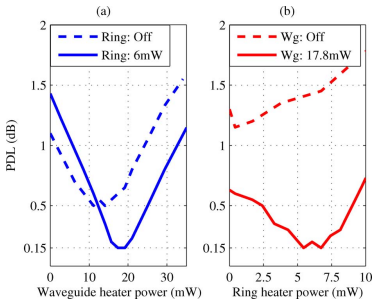

Fig. 4. Measured PDL at $\lambda = 1556$ nm as a function of waveguide and ring heater powers. (a) Ring heater fixed. (b) Waveguide heater fixed.

(see Fig. 2). Without changing the fiber alignment, PDL was then measured as a function of heater power at the transmission peaks using the PDL meter.

Initially, the ring heaters were switched OFF, and the power supplied to the waveguide heater was varied. At a wavelength of $\lambda = 1556$ nm this yields the dashed curve in Fig. 4(a). As expected, PDL decreases as the phase shift increases, reaching a minimum value of 0.5 dB at 14 mW of heating power. As more power is applied, the phase shift exceeds the optimum value so that PDL increases again. The fact that the device exhibits a higher PDL with 30 mW of power than without heating, can be attributed to imperfect fabrication or slight fiber misalignment that yield an initial nonzero phase shift between the arms. Only marginal variations in insertion loss of $\sim$0.2 dB were observed while heating the device.

The ring heaters are used to compensate for both the initial fabrication differences between the rings and differential thermal crosstalk from the waveguide arm heater. A trial and error approach was used to determine which of the two ring heaters cancels the combination of these two effects, and thus further reduces PDL. When the waveguide heater was switched OFF, and power was supplied only to the previously chosen ring heater (with the other ring heater OFF), PDL improvements were negligible. This is shown by the dashed curve in Fig. 4(b) and indicates that the initial fabrication differences between the rings were low. However, when the waveguide heater is fixed at 17.8 mW, different thermal crosstalk is induced in the rings, so that they must be matched again with the ring heaters. This can be seen in the solid curve in Fig. 4(b), where the waveguide heater is fixed at 17.8 mW and PDL reaches a minimum of 0.15 dB at 6-mW ring heater power. Conversely, as shown in the solid curve in Fig. 4(a), at this power level for the ring heater, the minimum PDL is achieved at 17.8-mW waveguide heating power. The fact that the waveguide heating powers that yield minimum PDL are slightly different depending on the power supplied to the ring heaters can again be explained by thermal crosstalk from the ring heater to the polarization diversity waveguide arm. The 0.15 dB of remaining PDL are attributed to minor asymmetries in the fiber alignment.

TABLE I
MEASURED PDL AT TRANSMISSION PEAKS WITH HEATERS ON AND OFF. WAVEGUIDE HEATER POWER $\sim$ 20 mW; RING HEATER POWER $\sim$ 4 mW

Wavelength (nm)	1542.5	1547.0	1551.5	1556.0	1560.5	1565.0
PDL (dB) heaters on	0.8	0.4	0.4	0.35	0.6	1
PDL (dB) heaters off	1.25	1.1	1.2	1.4	2.0	2.2

The optimum waveguide and ring heater power levels were found to be generally slightly different for different transmission peaks. However, choosing adequate levels, it is possible to achieve low PDL at several consecutive peaks, inside the 1-dB fiber-to-fiber coupling bandwidth. This is shown in Table I, from where it is clear that PDL well below 0.5 dB for the downstream wavelength as well as the continuous wave located at the next peak is readily achieved at $\lambda = 1551.5$ nm and $\lambda = 1556$ nm. Also notice that PDL improvements of up to 1.4 dB (at $\lambda = 1560.5$ nm) are achieved when the heaters are used. By readjusting the heaters, low PDL can be obtained in a different wavelength range.

V. CONCLUSION

We have shown experimentally that by using a π phase shift in one of the arms of a polarization diversity circuit the PDL induced by the near vertical grating couplers can be reduced from more than 1 to only 0.15 dB, at a fixed wavelength. This requires careful alignment of the input and output fibers and exact matching of the devices in each arm. In the wavelength router used to demonstrate this concept, it was also possible to achieve PDL below 0.5 dB at several consecutive transmission peaks. This technique should enable low PDL operation in a variety of polarization diversity configurations.

REFERENCES

[1] T. Barwicz, M. Watts, M. Popovic, P. Rakich, L. Socci, F. Kartner, E. Ippen, and H. Smith, "Polarization-transparent microphotonic devices in the strong confinement limit," *Nat. Photon.*, vol. 1, no. 1, pp. 57–60, 2007.

[2] H. Fukuda, K. Yamada, T. Tsuchizawa, T. Watanabe, H. Shinojima, and S. Itabashi, "Silicon photonic circuit with polarization diversity," *Opt. Express*, vol. 16, pp. 4872–4880, 2008.

[3] D. Taillaert, H. Chong, P. Borel, L. Frandsen, R. De La Rue, and R. Baets, "A compact two-dimensional grating coupler used as a polarization splitter," *IEEE Photon. Technol. Lett.*, vol. 15, no. 9, pp. 1249–1251, Sep. 2003.

[4] F. Van Laere, T. Stomeo, D. Taillaert, G. Roelkens, D. Van Thourhout, T. Krauss, and R. Baets, "Efficient polarization diversity grating couplers in bonded InP-membrane," *IEEE Photon. Technol. Lett.*, vol. 20, no. 4, pp. 318–320, Feb. 15, 2008.

[5] W. Bogaerts, D. Taillaert, P. Dumon, D. Van Thourhout, R. Baets, and E. Pluk, "A polarization-diversity wavelength duplexer circuit in silicon-on-insulator photonic wires," *Opt. Express*, vol. 15, no. 4, pp. 1567–1578, 2007.

[6] G. Roelkens, D. Vermeulen, D. Van Thourhout, R. Baets, S. Brision, P. Lyan, P. Gautier, and J. Fédéli, "High efficiency diffractive grating couplers for interfacing a single mode optical fiber with a nanophotonic silicon-on-insulator waveguide circuit," *Appl. Phys. Lett.*, vol. 92, pp. 131 101–131 103, 2008.

Silicon-on-Insulator polarization rotating micro-ring resonator

D. Vermeulen, P. De Heyn, T. Van Vaerenbergh, W. Bogaerts, G. Roelkens

Photonics Research Group, Department of Information Technology, Ghent University - imec, B-9000 Ghent, Belgium

Abstract: We propose a novel micro-ring resonator which uses quasi-TE polarized light in the bus waveguide to excite the quasi-TM polarized modes in a micro-ring. An all-pass filter is demonstrated on Silicon-on-Insulator.

1. Introduction

Resonant devices are considered to be a key technology in integrated photonic circuits. For high index contrast platforms such as Silicon-on-Insulator (SOI) the most investigated class of components are definitely the micro-ring resonators [ref]. They can be used as spectral filters for telecommunication and data communication purposes, as wavelength dependent electro-optic modulators and photodetectors, as transducers for label-free biosensing [1], as optical delay lines, ... In general quasi-TE polarized light is used in micro-ring resonators since it has the strongest confinement which enables light guiding in bends with very small radii with negligible bending losses. However, depending on the application and exact platform dimensions, the fundamental quasi-TM polarized mode can be preferred to resonate in the micro-ring. The lower confinement of the quasi-TM mode can be for example beneficial for a-thermal devices [2], sensors based on a cladding refractive index variation, high-Q rings due to a lower backscattering from the vertical sidewalls [3] and for large wavelength range tuning using liquid crystals [4]. Most of these applications, however, exhibit waveguides which are vertically asymmetrical.
In [5] we showed how an asymmetrical waveguide is a major problem for a grating coupler enabled platform. During the adiabatic transition from a broad multimode waveguide to a single-mode waveguide, several anti-crossings will be passed, thereby coupling the fundamental quasi-TM mode to higher order quasi-TE modes which are not guided when tapering down to a single-mode photonic wire waveguide. Circumvention of such an adiabatic taper has been demonstrated by using focusing techniques such as a focusing grating coupler, but with a lower coupling efficiency than similar grating couplers for quasi-TE polarized light. Secondly, for routing purposes one prefers the polarization which enables the most compact routing functionality, i.e. the TE polarization.
A straightforward solution would be to use a cascade of polarization rotators [6], polarization filters and ring-resonator. As a solution we propose a novel micro-ring resonator which uses quasi-TE polarized light in the bus waveguide to excite the quasi-TM polarized modes in a micro-ring, thus acting as a polarization rotator, polarization filter and ring resonator at the same time.

2. Design

The coupling section of the ring resonator is an asymmetrical directional coupler which acts as a polarization rotator [7, 8]. For a certain width of the bus waveguide, the quasi-TE mode in the bus waveguide will be phase matched to the quasi-TM mode in the micro-ring. In order to achieve successful coupling between these two quasi-polarized modes, a vertical asymmetry is necessary [5].
Our design is based on an SOI platform exhibiting a 220 nm thick Si core layer on a 2 μm thick buried oxide (BOX) layer. The asymmetry requirement is fulfilled by using an air top cladding. A deep etch of 220 nm is performed for defining the waveguides and ring resonator. A shallow etch of 70 nm allows us to use grating couplers for characterization. We choose a bus waveguide width of 320 nm and a micro-ring waveguide width of 600 nm. The gap of the coupling section is 300 nm and the ring radius is 30 μm. The bus waveguide has the same curvature as the micro-ring, resulting in a plane symmetric coupling section.

3. Measurements

The measurement result is shown in Figure 1. Because the grating couplers act as a coupling method for TE-polarized light and as polarization filter with an extinction ratio of 50 dB, we know that only the quasi-TE mode is excited in the bus waveguide. By calculating the theoretically expected Free Spectral Range (FSR) of the quasi-TM resonant mode

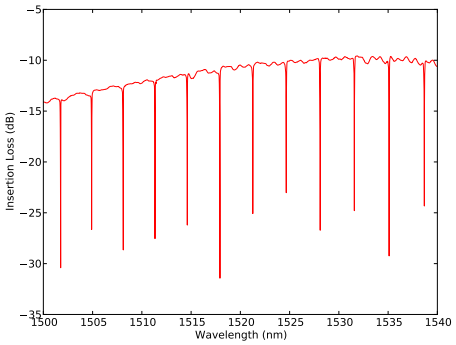

Fig. 1: Measurement result of the polarization rotating micro-ring resonator in an all-pass filter configuration.

and comparing it with the measured FSR, we can conclude that quasi-TE polarized light from the bus waveguide is coupled to the quasi-TM resonant mode in the ring. The mean extinction ratio (ER) over the 40 nm wavelength range is −16.2 dB, which means that the ring is critically coupled. The mean Q is 32660 and the mean finesse is 88. Furthermore, no peak splitting was detected.

4. Conclusion

We proposed a new kind of micro-ring resonator which makes use of a polarization rotating directional coupling section to excite the quasi-TM resonant mode. A critically coupled all-pass filter showing very good performance was demonstrated. This polarization micro-ring resonator is expected to be useful for a whole class of applications where TM-polarized light is preferred to resonate.

5. Acknowledgements

Diedrik Vermeulen thanks the Institute for the Promotion of Innovation by Science and Technology in Flanders (IWT) for a grant. Thomas Van Vaerenbergh is supported by the Flemish Research Foundation (FWO-Vlaanderen) for a PhD grant.

References and links

1. K. De Vos, I. Bartolozzi, E. Schacht, P. Bienstman, and R. Baets, "Silicon-on-Insulator microring resonator for sensitive and label-free biosensing." *Optics express*, vol. 15, no. 12, pp. 7610–5, Jun. 2007. [Online]. Available: http://www.ncbi.nlm.nih.gov/pubmed/19547087
2. J. Teng, P. Dumon, W. Bogaerts, H. Zhang, X. Jian, X. Han, M. Zhao, G. Morthier, and R. Baets, "Athermal Silicon-on-insulator ring resonators by overlaying a polymer cladding on narrowed waveguides." *Optics express*, vol. 17, no. 17, pp. 14 627–33, Aug. 2009. [Online]. Available: http://www.ncbi.nlm.nih.gov/pubmed/19687941
3. P. D. Heyn, B. Kuyken, D. Vermeulen, W. Bogaerts, and D. V. Thourhout, "High-Performance Low-Loss Silicon-on-Insulator Microring Resonators using TM-polarized Light," in *Optical Fiber Communication Conference*. Optical Society of America, 2011.
4. W. D. Cort, J. Beeckman, R. James, F. A. Fernandez, R. Baets, and K. Neyts, "Tuning silicon-on-insulator ring resonators with in-plane switching liquid crystals," *JOSA B*, vol. 28, no. 1, pp. 79–85, 2011.
5. D. Vermeulen, K. V. Acoleyen, S. Ghosh, S. Selvaraja, W. A. D. D. Cort, N. A. Yebo, E. Hallynck, K. D. Vos, P. P. P. Debackere, P. Dumon, W. Bogaerts, G. Roelkens, D. V. Thourhout, and R. Baets, "Efficient Tapering to the Fundamental Quasi-TM Mode in Asymmetrical Waveguides," in *European Conference on Integrated Optics*, 2010.
6. D. Vermeulen, S. Selvaraja, P. Verheyen, W. Bogaerts, D. V. Thourhout, and G. Roelkens, "High Efficiency Broadband Polarization Rotator on," in *Group IV Photonics*, 2010, pp. 42–44. [Online]. Available: http://ieeexplore.ieee.org/xpl/freeabs_all.jsp?arnumber=5643432&abstractAccess=no&userType=inst
7. L. Liu, Y. Ding, K. Yvind, and J. r. M. Hvam, "Silicon-on-insulator polarization splitting and rotating device for polarization diversity circuits," *Optics Express*, vol. 19, no. 13, pp. 12 646–12 651, 2011.
8. D. Dai and J. E. Bowers, "Novel concept for ultracompact polarization splitter-rotator based on silicon nanowires." *Optics express*, vol. 19, no. 11, pp. 10 940–9, May 2011. [Online]. Available: http://www.ncbi.nlm.nih.gov/pubmed/21643354

Reflectionless grating couplers for Silicon-on-Insulator photonic integrated circuits

D. Vermeulen,[1,2,*] Y. De Koninck,[1] Y. Li,[1] E. Lambert,[1] W. Bogaerts,[1] R. Baets,[1] and G. Roelkens[1]

[1] *Photonics Research Group, Department of Information Technology, Ghent University - imec, B-9000 Ghent, Belgium*
[2] *Acacia Communications, Inc., 3 Clock Tower Place, Suite 210, Maynard, MA 01754, USA*
[*] *Diedrik.Vermeulen@acacia-inc.com*

Abstract: We propose a novel grating coupler design which is inherently reflectionless by focusing the reflected light away from the entrance waveguide. The design rules for this reflectionless grating coupler are explained and the grating coupler design is investigated by means of 3D FDTD simulations for the case of a Silicon-on-Insulator based platform.

References and links

1. D. Taillaert, W. Bogaerts, P. Bienstman, T. F. Krauss, P. Van Daele, I. Moerman, S. Verstuyft, K. De Mesel, and R. Baets. "An out-of-plane grating coupler for efficient butt-coupling between compact planar waveguides and single-mode fibers," IEEE J. Quantum Electron. **38**(7):949–955, 2002.
2. D. Vermeulen, S. Selvaraja, P. Verheyen, G. Lepage, W. Bogaerts, P. Absil, D. Van Thourhout, and G. Roelkens. "High-efficiency fiber-to-chip grating couplers realized using an advanced CMOS-compatible Silicon-on-Insulator platform," Opt. Express **18**(17):18278–83, 2010.
3. A. Mekis, S. Gloeckner, G. Masini, A. Narasimha, T. Pinguet, S. Sahni, and P. Dobbelaere. "A grating-coupler-enabled CMOS photonics platform," IEEE J. Sel. Topics Quantum Electron. **99**:1–12, 2010.
4. L. Zhou, Z. Y. Li, Y. Zhu, Y. T. Li, Z. C. Fan, W. H. Han, Y. D. Yu, and J. Z. Yu. "A novel highly efficient grating coupler with large filling factor used for optoelectronic integration," Chinese Physics B **19**:124214, 2010.
5. X. Chen and H. K. Tsang. "Polarization-independent grating couplers for Silicon-on-Insulator nanophotonic waveguides," Opt. Lett. **36**(6):796–798, 2011.
6. X. Chen and H. K. Tsang. "Nanoholes grating couplers for coupling Between Silicon-on-Insulator waveguides and optical fibers," IEEE Photon. J. **1**(3):184–190, 2009.
7. C. R. Doerr, L. Chen, Y. K. Chen, and L. L. Buhl. "Wide bandwidth silicon nitride grating coupler," IEEE Photon. Technol. Lett. **22**(19):1461–1463, 2010.
8. C. Alonso-Ramos, A. Ortega-Moñux, I. Molina-Fernández, P. Cheben, L. Zavargo-Peche, and R. Halir. "Efficient fiber-to-chip grating coupler for micrometric SOI rib waveguides," Opt. Express **18**(14):15189, 2010.
9. N. Na, H. Frish, I. Hsieh, O. Harel, R. George, A. Barkai, H. Rong, and Others. "Efficient broadband silicon-on-insulator grating coupler with low backreflection," Opt. Lett. **36**(11):2101–2103, 2011.
10. D. Taillaert, P. Bienstman, and R. Baets. "Compact efficient broadband grating coupler for silicon-on-insulator waveguides," Opt. Lett. **29**(23):2749–51, 2004.
11. F. Van Laere, T. Claes, J. Schrauwen, S. Scheerlinck, W. Bogaerts, D. Taillaert, L. O'Faolain, D. Van Thourhout, R. Baets. "Compact focusing grating couplers for Silicon-on-Insulator integrated circuits," IEEE Photon. Technol. Lett. **19**(23):1919–1921, 2007.
12. A. F. Oskooi, D. Roundy, M. Ibanescu, P. Bermel, J. D. Joannopoulos, and S. G. Johnson. "Meep: A flexible free-software package for electromagnetic simulations by the FDTD method," Comput. Phys. Commun. **181**(3):687–702, 2010.

1. Introduction

Photonic integration is considered to be a key technology for future advancements in optical communication technologies. Scaling down the optical building blocks enables complex and ultra-compact photonic circuits at a fraction of the cost of conventional systems consisting out of discrete components. Choosing an appropriate platform for developing this miniaturization technology is guided by functionality, compatibility, performance, yield and cost. Regarding the last two issues, Silicon-on-Insulator (SOI) is by far the leading technology for low-cost and high-volume photonic integration since it can benefit from the processes developed in the mature electronics industry. Although the high refractive index contrast of SOI reduces the footprint of the integrated photonic devices considerably, it becomes more difficult to achieve a high-performance mode-size convertor between a single-mode optical fiber ($100\,\mu\text{m}^2$) and an integrated optical waveguide ($0.1\,\mu\text{m}^2$). A possible solution is a grating coupler which is a periodic structure that couples light out of the chip to free space or to an optical fiber [1]. Fiber-to-chip grating couplers with very high efficiency have been demonstrated [2]. However, as most papers focus on coupling efficiency, polarization dependency, ease of fabrication and bandwidth, a solution for the back reflection of these grating couplers is only recently being investigated. A typical reflection back in the silicon waveguide circuit for a high-efficiency grating coupler is around -17 dB [3]. Other reported high back reflections are -10 dB [4], [5] and -8 dB [6]. These levels of back reflections are unacceptable for integrated circuits which contain integrated lasers and amplifiers. Furthermore, back reflections are highly unwanted in interferometer based designs. Most approaches to reduce the reflection of the grating focus on optimizing the dimensions of the grating profile itself, thereby achieving back reflections of -22 dB [7], -28 dB [8] and -27 dB [9]. In this paper we will introduce a solution for curved grating couplers which decouples the reflection at the grating from the reflection back into the waveguide, by refocusing the reflected light away from the entrance waveguide.

2. Theoretical outline

There are two main sources which contribute to the reflection from a grating coupler back into the entrance waveguide. The most important source is the second order reflection of the grating, which can be relatively broadband for high-index contrast gratings. Typically one eliminates this second order reflection by tilting the optical fiber under a small angle of around 10° with respect to the surface normal [10]. The second source of back reflection is due to the Fresnel reflection at the waveguide/grating coupler interface. This reflection is highly dependent on the grating structure itself and is very difficult to eliminate. In the proposed grating coupler design, we will refocus both sources of reflection away from the entrance waveguide thereby extinguishing the reflection almost completely.

In [11] a compact focusing grating coupler is presented which uses a curved grating to focus the coupled light into a single-mode waveguide, achieving an eight-fold length reduction as compared to a standard linear grating and adiabatic taper, without performance penalty. For the reflectionless grating coupler we follow the same design rules. The grating is curved such that a plane wavefront originating from the tilted optical fiber is diffracted to the TE-polarized mode of a broad SOI waveguide, so that the wavefront is curved cylindrically and focusing occurs in the center of curvature of the wavefront. The easiest way to describe this system is to use a polar coordinate system (r, δ) with the origin placed at the exit point of the entrance waveguide, as shown in Fig. 1. The beam will expand in the slab region with an effective refractive index n_s and after a certain length r_0 it will encounter the grating, thereby experiencing a different effective refractive index n_g. As a first approximation we assume that these effective refractive indices n_s and n_g are equal and thus $\alpha = 180^\circ$ (no refraction between slab and grating region).

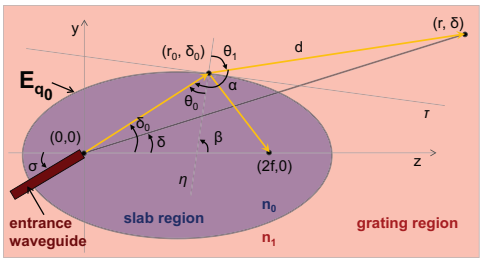

Fig. 1. Focusing grating coupler geometry parameters. The light (yellow arrows) is refracted and reflected at the first grating ellipse E_{q_0}. τ and η are the tangent and normal line respectively of ellipse E_{q0} at point (r_0, δ_0).

The phase matching condition is now [11]:

$$q\lambda_0 = rn_s - rn_c \cos\delta \sin\phi \tag{1}$$

where λ_0 is the vacuum wavelength and q is an integer number corresponding with each grating line. The fiber is tilted under an angle ϕ, the angle between the fiber and the chip surface normal, such that the projected propagation constant of the fiber only has a z-component proportional to $n_c \sin\phi$ where n_c is the refractive index of the top cladding. By rewriting Eq. (1) we can see that the grating lines will form confocal ellipses $E_{q_0}, E_{q_0+1}, ..., E_{q_0+n}$:

$$r = \frac{\frac{q\lambda_0}{n_s}}{1 - \frac{n_c \sin\phi \cos\delta}{n_s}} = \frac{a(1-e^2)}{1 - e\cos\delta} \tag{2}$$

with a common focal point $f_{1,q}$ at the origin. From this we can determine the eccentricity $e = \frac{n_c \sin\phi}{n_s}$, semi-major axis $a = \frac{q\lambda_0 n_s}{n_s^2 - n_c^2 \sin^2\phi}$ and second focal points $f_{2,q} = \frac{q\lambda_0 n_c \sin\phi}{n_s^2 - n_c^2 \sin^2\phi}$. The first grating line corresponds to q_0. The phase matching condition is fulfilled for all parts of the confocal ellipses. We can thus choose which part of the ellipses we use for designing a grating coupler because every part of the ellipse will couple the light out under the same angle ϕ. Normally one takes the right part of the confocal ellipses as shown in Fig. 2(a), such that the propagation vector $\vec{\beta}$ of the entrance waveguide is parallel to the projected wave vector $\vec{k}_z = (2\pi/\lambda) n_c \sin\phi \vec{e}_z$ of the diffracted light (waveguide angle $\sigma = 0°$). Although this seems like the most logical choice, this design will introduce the largest back reflection in the waveguide since the reflection from the grating lines will be refocused to the second focal points $f_{2,q}$ and coupled back into the entrance waveguide. This is solved by using another part of the confocal ellipses as grating coupler and rotating the waveguide by an angle σ of for example 45°, see Fig. 2(b). In this design the focal points and the grating are not inline hence the grating reflection is focused away from the entrance waveguide into a slab region, thereby fully eliminating the back reflection.

To obtain the appropriate first grating line number q_0, we calculate the in plane aperture opening angle ε of the entrance waveguide using a 3D mode propagation tool. This angle will determine the focusing length of the slab r_0 and thus q_0 such that the width of the diffracted beam matches the width of the Gaussian fiber mode. In [11] it was shown that this focusing length has no influence on the grating coupler performance and can be chosen freely. However, in the reflectionless grating coupler design, the larger the focusing length, the larger is the distance from entrance waveguide to the the closest focal point f_{2,q_0} whereto the reflected light is

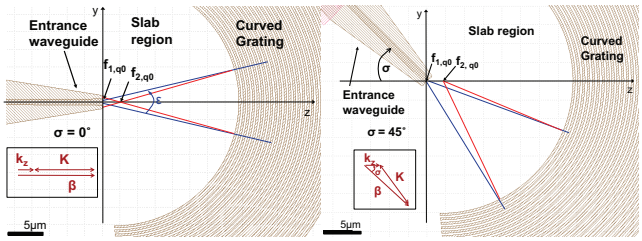

(a) $\sigma = 0^\circ$ (b) $\sigma = 45^\circ$

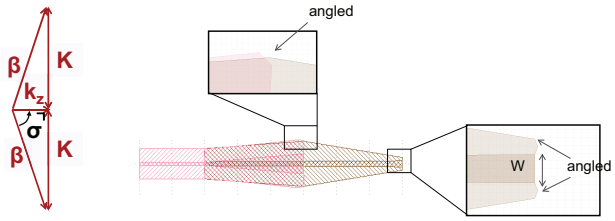

(c) $\sigma = \cos^{-1}\left(\frac{n_c \sin\phi}{n_s}\right)$ (d) Entrance waveguide design improvements

Fig. 2. Reflection from curved grating couplers for different waveguide angles σ. The k-diagram is drawn for $\sigma = 0^\circ$ (a), $\sigma = 45^\circ$ (b) and $\sigma = \cos^{-1}\left(\frac{n_c \sin\phi}{n_s}\right)$ (c) which corresponds to both the optimal reflection waveguide angle and second order reflection angle. ($\vec{K}$ = reciprocal lattice vector) The entrance waveguide is optimized for low reflection (d).

refocused, thereby minimizing the reflection coupled back into the entrance waveguide. On the other hand, a larger focusing length is accompanied by a broader waveguide aperture and thus a larger chance to recapture reflected light back into the entrance waveguide. Depending on the exact entrance waveguide geometry, a proper waveguide width should be chosen.
There exists a waveguide angle σ of the entrance waveguide wherefor the angle between the incident light and the reflected light is maximal. This optimal reflection waveguide angle $\sigma = \cos^{-1}\left(\frac{n_c \sin\phi}{n_s}\right)$ is derived by maximizing the reflection angle $\theta_0(\delta_0)$ given by

$$\theta_0 = \beta - \delta_0 = \frac{\pi}{2} + \tan^{-1}\left(\frac{n_c \sin\phi}{n_s \sin\delta_0} - \cot\delta_0\right) - \delta_0 \tag{3}$$

Figure 3(a) shows θ_0 from Eq. (3) as a function of δ_0 for a fiber angle ϕ of 15°, wavelength $\lambda_0 = 1.55\,\mu$m, SiO_2 cladding ($n_c = 1.45$) and $n_s = 2.852$ corresponding to the effective index of the TE slab mode propagating in an SOI slab with a 220 nm thick Si core surrounded by SiO_2. The optimal entrance waveguide angle $\sigma = \delta_{0,max}$ for these parameters is 82.4° and 68.9° for a fiber angle ϕ of 15° and 45° respectively. In Fig. 3(b) the optimal reflection waveguide angle and the corresponding reflection angle θ_0 are plotted as a function of the fiber tilt angle ϕ. We can conclude that a larger fiber tilt results in a larger reflection angle θ_0 and thus accordingly lower back reflection. A larger fiber tilt will also reduce the second order back reflection (case $\sigma = 0^\circ$) from the grating. However, for practical reasons one typically chooses a tilt angle ϕ between 5° and 20°.

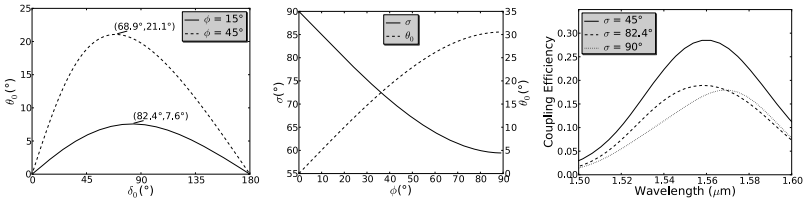

(a) (b) (c)

Fig. 3. The reflection angle θ_0 as a function of δ_0 for $\phi = 15^\circ$ (a) and the optimal entrance waveguide angle σ and corresponding θ_0 as a function of ϕ (b) for $\lambda_0 = 1.55\,\mu$m. Simulated coupling efficiency (c) for different waveguide angles σ (etch of 70 nm, $\phi = 15^\circ$).

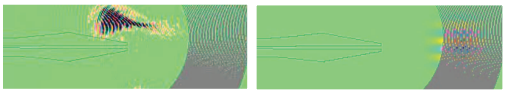

(a) (b)

Fig. 4. 3D FDTD simulations showing (a) the refocusing of the reflection using an oversaturated electrical field (Media 1) and (b) waveguide coupling when excited from the fiber (Media 2) ($\sigma = 90^\circ$, $\phi = 15^\circ$)

3. Design improvements

Achieving ultra-low reflections means reducing every possible reflection source. One important source of parasitic reflections is due to discontinuities such as at the exit of the entrance waveguide. These can be minimized by angling the trenches as is shown in Fig. 2(d). The grating reflected and refocused light can be reflected back onto the grating and thus back into the waveguide. Therefore we also need to make sure that the reflected light is not normally incident on any feature.

Another improvement is to differentiate between the effective refractive index of the grating n_g and the effective refractive index of the slab region n_s (see Fig. 1). The phase matching condition for the first grating line corresponding to q_0 will stay the same, i.e. Eq. (1). At this first grating line, the light will transition from a slab with refractive index n_s to a grating region with refractive index n_g and thus be refracted at this interface under an angle $\theta_1 = \sin^{-1}\left(\frac{n_s \sin\theta_0}{n_g}\right)$ according to Snell's law. The angle between the incoming beam and refracted beam is thus $\alpha = \pi + \theta_0 - \theta_1$. Solving the phase condition numerically

$$q\lambda_0 = r_0 n_s + d n_g - r\cos\delta n_c \sin\phi \tag{4}$$

together with the system of geometric equations $d^2 = r_0^2 + r^2 - 2r_0 r\cos(\delta_0 - \delta)$ and $r^2 = r_0^2 + d^2 - 2r_0 d\cos\alpha$ for every refraction point (r_0, δ_0) to (r, δ) will result in the subsequent grating lines for $q \geq q_0 + 1$.

4. 3D FDTD simulations

The grating couplers, designed using Eq. (4), were simulated using full-vectorial 3D FDTD software such as [12]. To calculate the reflection spectra, a pulse with a Gaussian time pro-

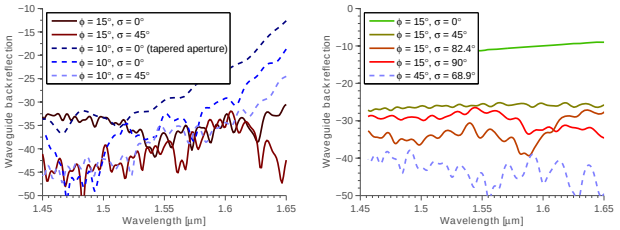

(a) Shallow etched grating couplers (b) Fully etched grating couplers

Fig. 5. Reflection spectra for shallow (a) and fully etched (b) grating couplers, each time for different values of the waveguide angle σ and fiber tilt angle ϕ.

file was launched in the single-mode access waveguide and the reflected flux was measured in that same waveguide (see Fig. 4(a) (Media 1)). The coupling efficiency was simulated by the normalized power in the single-mode waveguide after launching a Gaussian mode under the correct angles and polarization (see Fig. 4(b) (Media 2)). We have found that the optimal reflection waveguide angle does indeed have the lowest back reflection, but at the price of a coupling efficiency penalty of around 2 dB (see Fig. 3(c)). This is because this waveguide angle corresponds to the angle for second order Bragg reflection (case $\sigma = \cos^{-1}(n_c \sin\phi / n_s)$) when $\vec{K}.\vec{k}_z = 0$ (see Fig. 2(c)). Figure 5 shows the spectra of the reflection back in the entrance waveguide of the proposed grating coupler for different waveguide angles σ. For the shallow etched gratings (70 nm etch in a 220 nm Si core) and for fiber tilt angle $\phi = 10^\circ$, the second order back reflection present at the higher wavelengths decreases by 5 dB to 10 dB for waveguide angles up to 45° without coupling efficiency penalty (typical grating coupler efficiency is around 30%) achieving a back reflection of -40 dB (Fig. 5(a)). We see that mainly the second order reflection (case $\sigma = 0^\circ$) present at the higher wavelengths is reduced. This second order reflection can be easily reduced by increasing the fiber tilt angle to 15° and even more using the novel grating coupler design. The reflection reduction is the most pronounced in the case of fully etched grating couplers (220 nm etch in a 220 nm Si core) having a typical efficiency around 10%. The back reflection decreases from -7 dB to -28 dB for $\sigma = 45^\circ$ (Fig. 5(b)).

5. Conclusion

We have investigated a reflectionless grating coupler design by means of 3D FDTD simulations. The grating is curved and refocuses the reflection away from the entrance waveguide thereby realizing a 5 dB to 10 dB reflection reduction down to -40 dB for shallow etched gratings, the same back reflection performance of a typical optical fiber connector, without introducing a coupling efficiency penalty. Furthermore, we showed that this method can be used to reduce the reflection of highly reflective (-7 dB) deeply etched grating couplers to useful reflections of -28 dB. These devices could become key components in interferometer based designs and circuits using integrated lasers and amplifiers.

Acknowledgements

The authors would like to thank Chris Doerr for proof reading and making comments. Yanlu Li and Roel Baets acknowledge the Methusalem grant “Smart photonic chips” from the Flemish government. Y. De Koninck acknowledges the Fund for Scientific Research (FWO) for a grant.

5

Overall Conclusion

Silicon Photonics is thé most promising technology for high volume low-cost integration of optical transceivers. By leveraging on the processes and tools developed by the CMOS industry, the chip cost is minimized and the wafer and chip yield maximized. The packaging cost can be kept to a minimum by using out-of-plane optical couplers such as grating couplers to be able to wafer-scale test the wafer both optically and electrically and increase the packaging yield. I have investigated three kinds of transceiver applications which would benefit enormously from integrating the optical components. The most developed transceiver demonstrator in this work is a Point-To-Point (PTP) Fiber-To-The-Home (FTTH) transceiver array which targets the access market and employs the compact integration that Silicon Photonics offers to package 4 transceivers in a single SFP package. In the future an 8-channel and even 16 or 32-channel transceiver array should be possible. The biggest challenge is meeting the optical power budget. The biggest improvement would be to optimize the modulator for this specific application, reducing the 6 dB IL with a couple of dB. Together with fully optimized waveguide components, optimized fiber-to-chip coupling interfaces and by going to a laser with more than 13 dBm output power or integrating an amplifier, a 32-channel device is achievable with Silicon Photonics.
For the long-haul market a PM-DQPSK receiver having high spectral efficiency has been developed and demonstrated. Due to the low-cost fabrication process, this kind of receiver could also be used in future access markets which use coher-

ent DWDM technology to increase the bandwidth per user.
A third demonstrator that was investigated was a Wavelength Router (WR) for Flexible PON or FlexPON networks. Due to the large amount of optical equipment needed, this kind of network concept is only viable by integrating the photonic components and Silicon Photonics acts here as a technology enabler. The question is if the industry will accept active components in the field such as this wavelength router, rather than a passive optical splitter.
In general, after being pioneered and researched for the last decade by universities and pioneering companies, Silicon Photonics is taking off worldwide and will be present in almost all telecom and datacom transceiver markets. This is just the beginning of the mass adoption of Silicon Photonics technology. The results achieved in this work are definitely an important contribution to the Silicon Photonics technology platform. Needless to say, still a lot of work needs to be done to make Silicon Photonics the perfect platform. This includes integration of lasers, amplifiers and isolators in a CMOS-compatible way.

A

Published papers

This is a list of the published works resulting directly or indirectly from the research performed during my PhD. After each publication I specify the part of the research to which I contributed (partly of fully).

A.1 Patents

[1] (pending): idea/design/layout
[2] (pending) : idea/design/simulation/layout/fabrication/characterization
[3] (pending): idea/design/simulation
[4] (pending): idea/design/simulation/layout/characterization/writing
[5] (pending): idea/design/layout/writing
[6] (pending): feedback

A.2 Book Chapters

[7]: Main text written by Wim Bogaerts. I contributed with research results, measurements, artwork, detailed grating coupler sections and proof-reading.

A.3 International journals

[8]: design
[9]: design/simulation/layout/characterization/writing
[10]: layout
[11]: design/simulation/layout
[12]: feedback/expertise
[13]: design/layout
[14]: design/simulation/layout/characterization/writing
[15]: research results
[16]: design/simulation/layout/characterization/writing
[17]: design/layout
[18]: research results
[19]: simulation/characterization

A.4 International conferences

[20]: design/layout
[21]: research results
[22]: research results
[23]: design/simulation/layout/fabrication/characterization/writing
[24]: desing/simulation/layout
[25]: design/layout
[26]: feedback
[27]: design/simulation/layout
[28]: design/layout/characterization
[29]: design
[30]: research results
[31]: design/layout/characterization/writing
[32]: design/layout/writing
[33]: layout
[34]: research results
[35]: feedback
[36]: feedback
[37]: design/simulation/layout/fabrication/characterization/writing
[38]: feedback
[39]: design/simulation/layout/fabrication/characterization/writing
[40]: research results
[41]: debugging/feedback
[42]: design/simulation/layout/fabrication/writing

[43]: design/simulation/layout/writing
[44]: design/layout
[45]: design/simulation/layout/characterization/writing
[46]: design/layout
[47]: research results
[48]: design/simulation/layout/characterization
[49]: design/simulation/layout/characterization/writing
[50]: design/simulation/layout/characterization/writing
[51]: research results
[52]: design/simulation/layout/characterization/writing
[53]: simulation/characterization

A.5 National conferences

[54]: design/layout

List of published papers and patents

[1] D. Vermeulen, Y. De Koninck, Y. Li, and R. Baets. *REFLECTIONLESS GRATING COUPLER*, 2012.

[2] D. Vermeulen and G. Roelkens. *TRANSPARENT PHOTONIC INTEGRATED CIRCUIT (EP2386890 A1, EP2386891A1, US20110278441)*, 2011.

[3] Jonathan Schrauwen, D. Taillaert, and D. Vermeulen. *COUPLING METHODS USING A TAPER (EP2442165A1, US20120093456)*, 2010.

[4] D. Vermeulen, G. Roelkens, and D. Van Thourhout. *GRATING STRUCTURES FOR SIMULTANEOUS COUPLING TO TE AND TM WAVEGUIDE MODES (US 20100322555 A1)*, 2010.

[5] G. Roelkens and D. Vermeulen. *METHODS AND SYSTEMS FOR REDUCING POLARIZATION DEPENDENT LOSS (EP2494393 A1, US20120207428, WO2011051358A1)*, 2010.

[6] R. Baets, D. Vermeulen, Danae Delbeke, and E. Hallynck. *METHOD AND SYSTEM FOR COUPLING RADIATION (EP2321680A1, US20110103743, WO2009156412A1)*, 2011.

[7] W. Bogaerts and D. Vermeulen. *Off-chip coupling*. In Handbook of Silicon Photonics. 2013.

[8] Y. Li, D. Vermeulen, Y. De Koninck, Gunay Yurtsever, G. Roelkens, and R. Baets. *Compact grating couplers on silicon-on-insulator with reduced backreflection.* Optics letters, 37(21):4356–8, 2012.

[9] D. Vermeulen, Y. De Koninck, Y. Li, E. Lambert, W. Bogaerts, R. Baets, and G. Roelkens. *Reflectionless grating couplers for Silicon-on-Insulator photonic integrated circuits.* Optics Express, 20(20):22278, 2012.

[10] Nannicha Hattasan, B. Kuyken, Francois Leo, E. M. P. Ryckeboer, D. Vermeulen, and G. Roelkens. *High-Efficiency SOI Fiber-to-Chip Grating Couplers and Low-Loss Waveguides for the Short-Wave Infrared.* IEEE Photonics Technology Letters, 24(17):1536–1538, 2012.

[11] M. Aamer, Ana M. Gutierrez, A. Brimont, D. Vermeulen, G. Roelkens, J. M. Fedeli, A. Hakansson, and P. Sanchis. *CMOS Compatible Silicon-on-Insulator Polarization Rotator Based on Symmetry Breaking of the Waveguide Cross Section.* IEEE Photonics Technology Letters, 24(22):2031–2034, 2012.

[12] Linghua Wang, Y. Li, Marco Garcia Porcel, D. Vermeulen, Xiuyou Han, Jinyan Wang, Xigao Jian, R. Baets, Mingshan Zhao, and Geert Morthier. *A polymer-based surface grating coupler with an embedded Si3N4 layer.* Journal of Applied Physics, 111(11):114507, 2012.

[13] P. De Heyn, D. Vermeulen, D. Van Thourhout, and G. Roelkens. *Silicon-on-Insulator All-Pass Microring Resonators Using a Polarization Rotating Coupling Section.* IEEE Photonics Technology Letters, 24(14):1176–1178, 2012.

[14] D. Vermeulen, S.K. Selvaraja, P. Verheyen, P. Absil, W. Bogaerts, D. Van Thourhout, and G. Roelkens. *Silicon-on-Insulator Polarization Rotator Based on a Symmetry Breaking Silicon Overlay.* IEEE Photonics Technology Letters, 24(6):482–484, 2012.

[15] G. Roelkens, D. Vermeulen, S.K. Selvaraja, R. Halir, W. Bogaerts, and D. Van Thourhout. *Grating-Based Optical Fiber Interfaces for Silicon-on-Insulator Photonic Integrated Circuits.* IEEE Journal of Selected Topics in Quantum Electronics, 17(3):571–580, 2011.

[16] D. Vermeulen, S.K. Selvaraja, P. Verheyen, G. Lepage, W. Bogaerts, P. Absil, D. Van Thourhout, and G. Roelkens. *High-efficiency fiber-to-chip grating couplers realized using an advanced CMOS-compatible silicon-on-insulator platform.* Optics express, 18(17):18278–83, 2010.

[17] R. Halir, D. Vermeulen, and G. Roelkens. *Reducing Polarization-Dependent Loss of Silicon-on-Insulator Fiber to Chip Grating Couplers.* IEEE Photonics Technology Letters, 22(6):389–391, 2010.

[18] G. Roelkens, D. Vermeulen, F. Van Laere, S.K. Selvaraja, S. Scheerlinck, D. Taillaert, W. Bogaerts, P. Dumon, D. Van Thourhout, and R. Baets. *Bridging the Gap Between Nanophotonic Waveguide Circuits and Single Mode Optical Fibers Using Diffractive Grating Structures.* Journal of Nanoscience and Nanotechnology, 10(3):1551–1562, 2010.

[19] G. Roelkens, D. Vermeulen, D. Van Thourhout, R. Baets, S. Brision, P. Lyan, P. Gautier, and J. M. Fedeli. *High efficiency diffractive grating couplers for interfacing a single mode optical fiber with a nanophotonic silicon-on-insulator waveguide circuit.* Applied Physics Letters, 92(13):131101, 2008.

[20] A. Hakansson, M. Aamer, N. Sotiropoulos, Antoine Brimont, Pablo Sanchis, J. M. Fedeli, Delphine Marris-Morini, Eric Cassan, L. Vivien, Karen Gilbert, Philippe Grosse, Jean Michel Hartmann, D. Vermeulen, and G. Roelkens. *Compact silicon differential receiver with integrated zero biased balanced detection.* The 9th International Conference on Group IV Photonics (GFP), 6:165–167, 2012.

[21] G. Roelkens, S Keyvaninia, S. Stankovic, N Hattasan, A Gassenq, Y. De Koninck, M Tassaert, S Ghosh, P Mechet, D. Vermeulen, G Morthier, R. Baets, and D. Van Thourhout. *III-V / Silicon photonic integrated circuits for communication and sensing applications.* In Photonics West (invited), 2013.

[22] G. Roelkens, D. Vermeulen, Y. Li, Y. De Koninck, S.K. Selvaraja, K. Van Acoleyen, and R. Baets. *High index contrast gratings for silicon photonic integrated circuits.* In Photonics West (invited), 2013.

[23] D. Vermeulen, G. Roelkens, D. Van Thourhout, and C. R. Doerr. *Silicon Photonics for Optical Fiber Communication Applications.* In APC (invited), China, 2012.

[24] S.K. Selvaraja, Gayle Murdoch, Alexey Milenin, Christie Delvaux, Patrick Ong, Shibnath Pathak, D. Vermeulen, Gunther Sterckx, Gustaf Winroth, P. Verheyen, Guy Lepage, W. Bogaerts, R. Baets, J. Van Campenhout, and P. Absil. *Advanced 300-mm Waferscale Patterning for Silicon Photonics Devices with Record Low Loss and Phase Errors.* In 17th OptoElectronics and Communications Conference (OECC), pages PDP2–2 p15, Busan, South Korea, 2012.

[25] P. De Heyn, D. Vermeulen, T. Van Vaerenbergh, B. Kuyken, and D. Van Thourhout. *Ultra-high Q and finesse all-pass microring resonators on Silicon-on-Insulator using rib waveguides.* In 16th European Conference on Integrated Optics, Barcelona, Spain, 2012.

[26] N. Sotiropoulos, H. De Waardt, A. M. J. Koonen, D. Vermeulen, and G. Roelkens. *Performance of 80 Gb/s MMI-Based DQPSK Demodulator on SOI*. In 6th European Conference on Integrated Optics (ECIO), Barcelona, Spain, 2012.

[27] M. Aamer, A M Gutierrez, A Brimont, A Griol, P Sanchis, D. Vermeulen, and P Roelkens. *Experimental demonstration of an ultra compact SOI polarization rotator*. In 16th European Conference on Integrated Optics (ECIO), Barcelona, Spain, 2012.

[28] T. Claes, D. Vermeulen, P. De Heyn, K. De Vos, G. Roelkens, D. Van Thourhout, and P. Bienstman. *Towards a silicon dual polarization ring resonator sensor for multiplexed and label-free structural analysis of molecular interactions*. page 159, Barcelona, Spain, 2012.

[29] Y. Li, D. Vermeulen, Y. De Koninck, G. Yurtsever, G. Roelkens, and R. Baets. *Fiber couplers for silicon-on-insulator photonic IC's with optimized on-chip return loss*. In Optical Fiber Communication Conference (OFC), volume 1, page JTh2A.8, 2012.

[30] G. Roelkens, S Keyvaninia, S. Stankovic, M Tassaert, N Hattasan, A Gassenq, P. De Heyn, Y. De Koninck, R Kumar, M Muneeb, D. Vermeulen, G Morthier, R. Baets, and D. Van Thourhout. *III-V-on-silicon membrane photonics for near- infrared and mid-infrared applications*. In 16th European Conference on Integrated Optics (ECIO), Barcelona, Spain, 2012.

[31] D. Vermeulen, P. De Heyn, T. Van Vaerenbergh, W. Bogaerts, and G. Roelkens. *Silicon-on-Insulator polarization rotating micro-ring resonator*. In IEEE Photonics Conference (IPC), volume 4, pages 875–876, Arlington, United States, 2011.

[32] D. Vermeulen, Y. De Koninck, Y. Li, E Lambert, W. Bogaerts, R. Baets, and G. Roelkens. *Reflectionless grating coupling for silicon-on-insulator integrated circuits*. In Group IV Photonics (GFP), 2011 8th IEEE International Conference on, volume 1, pages 74–76, London, United Kingdom, 2011.

[33] B. Kuyken, N Hattasan, D. Vermeulen, S.K. Selvaraja, W. Bogaerts, William M. J. Green, R. Baets, and G. Roelkens. *Highly efficient broadband silicon-on-insulator grating couplers for the short wave infrared wavelength range*. In Integrated Photonics Research, Silicon and Nano-Photonics (IPR), page IMB6, Toronto, Canada, 2011.

[34] G. Roelkens, S. Stankovic, S Keyvaninia, D. Vermeulen, M Muneeb, R. Baets, and D. Van Thourhout. *III-V / silicon photonic integrated circuits for communication applications*. In OECC, page 8S1, Taiwan, 2011.

[35] Thijs Spuesens, Liu Liu, D. Vermeulen, Jing Zhao, P Rojo Romeo, P Regreny, L Grenouillet, J. M. Fedeli, and D. Van Thourhout. *Integration of photodetectors with lasers for optical interconnects using 200 mm waferscale III-V/SOI technology.* The Optical Fiber Communication Conference and Exposition (OFC) and The National Fiber Optic Engineers Conference (NFOEC), 2011.

[36] P. De Heyn, B. Kuyken, D. Vermeulen, W. Bogaerts, and D. Van Thourhout. *High-Performance Low-Loss Silicon-on-Insulator Microring Resonators using TM-polarized Light.* In The Optical Fiber Communication Conference and Exposition (OFC) and The National Fiber Optic Engineers Conference (NFOEC), Los Angeles, United States, 2011.

[37] D. Vermeulen, S.K. Selvaraja, R. Halir, W. Bogaerts, D. Van Thourhout, and G. Roelkens. *Photonic Integrated Circuits on SOI for Optical Fiber Communication Applications.* In 15th Annual Symposium of the IEEE Photonics Benelux Chapter, Delft, Netherlands, 2010.

[38] P. De Heyn, B. Kuyken, D. Vermeulen, W. Bogaerts, and D. Van Thourhout. *Improved intrinsic Q of silicon-on-insulator microring resonators using TM-polarized light.* In Annual Symposium of the IEEE Photonics Benelux Chapter, pages 197–200, Delft, Netherlands, 2010.

[39] D. Vermeulen, S.K. Selvaraja, P. Verheyen, W. Bogaerts, D Van Thourhout, and G. Roelkens. *High Efficiency Broadband Polarization Rotator on Silicon-On-Insulator.* In Group IV Photonics, pages 42–44, 2010.

[40] G. Roelkens, D. Vermeulen, R. Halir, L Liu, T Spuesens, R Kumar, P Mechet, K Huybrechts, S Keyvaninia, S. Stankovic, M Tassaert, P. De Heyn, Katarzyna Komorowska, S.K. Selvaraja, D. Van Thourhout, Geert Morthier, and R. Baets. *III-V/silicon photonic integrated circuits for FTTH and on-chip optical interconnects.* In IB2COM, Malaga, Spain, 2010.

[41] Emmanuel Lambert, Martin Fiers, W. Bogaerts, D. Vermeulen, and P. Bienstman. *A Python software framework for the design of photonic integrated circuits.* In EuroScipy, Paris, France, 2010.

[42] D. Vermeulen, T. Spuesens, P. De Heyn, P. Mechet, R. Notzel, S. Verstuyft, D. Van Thourhout, and G. Roelkens. *III-V/silicon-on-insulator photonic integrated circuit for fiber-to-the-home central office transceivers in a point-to-point network configuration.* In ECOC, page Tu.5.C.2, Torino, Italy, 2010.

[43] D. Vermeulen, K. Van Acoleyen, S. Ghosh, S. K. Selvaraja, W. A. D. De Cort, N. A. Yebo, E. Hallynck, K. De Vos, P. P. P. Debackere, P. Dumon, W. Bogaerts, G. Roelkens, D. Van Thourhout, and R. Baets. *Efficient Tapering to the*

Fundamental Quasi-TM Mode in Asymmetrical Waveguides. In European Conference on Integrated Optics, 2010.

[44] R. Halir, D. Vermeulen, and G. Roelkens. *Silicon-on-insulator tunable wavelength router with minimized polarization dependent loss.* In The Optical Fiber Communication Conference and Exposition (OFC) and The National Fiber Optic Engineers Conference (NFOEC), volume 2, United States, 2010.

[45] D. Vermeulen, S.K. Selvaraja, P. Verheyen, G Lepage, W. Bogaerts, and G. Roelkens. *High-efficiency silicon-on-insulator fiber-to-chip grating couplers using a silicon overlay.* In Group IV Photonics, pages post–deadline, San Francisco, United States, 2009.

[46] S.K. Selvaraja, D. Vermeulen, Marc Schaekers, Erik Sleeckx, W. Bogaerts, G. Roelkens, P. Dumon, D. Van Thourhout, and R. Baets. *Highly efficient grating coupler between optical fiber and silicon photonic circuit.* In Lasers and Electro-Optics, 2009 and 2009 Conference on Quantum electronics and Laser Science Conference. CLEO/QELS 2009. Conference on, volume 1, pages 1–2, 2009.

[47] G. Roelkens, D. Taillaert, F. Van Laere, D. Vermeulen, J. Schrauwen, S. Scheerlinck, T. Claes, W. Bogaerts, P. Dumon, S.K. Selvaraja, D. Van Thourhout, and R. Baets. *Interfacing optical fibers and high refractive index contrast waveguide circuits using diffractive grating couplers.* In Photonics West, volume 7218, pages 721808–721808–10, San Jose, United States, 2009.

[48] D. Vermeulen, G. Roelkens, D. Van Thourhout, and R. Baets. *SOI 1D and 2D photonic crystal structures for polarization independent fiber-to-chip coupling and duplexing operation.* In 8th International Photonic and Electromagnetic Crystal Structures Meeting (PECS-VIII), volume 45, Sydney, Australia, 2009.

[49] D. Vermeulen, G. Roelkens, J. Brouckaert, D. Van Thourhout, and R. Baets. *Towards an integrated fiber-to-the-home transceiver on a silicon nanophotonics platform.* In CMOS Photonics, 5th Optoelectronic and Photonic Winter School, Trento, Italy, 2009.

[50] D. Vermeulen, G. Roelkens, J. Brouckaert, D. Van Thourhout, and R. Baets. *Towards an integrated fiber-to-the-home transceiver on a silicon nanophotonics platform.* In 13th Annual Symposium of the IEEE/LEOS Benelux Chapter, pages 87–90, Enschede, the Netherlands, 2008.

[51] W. Bogaerts, Liu Liu, S.K. Selvaraja, P. Dumon, J. Brouckaert, D. Taillaert, D. Vermeulen, G. Roelkens, D. Van Thourhout, and R. Baets. *Silicon nanophotonic waveguides and their applications.* In Asia-Pacific Optical

Communications (APOC), pages 71341O–71341O–13, Hangzhou, China, 2008.

[52] D. Vermeulen, G. Roelkens, J. Brouckaert, D. Van Thourhout, R. Baets, R. Duijn, E. Pluk, and G. Van den Hoven. *Silicon-on-insulator nanophotonic waveguide circuit for fiber-to-the-home transceivers.* In 2008 34th European Conference on Optical Communication (ECOC), volume 2, pages 1–2, 2008.

[53] G. Roelkens, D. Vermeulen, D. Van Thourhout, R. Baets, S. Brision, P. Lyan, P. Gautier, and J. M. Fedeli. *High efficiency SOI fiber-to-waveguide grating couplers fabricated using CMOS technology.* In 2008 Summer Optics and Photonics Congress (IPNRA), Boston, USA, 2008.

[54] D. Vermeulen, G. Roelkens, and D. Van Thourhout. *Photonic integrated wavelength router on SOI for optical fiber communication applications.* In 11e UGent - Firw Doctoraatssymposium, 2010.

List of Figures